2008

Rice straw fiber polymer composites: thermal and mechanical performance

Fei Yao
Louisiana State University and Agricultural and Mechanical College

RICE STRAW FIBER POLYMER COMPOSITES: THERMAL AND MECHANICAL PERFORMANCE

A Dissertation

Submitted to the Graduate Faculty of the
Louisiana State University and
Agricultural and Mechanical College
in partial fulfillment of the
requirements for the degree of
Doctor of Philosophy

in

The School of Renewable Natural Resources

by
Fei Yao
B.S., Nanjing Forestry University, 2002
M.S., Nanjing Forestry University, 2004
December 2008

ACKNOWLEDGEMENTS

Many people contributed to the successful completion of this project. I am deeply grateful to Dr. Qinglin Wu, my committee chair and mentor, for his guidance, advice, encouragement and assistant throughout my Ph.D program. There is no doubt in my mind that his talent, diligence and persistence has thoroughly infected me and will be shining me in the future. I greatly appreciate my committee members, Dr. Ioan I. Negulescu, Dr. Jonathan Y. Chen, Dr. Richard P. Vlosky, and Dr. Jim J. Wang for their suggestion and support. I could not have asked for a better academic committee than them. It has been an honor and privilege for me to have them on my committee.

Very special thanks go to Dr. Yong Lei, my laboratory fellow and reliable friend, for his constructive suggestion and sincere help both in and out of academic fields throughout these years. Special thanks go to Dr. Hongzhi Liu, my former laboratory fellow, for his valuable discussion on several chapters. Thanks also go to other laboratory fellows and friends, Mr. Yanjun Xu, Dr. Peng Tian, Dr. Weihong Guo, Dr. Haiyun Liu, Mr. Birm June Kim, and Dr. Dagang Liu, for their help on experiments.

I am grateful to my host family, Mr. and Mrs. Rackley, and their families, for their invaluable suggestion, durative support and love-filled encouragement. They always provide me expeditious assistance whenever and wherever I and my wife need throughout our American life. Special appreciation goes to two friends, Mr. Price Blake and Mr. Bradley Aucoin, for their warmhearted help on language-editing. I wish to thank two friends, Ms. Feifei Han and Dr. Yimin Xiong, for their patience, support and understanding during the preparation of this dissertation.

I am deeply indebted to my wife, Yunyun Lu, for her patience, companionship, encouragement, understanding, and deep love. Her arrival at Baton Rouge in summer 2006 gave me best confidence and support to endure and complete this program. I also appreciate my parents, Yuan Yao and Jianhua Jiang, for their solicitude, encouragement and countless love. They support every single decision I made and they are proud of every tiny achievement I earned. They deserve my deepest appreciation and respect.

I hope all of them share this tremendous joy with me.

TABLE OF CONTENTS

LIST OF TABLES

LIST OF FIGURES

NOMENCLATURE

A	pre-exponential factor (s^{-1})
A3	Avrami-Erofeev equation (random instant nucleation and three-dimensional growth of nuclei)
ANOVA	analysis of variance
CDF	cumulative distribution function
d	distance between crystallographic planes
D2	2D-diffusion kinetic model
D3	Jander kinetic model
D4	Ginstling-Brounshtein kinetic model
DMA	dynamic mechanical analysis
DSC	differential scanning calorimetry
DTG	differential thermogravimetric
D^2TG	second time derivative of thermogravimetric
E	activation energy (kJ/mol)
E_a	apparent activation energy (kJ/mol)
E'	storage modulus
E''	loss modulus
EPDM	ethylene/propylene/diene terpolymer
EPR	ethylene/propylene copolymer
EPR-g-MA	maleic anhydride grafted ethylene/propylene copolymer
$f(\alpha)$	general expression of kinetic model
$g(\alpha)$	integral form of kinetic model $(df(\alpha)/d\alpha)$
HDPE	high density polyethylene
$JMA(n)$	Johnson-Mehl-Avrami kinetic model
k	Arrhenius rate constant
K	shape factor of crystalline thickness
KCE	kinetic compensation effect
L_{hkl}	crystalline thickness perpendicular to the reflection plane
LDPE	low density polyethylene
LLDPE	linear low density polyethylene
M_w	weight average molar mass (or average molecular weight)
MA	maleic anhydride
MFI	melt flow index
n	kinetic exponent
NFPC	natural fiber reinforced polymer composite
PDF	probability density function
PE	polyethylene
PE-g-MA	maleic anhydride grafted polyethylene
PP-g-MA	maleic anhydride grafted polypropylene
PT	Prout-Tompkins kinetic model
PVC	Polyvinyl chloride

R	universal gas constant ($8.314\ J/mol \cdot K$)
R^2	coefficient of determination
RHDPE	recycled high density polyethylene
RHF	rice husk fiber
$RO(n)$	reaction order law
RS	rise straw
$SB(m,n)$	autocatalytic (Šesták-Berggren) kinetic model
SEBS	styrene/ethylene-butylenes/styrene triblock compolymer
SEBS-g-MA	maleic anhydride grafted styrene/ethylene-butylenes/styrene triblock compolymer
SEM	scanning electron microscopy
SLF	rice straw leaf fiber
SSF	rice straw stem fiber
t	time (s)
T	absolute temperature (K)
T_c	crystallization temperature (°C or K)
T_m	melting temperature (°C or K)
T_o	onset temperature (°C or K)
T_p	peak temperature (°C or K)
T_s	shift temperature (°C or K)
$\tan\delta$	damping factor (loss-modulus/storage-modulus)
TG	thermogravimetric
TGA	thermogravimetric analysis
uEPR	unfunctionalized ethylene/propylene copolymer
VHDPE	virgin high density polyethylene
w_0	sample weight at $t = 0$ (start point)
w_f	sample weight at $t = \infty$ (final point)
w_i	initial actual isothermal conversion fraction
w_t	sample weight at $t = t$
WF	wood fiber
WL	weight loss (%)
WL_o	weight loss at onset point (%)
WL_p	weight loss at peak point (%)
WL_s	weight loss at shift point (%)
WPC	Wood Plastic Composite
WSF	rice whole straw fiber
x	reduced activation energy (E/RT)
X_R	normalized crystallization degree
XRD	X-ray diffraction analysis
$y(\alpha)$	defined function by Málek method
$z(\alpha)$	defined function by Málek method
α	conversion rate (dimensionless)

α_M	fractional extent of reaction at the maximum of $y(\alpha)$ function
α_p	fractional extent of reaction at the maximum of DTG curve
α_p^{∞}	fractional extent of reaction at the maximum of $z(\alpha)$ function
α_{WL}	adjusted conversion rate
β	heating rate ($K/\min$ or °C/min)
β_0	line broadening (rad)
λ	wavelength of the X-ray (Å)
μ	location parameter
$\pi(x)$	expression of temperature integral
θ	half of the angle of diffraction (degree)
σ	shape parameter
ΔH	melting (or crystallization) enthalpy of composite
ΔH_M	melting (or crystallization) enthalpy of pure polymer

ABSTRACT

Rice straw fiber can be considered as important potential reinforcing filler for thermoplastic composite because of its lignocellulosic characteristics. It is thus of practical significance to understand and predict the thermal decomposition process of rice straw fibers. A method proposed by Málek, Šesták, and co-workers was used to investigate and model thermal decomposition process of common natural fibers with detailed analysis on rice straw system. Assuming a global model occurring within the entire degradation of natural fibers with consideration of fiber as one pseudo-component, $RO(n > 1)$ model can be used to describe both isothermal and non-isothermal degradation process of most selected fibers within acceptable error limits of 3 and 5%, respectively. The parameters of kinetic model were given in this dissertation. The model obtained has practical significance for introducing straw fiber into some engineering plastics with comparatively lower melting temperature.

Influences of different rice straw components, and compatibilizers on various properties of rice-straw based polymer composites were also investigated. Rice straw fibers can work well with both VHDPE and RHDPE as reinforcing filler. Also, different components of rice straw had no significant influence on mechanical properties of composites. The PE-g-MA/EPR ratio affected mechanical properties of composites modified by combined compatibilizers. The optimum PE-g-MA/EPR ratio was considered to be 2:1 and 1:1 for PE-g-MA/uEPR and PE-g-MA/EPR-g-MA modified composites, respectively. At the optimum ratio, composites modified by combined compatibilizers showed better strength and impact toughness, and acceptable modulus compared to those modified by either EPR or EPR-g-MA.

It was found that 13% weight loss seemed to be the limit for rice straw to maintain its strength in a composite system. High-temperature one-step extrusion was feasible for

manufacturing HDPE/nylon-6/rice-straw composites without significant strength loss caused by thermal degradation of fiber. The two-step method failed to exhibit better performance than the one-step method.

CHAPTER 1 INTRODUCTION

1.1 LITERATURE REVIEW

Natural fiber reinforced thermoplastic composites have recently gained importance in various applications such as building materials and automotive components. The natural fibers offer advantages of large quantity, annual renewability, low cost, light weight, competitive specific mechanical properties, reduced energy consumption, and environmental friendliness. The natural fibers used to reinforce thermoplastics mainly include wood, cotton, flax, hemp, jute, sisal, and sugarcane fibers (Bledzki and Gassan 1999; Mohanty et al. 2000; Wollerdorfer and Bader 1998).

Rice straw fiber can also be considered as important potential reinforcing filler for thermoplastic composite because of its lignocellulosic characteristics. Global paddy production reached 628 million tons in 2005 with an additional one percent increase in 2006 (FAO, 2006). The U.S. rice production in 2006/07 was at 10 million tons (USDA, 2006). With an approximate rice-to-straw ratio of 1.0, an equivalent amount of rice straw (i.e., 10 million tons) was produced.

Chemically, lignocellulosic rice straw fiber has similar compositions as other natural fibers used in thermoplastics. As a result, it is subjected to thermal degradation during composite processing (Saheb and Jog 1999). It is thus of practical significance to understand and predict the thermal decomposition process of rice straw fibers. The knowledge will help better design composite process and estimate the influence on composite properties by thermal decomposition of natural fibers.

Previous research in thermal decomposition of natural fibers was primarily motivated by applications such as renewable biomass energy and natural fuels (Brown et al. 2000; Mohan et al. 2006; Yang et al. 2005), and forest fire propagation control (Chen et al. 2006; Liu and Fan 1998).

Due to the complexity of thermal decomposition reactions of natural fibers, extensive research has been done in determining individual behaviors of the main components (or pseudo-components) of natural fibers (e.g., pure cellulose, lignin, and hemicelluloses). For practical engineering applications, however, it may be sufficient to consider only the basic characteristics of the thermal decomposition process with some simplified mechanisms (Gronli et al. 2002). For natural fiber reinforced polymer composite processing, it is of more practical relevance to understand and predict the thermal decomposition of the reinforcing fibers based on the simplified kinetic scheme and parameters under specific process temperature of polymer/natural fiber composite. However, there have been few fundamental studies in this field.

Moreover, the reported values of kinetic parameters for natural fibers were in a large range, e.g., activation energy for pure cellulose from 100 and 250 kJ/mol (Varhegyi et al. 1989). This variability was primarily caused by different kinetic schemes used and pre-assumption of the reaction function and reaction order in kinetic modeling process. The suitable kinetic models for natural fibers remain to be developed (Capart et al. 2004). A method proposed by Málek, Šesták, and co-workers allows fairly reliable kinetic analysis and interpretation of non-isothermal TG-DTG data (Malek 1992; Malek et al. 2001).

The utilization of compatibilizers in natural fiber reinforced polymer composites (NFPC) intends to improve poor interphase between hydrophilic wood and hydrophobic polyolefin matrix. Among numerous compatibilizers that have been studied in two recent decades, maleic anhydride (MA) grafted polyethylene and propylene (PE-g-MA or PP-g-MA) are considered some of the most effective interphase modifiers for polyolefin/wood composite due to the polar interaction and covalent link between anhydride carbonyl and hydroxyl groups of wood surfaces (Kazayawoko et al. 1999a; Kazayawoko et al. 1999b; Kazayawoko et al. 1997; Lu and Wu 2005; Matuana et al. 2001), as well as their good compatibility with matrix (Lai et al. 2003; Li and

Matuana 2003; Wang et al. 2003). In addition, various polyolefinic elastomers are also of interest because of their enhancement performance on the impact strength of the composites. However, the addition of elastomers alone fails to effectively improve the strength and modulus of final composites. The system can sometimes even weaken the properties, although the impact toughness is more or less improved depending on the nature and content of elastomers used. To optimize the balance between stiffness/strength and toughness of NFPC, the combination of elastomers with maleated polyolefins as combined modifiers has been reported (Oksman and Clemons 1998; Rana et al. 2003; Sombatsompop et al. 2005). Although some work has been done, there is lack of further understanding on the effect of various compatibilizers on mechanical properties and fracture behaviors of HDPE/RS system. Also, very limited work concerning the feasibility of high-temperature extrusion process on manufacturing engineering plastics based rice straw composites has been done.

Based on the above-mentioned situation, the study described in this dissertation intends to (1) investigate thermal decomposition process of common natural fibers; and establish corresponding modeling and prediction of the thermal decomposition behavior of various natural fibers, especially rice straw fiber, in relation to polymer composite processing; and explore the feasibility and limit of producing rice straw filled high melting-temperature plastic composites using obtained models; and (2) investigate the influence of different rice straw components, interphase compatibilizers on various properties of rice-straw based polymer composites using HDPE as matrix.

1.2 ORGANIZATION OF DISSERTATION

This dissertation is organized as follows:

Chapter 1 (this chapter) is the overall introduction of the study.

Chapters 2-4 consists of Part I, focusing on fundamental thermal degradation kinetics model of rice straw and other common natural fibers. Specifically, Chapter 2 describes thermal decomposition process of common natural fibers and their activation energy values through a dynamic thermogravimetric analysis. Chapter 3 presents corresponding modeling of the thermal decomposition process of natural fibers by employing a comparatively reliable method. The reaction mechanism and parameters of thermal decomposition process of natural fibers are then described. Chapter 4 is devoted to the details of the thermal degradation process of rice straw fibers under both isothermal and non-isothermal conditions in order to better understand its thermal behavior for future application.

Chapters 5-7 consists of Part II, focusing on specific application of rice straw fibers into various polymer matrixes. Specifically, Chapter 5 presents the influence of various untreated rice straw fiber components on mechanical, thermal, and crystalline properties of the reinforced HDPE composites using both virgin and recycled HDPE materials. Chapter 6 shows the influence of various compatibilizers and their combination on mechanical and thermal-related properties as well as morphologies of the rice straw reinforced virgin HDPE composites. Chapter 7 concerns the feasibility of high-temperature extrusion process on manufacturing HDPE/nylon-6 based rice straw composites.

Chapter 8 provides the overall conclusion for this dissertation.

1.3 REFERENCES

Bledzki, A. K., and Gassan, J. (1999). "Composites reinforced with cellulose based fibres." *Progress in Polymer Science*, 24(2), 221-274.

Brown, M. E., Maciejewski, M., Vyazovkin, S., Nomen, R., Sempere, J., Burnham, A., Opfermann, J., Strey, R., Anderson, H. L., Kemmler, A., Keuleers, R., Janssens, J., Desseyn, H. O., Li, C. R., Tang, T. B., Roduit, B., Malek, J., and Mitsuhashi, T. (2000). "Computational aspects of kinetic analysis Part A: The ICTAC kinetics project-data, methods and results." *Thermochimica Acta*, 355(1-2), 125-143.

Capart, R., Khezami, L., and Burnham, A. K. (2004). "Assessment of various kinetic models for the pyrolysis of a microgranular cellulose." *Thermochimica Acta*, 417(1), 79-89.

Chen, H. X., Liu, N. A., and Fan, W. C. (2006). "Two-step consecutive reaction model and kinetic parameters relevant to the decomposition of Chinese forest fuels." *Journal of Applied Polymer Science*, 102(1), 571-576.

Gronli, M. G., Varhegyi, G., and Di Blasi, C. (2002). "Thermogravimetric analysis and devolatilization kinetics of wood." *Industrial & Engineering Chemistry Research*, 41(17), 4201-4208.

Kazayawoko, M., Balatinecz, J. J., and Woodhams, R. T. (1997). "Diffuse reflectance Fourier transform infrared spectra of wood fibers treated with maleated polypropylenes." *Journal of Applied Polymer Science*, 66(6), 1163-1173.

Kazayawoko, M., Balatinecz, J. J., and Matuana, L. M. (1999a). "Surface modification and adhesion mechanisms in woodfiber-polypropylene composites." *Journal of Materials Science*, 34(24), 6189-6199.

Kazayawoko, M., Balatinecz, J. J., and Sodhi, R. N. S. (1999b). "X-ray photoelectron spectroscopy of maleated polypropylene treated wood fibers in a high-intensity thermokinetic mixer." *Wood Science and Technology*, 33(5), 359-372.

Lai, S. M., Yeh, F. C., Wang, Y., Chan, H. C., and Shen, H. F. (2003). "Comparative study of maleated polyolefins as compatibilizers for polyethylene/wood flour composites." *Journal of Applied Polymer Science*, 87(3), 487-496.

Li, Q. X., and Matuana, L. M. (2003). "Surface of cellulosic materials modified with functionalized polyethylene coupling agents." *Journal of Applied Polymer Science*, 88(2), 278-286.

Liu, N. A., and Fan, W. C. (1998). "Modelling the thermal decompositions of wood and leaves under a nitrogen atmosphere." *Fire and Materials*, 22(3), 103-108.

Lu, J. Z., and Wu, Q. L. (2005). "Surface and interfacial characterization of wood-PVC composite: Imaging morphology and wetting behavior." *Wood and Fiber Science*, 37(1), 95-111.

Malek, J. (1992). "The kinetic-analysis of nonisothermal data." *Thermochimica Acta*, 200, 257-269.

Malek, J., Mitsuhashi, T., and Criado, J. M. (2001). "Kinetic analysis of solid-state processes." *Journal of Materials Research*, 16(6), 1862-1871.

Matuana, L. M., Balatinecz, J. J., Sodhi, R. N. S., and Park, C. B. (2001). "Surface characterization of esterified cellulosic fibers by XPS and FTIR spectroscopy." *Wood Science and Technology*, 35(3), 191-201.

Mohan, D., Pittman, C. U., and Steele, P. H. (2006). "Pyrolysis of wood/biomass for bio-oil: A critical review." *Energy & Fuels*, 20(3), 848-889.

Mohanty, A. K., Misra, M., and Hinrichsen, G. (2000). "Biofibres, biodegradable polymers and biocomposites: An overview." *Macromolecular Materials and Engineering*, 276(3-4), 1-24.

Oksman, K., and Clemons, C. (1998). "Mechanical properties and morphology of impact modified polypropylene - Wood flour composites." *Journal of Applied Polymer Science*, 67(9), 1503-1513.

Rana, A. K., Mandal, A., and Bandyopadhyay, S. (2003). "Short jute fiber reinforced polypropylene composites: effect of compatibiliser, impact modifier and fiber loading." *Composites Science and Technology*, 63(6), 801-806.

Saheb, D. N., and Jog, J. P. (1999). "Natural fiber polymer composites: A review." *Advances in Polymer Technology*, 18(4), 351-363.

Sombatsompop, N., Yotinwattanakumtorn, C., and Thongpin, C. (2005). "Influence of type and concentration of maleic anhydride grafted polypropylene and impact modifiers on mechanical properties of PP/wood sawdust composites." *Journal of Applied Polymer Science*, 97(2), 475-484.

Varhegyi, G., Antal, M. J., Szekely, T., and Szabo, P. (1989). "Kinetics of the Thermal-Decomposition of Cellulose, Hemicellulose, and Sugar-Cane Bagasse." *Energy & Fuels*, 3(3), 329-335.

Wang, Y., Yeh, F. C., Lai, S. M., Chan, H. C., and Shen, H. F. (2003). "Effectiveness of functionalized polyolefins as compatibilizers for polyethylene/wood flour composites." *Polymer Engineering and Science*, 43(4), 933-945.

Wollerdorfer, M., and Bader, H. (1998). "Influence of natural fibres on the mechanical properties of biodegradable polymers." *Industrial Crops and Products*, 8(2), 105-112.

Yang, Y. B., Ryu, C., Khor, A., Yates, N. E., Sharifi, V. N., and Swithenbank, J. (2005). "Effect of fuel properties on biomass combustion. Part II. Modelling approach - identification of the controlling factors." *Fuel*, 84(16), 2116-2130.

CHAPTER 2* THERMAL DECOMPOSITION KINETICS OF NATURAL FIBERS: ACTIVATION ENERGY WITH DYNAMIC THERMOGRAVIMETRIC ANALYSIS

2.1 INTRODUCTION

In recent years, natural fibers in form of fiber and/or particulate have been widely used as reinforcing fillers in thermoplastic composite materials. These natural fillers are lighter, and cheaper, and provide much higher strength per unit mass than most inorganic fillers. Besides ecological considerations, several technical aspects promote the renewed interest for the fibers as supplement or replacement for traditional fillers (e.g., glass fibers) in polymer composites (Bledzki and Gassan 1999; Mohanty et al. 2000; Wollerdorfer and Bader 1998). Natural fibers from agricultural residues and forest products processing are mainly consist of natural lignocellulosic polymers. As a result, they are subjected to thermal degradation during composite processing (Bledzki et al. 2002; Saheb and Jog 1999). It is thus of practical significance to understand and predict the thermal decomposition process of natural fibers and the knowledge will help better design composite process and estimate the influence on composite properties by thermal decomposition of natural fibers.

Previous research in thermal decomposition of natural fibers was primarily motivated by applications such as renewable biomass energy/natural fuels (Brown et al. 2001; Mohan et al. 2006; Yang et al. 2005), and forest fire propagation control (Chen et al. 2006; Liu and Fan 1998). Due to the complexity of thermal decomposition reactions of natural fibers, extensive researches have been done in determining individual behaviors of the main components (or pseudo-components) of natural fibers (e.g., pure cellulose, lignin, and hemicelluloses). In this case, improvement of classic "Broido-Shafizadeh" model (Bradbury et al. 1979) and calculation of

* Reprint in part with permission from Polymer Degradation and Stability, Volume 93, Issue 1, Pages 90-98. Yao, F., Wu, Q. L., Lei, Y., Guo, W. H. & Xu, Y. J. 2008. Thermal decomposition kinetics of natural fibers: Activation energy with dynamic thermogravimetric analysis.

decomposition activation energy of pure cellulose is the primary focus. Antal and Varhegyi (1995), and Antal et al. (Antal et al. 1998) reviewed the pyrolysis of pure, ash-free cellulose and described it with a single-step, irreversible, first-order rate law containing high activation energies (238 or 228 kJ / mol). Milosavljevic and Suuberg (1995) reviewed global cellulose pyrolysis kinetics and found that low activation energies (140-155 kJ / mol) were obtained when cellulose was rapidly heated to above 600 K . Nada and Hassan (2000) investigated cellulose and some cellulose derivatives and concluded their activation energies of 53-182 kJ / mol . Capart et al. (2004) calculated kinetics parameters of microgranular cellulose using dynamic and isothermal methods in nitrogen atmosphere and described it with two reactions with activation energies of 202 and 255 kJ / mol , respectively. Besides of pure cellulose, the pyrolysis of lignin and hemicelluloses (i.e., xylan) has also been studied (Bilbao et al. 1989; Jakab et al. 1995). In developing fiber decomposition kinetics, different reaction schemes have also been considered for a better interpretation for fiber decomposition process. Koufopanos et al. (1989) established multi-step reaction mechanisms for wood and wood components. Diebold (1994) later developed an elaborate seven-step global kinetics scheme for cellulose pyrolysis. Orfao et al (1999) introduced three independent reactions model to pyrolysis kinetics of some lignocellulosic materials, while Di Blasi (2002) used three parallel reactions to describe the fast pyrolysis process of wood. More recently, Chen et al. (2006) employed a two-step consecutive reaction model for some forest fuels. For practical engineering applications, however, it may be sufficient to consider only the basic characteristics of the thermal decomposition process with some simplified mechanisms (Gronli et al. 2002). For natural fiber reinforced polymer composite processing, it is of more practical relevance to understand and predict the thermal decomposition of the reinforcing fibers based on the simplified kinetic scheme and parameters under specific

process temperature of polymer/natural fiber composite. However, there have been few fundamental studies in this field.

The reported values of kinetic parameters for natural fibers were in a large range, e.g., activation energy for pure cellulose from100 and 250 kJ / mol (Varhegyi et al. 1989). This variability was primarily caused by different kinetic schemes used and pre-assumption of the reaction function and reaction order in kinetic modeling process. The suitable kinetic models for natural fibers remain to be developed (Capart et al. 2004). The "model-free" iso-conversional methods are considered as a helpful solution for truly determining activation energy in this case (Maciejewski 2000). The approach allows obtaining the dependence of the kinetic parameters with the conversion from thermogravimetric (TG) and differential thermogravimetric (DTG) curves measured at different heating rates without making any assumptions about the reaction function and reaction order. Consequently, the method makes it possible to avoid the risk of obtaining wrong kinetics parameters, especially activation energy, due to pre-assuming inappropriate reaction function (Brown et al. 2000; Maciejewski 2000). The approach has been used to determine the thermal degradation kinetics of some polymer/natural fiber composites (Alvarez and Vazquez 2004).

Despite of previous research that has contributed to the understanding of thermal decomposition kinetics of natural fibers, a simplified prediction approach for thermal decomposition of the fibers under the normal processing temperatures of polymer composites has not been established so far. The objective of this work was to investigate thermal decomposition process of common natural fibers and to establish their activation energy values through a dynamic thermogravimetric analysis by model-free methods. Future publication will deal corresponding modeling and prediction of the thermal decomposition behavior of natural fibers in relation to polymer composite processing.

2.2 THEORETICAL APPROACH

The fundamental rate equation used in all kinetic studies is generally described as:

$$d\alpha / dt = kf(\alpha) \tag{2.1}$$

where k is the rate constant and $f(\alpha)$ is the reaction model, a function depending on the actual reaction mechanism. Eq. (2.1) expresses the rate of conversion, $d\alpha / dt$, at a constant temperature as a function of the reactant concentration loss and rate constant. In this study, the conversion rate α is defined as:

$$\alpha = (W_0 - W_t)/(W_0 - W_f) \tag{2.2}$$

where W_t, W_0 and W_f are time t, initial and final weights of the sample, respectively. The rate constant k is generally given by the Arrhenius equation:

$$k = A\exp(-E/RT) \tag{2.3}$$

where E is the apparent activation energy (kJ/mol), R is the gas constant ($8.314\ J/K \cdot mol$), A is the pre-exponential factor (s^{-1}), T is the absolute temperature (K). The combination of Eqs. (2.1) and (2.3) gives the following relationship:

$$d\alpha / dt = A\exp(-E/RT) f(\alpha) \tag{2.4}$$

For a dynamic TGA process, introducing the heating rate, $\beta = dT/dt$ into Eq. (2.4), Eq. (2.5) is obtained as:

$$d\alpha / dT = (A/\beta)\exp(-E/RT) f(\alpha) \tag{2.5}$$

Eqs.(2.4) and (2.5) are the fundamental expressions of analytical methods to calculate kinetic parameters on the basis of TGA data.

The most common "model-free" methods used in this study are summarized in Table 2.1. The Friedman method is the isoconversional method, which directly leads to $-E_a/R$ for a given value of α by plotting the term $\ln(d\alpha/dt)$ against $1/T$. In the Kissinger method, $\ln(\beta/T_p^2)$ is

plotted against $1/T_p$ for a series of experiments at different heating rates with the peak temperature, T_p, obtained from the DTG curve. The isoconversional Flynn-Wall-Ozawa (F-W-O) method is the integral method, which leads to $-E_a/R$ from the slope of the line determined by plotting $\log(\beta)$ against $1/T$ at any certain conversion rate. The modified Coats-Redfern method is a multi-heating rate application of the Coats-Redfern equation. Plotting the left hand side for each heating rate versus $1/T$ at that heating rate gives a family of straight lines of slope $-E_a/R$. The full solution is to be done iteratively by first assuming a value of Ea and then recalculating the left hand side until convergence occurs. Here, a quick solution, however, is also available by moving $(1-2RT/E_a)$ into the intercept and assuming that it is a constant.

Table 2.1 Kinetic methods used in evaluating activation energy in this study.

Method	Expression	Plots
Friedman (1964)	$\ln(d\alpha/dt) = \ln[Af(\alpha)] - E_a/RT$	$\ln(d\alpha/dt)$ *vs.* $1/T$
Kissinger (1956)	$\ln(\beta/T_p^{\,2}) = \ln(AR/E_a) + (1/T_p)(-E_a/R)$	$\ln(\beta/T_p^{\,2})$ *vs.* $1/T_p$
Flynn-Wall-Ozawa (Flynn and Wall 1966; Ozawa 1965)	$\log\beta = \log\frac{AE_a}{Rg(\alpha)} - 2.315 - 0.4567E_a/RT$	$\log\beta$ *vs.* $1/T$
Modified Coats-Redfern (Brown et al. 2000)	$\ln\left[\frac{\beta}{T^2(1-2RT/E_a)}\right] = \ln\left[-\frac{AR}{E_a\ln(1-\alpha)}\right] - \frac{E_a}{RT}$	$\ln(\beta/T^2)$ *vs.* $1/T$

2.3 EXPERIMENTAL

2.3.1 Materials Preparation

Ten natural fibers including wood, bamboo, agricultural residue, and bast fibers were selected in this study. The information on chemical composition reported in the literature for various fibers is summarized in Table 2.2. All raw materials were washed with water to remove

the impurity and then dried in an oven at 75°C for 12 h. Dried materials were then ground with a Wiley mill, and then screened. The samples with the particle size between 20 and 28 meshes were collected for test.

Table 2.2 Chemical composition of selected samples.

Species		Cellulose (wt%)	Hemicelluloses (wt%)	Lignin (wt%)	Ash (wt%)
Wood	Pine (softwood)	40-45	25-30	26-34	-
	Maple (hardwood)	45-50	21-36	22-30	-
Bamboo	Bamboo	42.3-49.1	24.1-27.7	23.8-26.1	1.3-2.0
Ag-residue	Rice straw	41-57	33	8-19	8-38
	Rice husk	35-45	19-25	20	14-17
	Bagasse	40-46	24.5-29	12.5-20	1.5-2.4
	Cotton stalk	43.1	26.9	27.3	1.3
Bast fiber	Jute	61-71.5	12-20.4	11.8-13	2
	Hemp	70.2-74.4	17.9-22.4	3.7-5.7	-
	Kenaf	31-39	21.5	15-19	-

(Bledzki and Gassan 1999; Bledzki et al. 2002; Higuchi 1957; Jackson 1977; Lu et al. 2006; Marti-Ferrer et al. 2006; Mohanty et al. 2000; Nada et al. 2006; Sundstøl 1984)

2.3.2 Test Procedures

Thermal decomposition was observed in terms of global mass loss by using a TA Instrument TGA Q50 thermogravimetric analyzer. This apparatus detects the mass loss with a resolution of 0.1 μg as a function of temperature. The samples were evenly and loosely distributed in an open sample pan of 6.4 mm diameter and 3.2 mm deep with an initial sample amount of 8-10 mg. Due to different bulk density, the depth of the sample layer filled in the pan was about 1-2 mm. The temperature change was controlled from room temperature (25±3°C) to

800°C at six different heating rates of 2, 3.5, 5, 7.5, 10, and 15°C/min. The sampling segment was set as 0.5 second per point. The thermal decomposition was carried out at low or moderate heating rates to keep possible heat/mass-transfer intrusions at a minimum (Gronli et al. 2002). A high purity nitrogen stream (99.5% nitrogen, 0.5% oxygen content) was continuously passed into the furnace at a flow rate of 60 mL/min at room temperature and atmospheric pressure. Before starting each run, the nitrogen was used to purge the furnace for 30 min to establish an inert environment in order to prevent any unwanted oxidative decomposition.

2.3.3 Data Processing

The TG and DTG curves obtained from TGA runs were carefully smoothed at a smoothing region width of 0.2°C by using least squares smoothing method, and analyzed by using Universal Analysis 2000 software from TA Instruments. Activation energy values were calculated with a specially designed program in MS Excel, which takes specific TG and derivative thermogravimetric (DTG) data from the Universal Analysis software. To verify the reproducibility of obtained mass loss curves, two sample runs were performed under the same experimental conditions for each kind of fiber at each selected heating rate first. The approximate overlapping of two weight loss curves from two separate test runs was considered as reasonable agreement; otherwise, another two runs were performed then to determine which one should be chosen.

2.4 RESULTS AND DISCUSSION

2.4.1 Overall Decomposition Process of Natural Fibers

Fig. 2.1 presents the overall thermogravimetric decomposition process of natural fibers at a heating rate of 2°C/min. As shown in Fig. 2.1a, a distinct DTG peak, resulted mainly from the thermal decomposition of cellulose, was observed with an obvious “shoulder” (arrow), which was normally considered as the result of thermal decomposition of hemicelluloses in an inert

atmosphere (Antal and Varhegyi 1995). These low-temperature hemicelluloses shoulder peaks, however, were overlapped in the cellulose main peaks and consequently they were not obvious

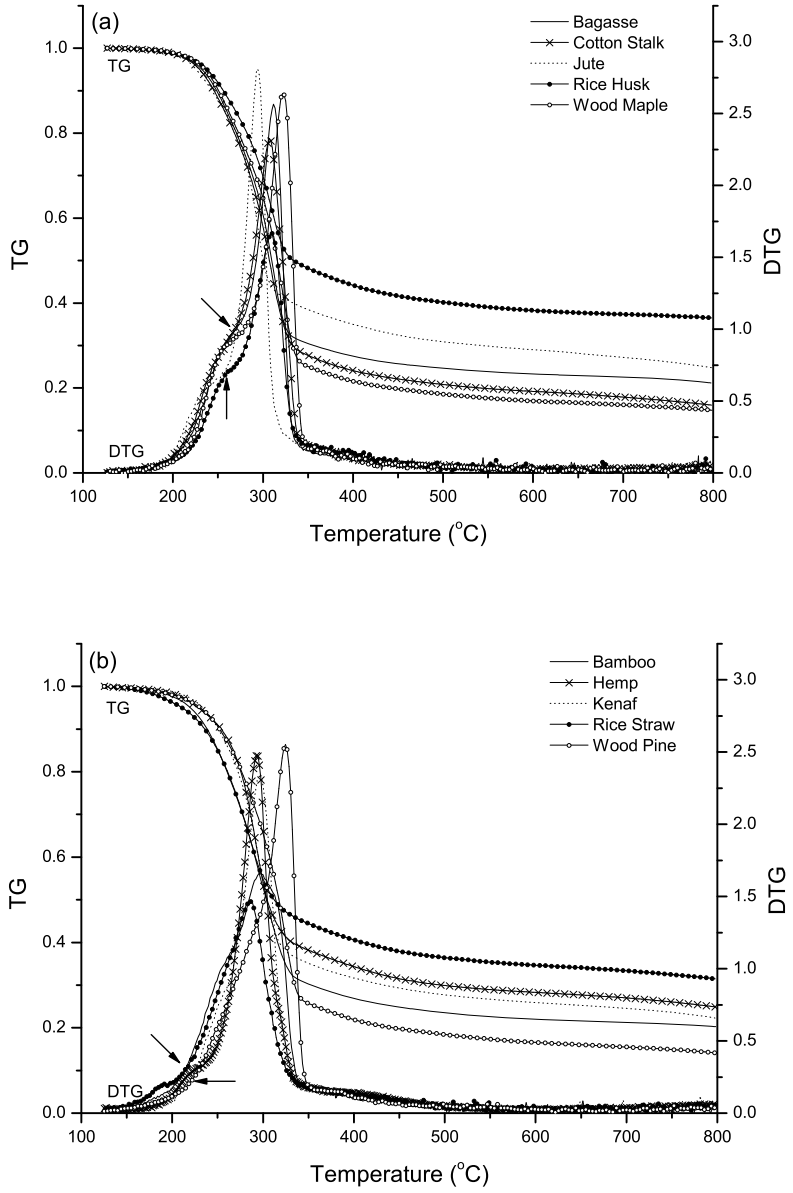

Fig. 2.1 Overall thermogravimetric decomposition process of natural fibers at a heating rate of 2°C/min.

in some cases (Fig. 2.1b arrow). The high-temperature "tails" shown in all curves of both Fig. 2.1a and 2.1b were normally presented by the degradation of lignin (Antal and Varhegyi 1995). The close similarity of TG and DTG curves for different fibers shown in Fig. 2.1 indicated that thermal decomposition process of selected natural fibers has the similar characteristics as a result of being lignocellulosic material.

2.4.2 Thermal Decomposition Characteristics of Natural Fibers

Thermal decomposition parameters were determined from the TG, DTG, and second time derivatives, D^2TG, curves as described below using rice husk data at a heating rate of 5°C /min as an example (Fig. 2.2). The extrapolated onset temperature of decomposition, T_o, was obtained by extrapolating the slope of the DTG curve in correspondence with the first local maximum in D^2TG curve and down to the zero level of the DTG axis (Gronli et al. 2002). The peak temperature, T_p, was determined by DTG peak where the maximum decomposition rate was obtained. The weight loss percentage corresponding to T_p is symbolized with WL_p. The final, tailing region indicated the end of cellulose decomposition. The further reactions mainly contained continued decomposition of lignin and tar or char from main components decomposition. The shift temperature, T_s, is defined here by extrapolating the slope of DTG curve corresponding to the local minimum in D^2TG curve in this region and down to the zero level of DTG axis. The weight loss percentage corresponding to T_s is marked with WL_s. The residue presented the residual solid mass fraction percentage detected at the final temperature, 800°C. It was well known that the characteristic temperature point would move to a higher value with increases in the heating rate. To avoid the influence of linear heating procedure on determining three important characteristic temperature parameters, T_o, T_p, T_s, six temperature values from six heating rates of individual fiber type were extrapolated to a value where $\beta = 0$

for each of the three temperature parameters. In addition, each of three weight loss percentage parameters, WL_p, WL_s and Residue, was obtained by averaging six corresponding weight loss percentage values from six heating rates of individual fiber type and the standard deviation values were also calculated and listed. Average values were thereafter given for each category.

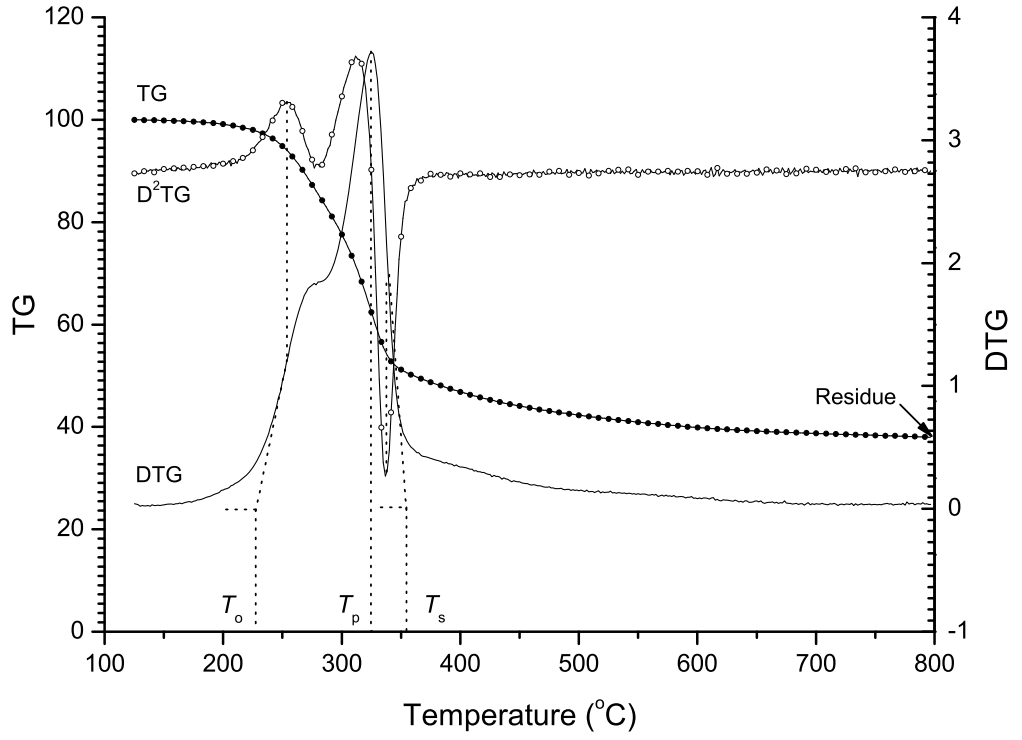

Fig. 2.2 Determination of decomposition characteristic parameters of natural fibers using rice husk fiber as an example at a heating rate of 5°C /min.

The decomposition characteristics of selected fibers are summarized in Table 2.3. The parameter T_o indicates an onset decomposition temperature range of about 215±10°C for all natural fibers except a higher value for pine. Weight loss in this period (referred to WL_o) was

observed around 5% for all fibers, while rice straw and pine fibers showed higher values indicating a comparatively faster initial decomposition than other fibers. The parameter T_p presents that the maximum decomposition rate of main natural fibers happened in a range of 290±10°C, while wood fibers had higher values (an average of 310°C for maple and pine fibers) with respect to the others. The weight loss at this point, indicated by parameter WL_p, reached nearly 45% or higher for most fibers. Due to possible inorganic component occurred in the surface layer, rice husk and straw fibers experienced smaller decomposition, around 35%, during this period. From peak to shift temperature, natural fibers had a rapid degradation in a narrow temperature range. Most fibers completed almost 60% or higher weight loss at 310±10°C as shown by WL_s and T_s, respectively. Further heating to the final temperature of 800°C led to an average residue value of 20±4% for most fibers, except rice husk and straw fibers, which had significant higher residue weight due to higher inorganic content. Small standard deviation values of parameter WL_o, WL_p, and WL_s as well as residual weight indicated that the weight loss fraction was probably the intrinsic property of natural fibers, which was not affected by heating rate. The temperatures and weight loss difference between offset and shift points, $(T_s - T_o)$ and $(WL_s - WL_o)$ respectively, showed again that main thermal decomposition fraction (around 60%) happened in a temperature range of around 100°C (215-310±10°C in terms of extrapolated temperatures) for most natural fibers. The period was overlapped with the processing temperatures of some engineering thermoplastics, e.g., polyamides, polyesters, and polycarbonates (Mohanty et al. 2000). Considering future introduction of more variety of polymers in natural fiber reinforced polymer composite, the decomposition activation energies of natural fibers in this period needs to be quantified.

Table 2.3 Decomposition characteristics of the select fibers including extrapolated peak and shift temperatures, weight loss and residue percentages obtained from different heating rates.

Natural Fiber	$T_{o\,\beta\to 0}$ [a] (°C)	WL_o (%)	$T_{p\,\beta\to 0}$ (°C)	WL_p (%)	$T_{s\,\beta\to 0}$ (°C)	WL_s (%)	Residue (%)	$T_s - T_o$ (°C)	$WL_s - WL_o$ (%)
Bagasse	222.3[b]	5.3 (0.2)	299.3	53.7 (1.1)	313.9	68.0 (1.3)	20.4 (2.1)	91.6	62.7
Bamboo	214.1	6.3 (0.7)	285.9	44.6 (1.6)	321.0	68.5 (0.4)	20.5 (0.2)	106.9	62.3
Cotton Stalk	221.6	5.3 (0.5)	293.4	50.4 (1.1)	318.9	70.0 (0.5)	17.1 (0.8)	97.3	64.7
Hemp	205.1	3.1 (0.5)	282.3	38.2 (1.4)	308.2	58.2 (1.1)	24.6 (0.5)	103.1	55.1
Jute	205.1	2.8 (0.2)	283.1	44.2 (1.9)	298.2	58.5 (1.5)	25.2 (0.4)	93.1	55.8
Kenaf	219.0	4.9 (0.5)	284.1	42.9 (1.1)	309.2	62.7 (1.1)	22.4 (0.3)	90.2	57.8
Rice Husk	223.3	4.0 (0.2)	297.4	37.7 (0.4)	322.0	50.1 (0.7)	37.0 (0.7)	98.7	46.1
Rice Straw	228.5	10.6 (0.3)	273.6	35.0 (1.5)	311.3	51.5 (0.6)	33.6 (2.3)	82.8	40.9
Wood-Maple	220.9	4.4 (0.1)	308.3	58.6 (0.5)	323.7	73.8 (0.8)	15.4 (0.6)	102.8	69.4
Wood-Pine	234.6	7.7 (0.3)	311.5	58.8 (0.9)	328.0	72.7 (0.5)	14.9 (0.7)	93.4	64.9
All fiber average[c]	219.5 (9.3)	5.4 (2.3)	291.9 (12.2)	46.4 (8.6)	315.4 (8.9)	63.4 (8.5)	23.1 (7.4)	96.0 (7.2)	57.9 (8.9)

[a] Capital: T = temperature, WL = weight loss; subscript: o = onset, p = DTG peak, s = shift, $\beta \to 0$ = extrapolated values to the heating rate of 0 °C/min.
[b] Values from six heating rates with mean value and standard deviation.
[c] Values from ten types of selected fibers with mean value and standard deviation.

2.4.3 Determination of Apparent Activation Energy

The plots of isoconversional Friedman, F-W-O, and modified Coats-Redfern methods show a general trend of activation energy. As an example, the Friedman plot for the bamboo fiber is shown in Fig. 2.3a, while Fig. 2.3b and 2.3c show the specific results of application of F-W-O and modified Coats-Redfern methods using sugarcane bagasse and jute fibers as examples, respectively. It is shown in Fig. 2.3a and 2.3b that the fitted lines are nearly parallel, which indicates approximate activation energies at different conversions and consequently implies the possibility of single reaction mechanism (or the unification of multiple reaction mechanisms). The reaction mechanism, however, also might change in comparatively higher conversion periods according to unsatisfied parallel line of α = 0.8 in Fig. 2.3c. The trends of other fibers (not shown in Fig. 2.3) are similar to those shown in this figure, indicating the possible single reaction mechanism in low conversion and the changed mechanisms when reaches higher conversions (normally around 0.7 or higher).

The change of reaction mechanism in higher conversions might be caused by the complex reactions in decomposition process of the main fiber components according to previous research on cellulose and "Broido-Shafizadeh" model (Antal and Varhegyi 1995; Bradbury et al. 1979). This change, also, leads to the complexity of modeling the whole process of fiber decomposition. Since aforementioned temperature range of 215-310±10°C with main thermal decomposition fraction of 60% is more meaningful for polymer composite and decomposition mechanism might change when conversion rate is higher than 0.7, emphasis was placed on a conversion range from 0.1 to 0.6, instead of the entire process, which might offer a simplified and more meaningful way to modeling thermal decomposition behavior of natural fibers. The decomposition conversion thereafter is less meaningful for polymer composites due to too high temperature and sample weight loss.

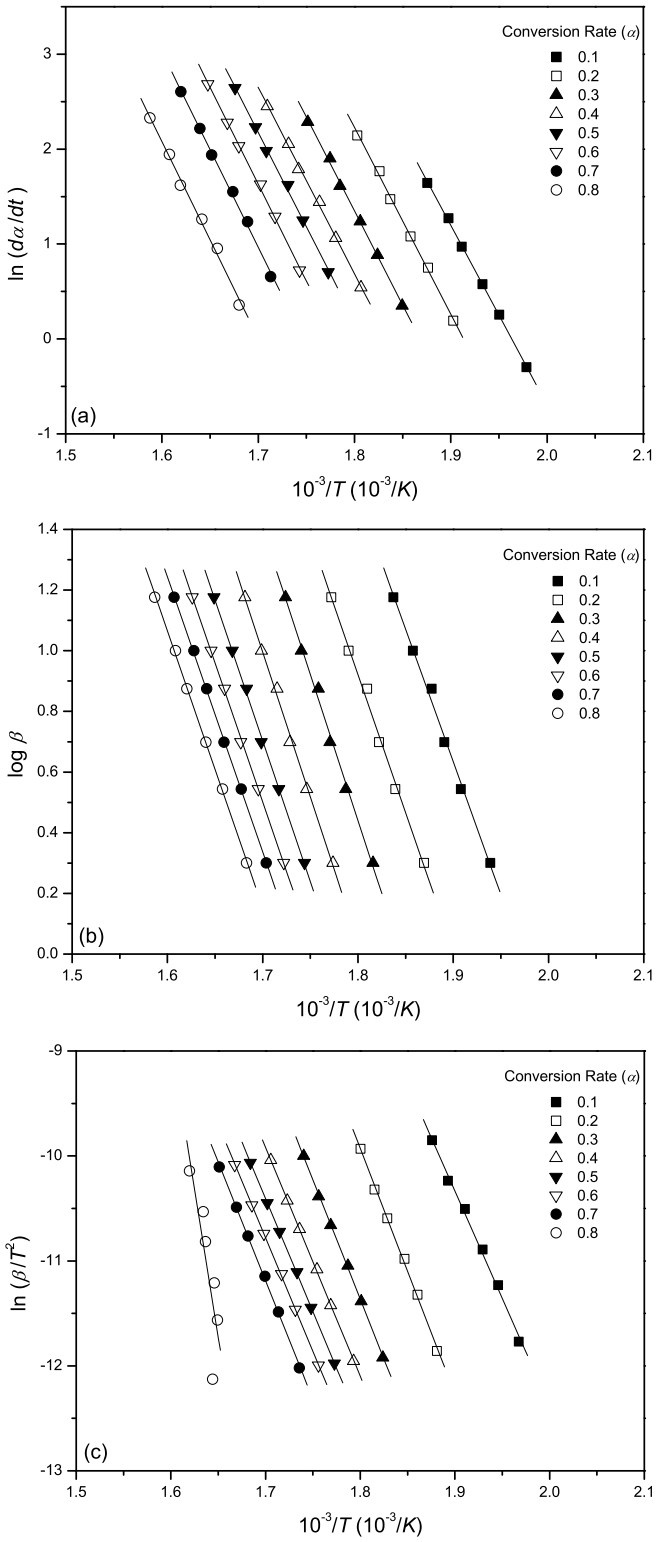

Fig. 2.3 Typical isoconversional plot of (a) Friedman method (bamboo), (b) F-W-O method (sugarcane bagasse) and (c) modified Coast-Redfern method (jute).

Table 2.4 summarizes the average apparent activation energies calculated from the conversion range of 0.1-0.6 through isoconversional Friedman, F-W-O, and modified Coats-Redfern methods for all selected fibers. To accurately obtain activation energy values, all data was calculated with a conversion spacing of 0.01 using the purpose- designed Excel program. Means and standard deviations listed here were calculated from 50 fractions. As shown in Table 2.4, the differential Friedman method led to an apparent activation energy range of approximate 157-169 kJ/mol for most fibers (except hemp, jute and rice straw fibers) in the conversion range. Similar results from F-W-O and modified Coats-Redfern method also confirmed this observation, where the range was around 156-171 and 154-170 kJ/mol, respectively, for those fibers. The result indicates that thermal decomposition activation energy values for all natural fibers are in the reported range. Fig. 2.4 shows the plots of activation energy as a function of conversion for α = 0.07-0.73 for all fibers based on three isoconversional methods. The reported activation energy range is also clearly observed in Fig. 2.4 with a "band" shape between 150 and 175 kJ/mol. As the thermal decomposition process proceeded in natural fibers, the activation energy remained unchanged or only slightly changed after the initial stage and then remained constant until α = 0.60 for those fibers. The slight increase of activation energies before α = 0.2 implied the possible occurrence of accelerated decomposition process of main composition which is approaching balance in the initial stage. It is noted that this accelerated process might be different with the one at the very beginning period (α = 0-0.07, not plotted in Fig 2.4) which is mainly caused by the decomposition of low molecular composition indicated by WL_o. The changing value after α = 0.7 until final conversion implied the multi-step reaction mechanisms (Ozawa 1965). The moderate standard deviation values for E_a implies that the degradation mechanism (or unification of multiple reaction mechanisms) for those fibers remains unchanged

Table 2.4 Average apparent activation energy of select fibers calculated by three model-free methods in a period of α = 0.1-0.6.

Natural Fiber	Friedman		F-W-O		Modified Coats-Redfern	
	$E_a\ (kJ/mol)$	R^2	$E_a\ (kJ/mol)$	R^2	$E_a\ (kJ/mol)$	R^2
Bagasse	168.5 (7.5)[a]	0.9972 (0.0022)	169.5 (4.8)	0.9967 (0.0019)	168.7 (4.9)	0.9963 (0.0021)
Bamboo	164.1 (2.2)	0.9982 (0.0003)	162.8 (2.5)	0.9989 (0.0003)	161.9 (2.3)	0.9987 (0.0003)
Cotton stalk	165.3 (8.5)	0.9953 (0.0010)	169.9 (5.1)	0.9959 (0.0005)	169.1 (5.7)	0.9954 (0.0006)
Hemp	180.9 (9.4)	0.9939 (0.0042)	177.9 (3.9)	0.9925 (0.0065)	177.7 (4.1)	0.9918 (0.0072)
Jute	183.1 (9.4)	0.9993 (0.0008)	184.2 (5.8)	0.9991 (0.0011)	184. 3 (6.3)	0.9990 (0.0012)
Kenaf	169.8 (3.5)	0.9964 (0.0006)	170.3 (1.6)	0.9965 (0.0009)	169.6 (1.9)	0.9960 (0.0010)
Rice husk	168.2 (2.5)	0.9926 (0.0050)	167.4 (2.2)	0.9944 (0.0036)	166.5 (2.1)	0.9938 (0.0040)
Rice straw	197.6 (3.0)	0.9814 (0.0047)	195.9 (1.5)	0.9812 (0.0055)	196.9 (1.3)	0.9812 (0.0060)
Wood-Maple	156.0 (2.7)	0.9865 (0.0050)	155.8 (3.8)	0.9857 (0.0028)	154.3 (3.6)	0.9838 (0.0031)
Wood-Pine	161.5 (3.0)	0.9965 (0.0041)	161.8 (3.2)	0.9946 (0.0060)	160.4 (3.1)	0.9940 (0.0067)
All fiber average[b]	171.5 (12.3)	0.9928 (0.0064)	171.5 (11.7)	0.9935 (0.0058)	170.9 (12.5)	0.9928 (0.0064)

[a] Values from fifty conversion fractions with mean value and standard deviation
[b] Values from ten types of fibers with mean value and standard deviation

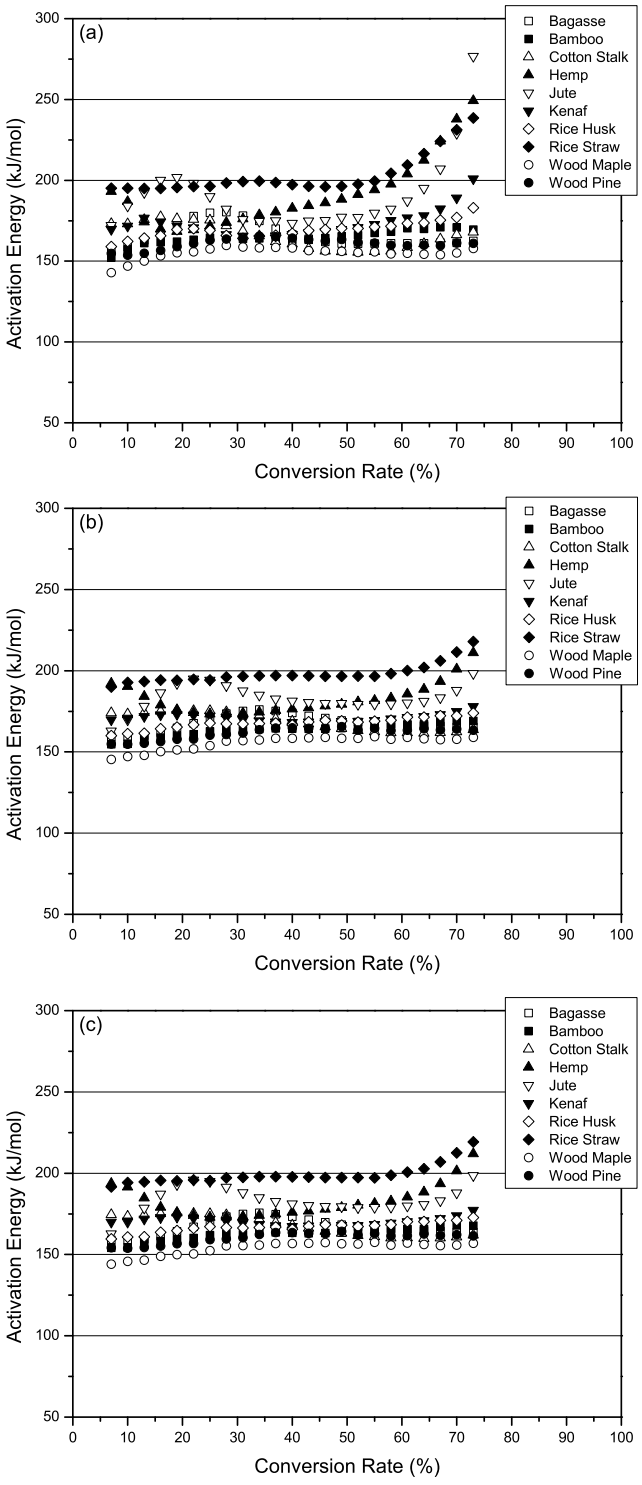

Fig. 2.4 A comparison of apparent activation energy as a function of decomposition conversion rate (α) for all selected fibers calculated by (a) Friedman, (b) F-W-O method and (c) modified Coast-Redfern method.

throughout the whole selected conversion range and could be attributed to comparatively low temperature (about 310°C). The E_a values of hemp and jute fibers reached around $180\,kJ/mol$ in three methods. The presence of low E_a in low conversion and high E_a in high conversion (Fig. 2.4) in hemp fiber might imply the different decomposition mechanisms in whole process (Ouajai and Shanks 2005). As shown with a very small standard deviation, the E_a values of rice straw fibers were approximately $200\,kJ/mol$, which is significantly higher than these of other fibers. The result indicates a single mechanism with a better stability of rice straw fiber compared to the other fibers associated with the weight loss fraction and residue results in Table 2.3. Table 2.4 also indicates strong linear correlation among the independent and dependent variables, as well as the consistence of the technique in calculating the activation energy value.

Table 2.5 shows the apparent activation energy values calculated by Kissinger's method for all selected fibers. Fig. 2.5 shows the linear plots of $\ln(\beta/T_p^2)$ versus $1/T_p$ for various fibers from the Kissinger method. Even though Kissinger's method is a special case in determining E_a and it may not display overall trend of E_a due to the fact that only data from a certain conversion rate is used. In this study, it is observed that E_a was stable in a conversion range of 0.1-0.6 according to the aforementioned results by isoconversional methods. Therefore, the results from Kissinger's method are meaningful for determining E_a in this case. An approximate activation energy range of 150-175 kJ/mol is obtained (Table 2.5) which supports the aforementioned results. Hemp and rice straw fibers show higher activation energies than these of other fibers, while jute fiber shows a moderate one.

It is noticed that the values by Kissinger's method are holistically lower than the ones by isoconversional methods, while values by isoconversional methods is nearly same from one to another. As suggested by ICTAC Kinetics Project (Brown et al. 2000), however, different

Table 2.5 Apparent activation energy of select fibers calculated by Kissinger method

Natural Fiber	$E_a\ (kJ/mol)$	R^2
Bagasse	161.1	0.9986
Bamboo	161.6	0.9764
Cotton stalk	146.0	0.9828
Hemp	171.1	0.9994
Jute	165.6	0.9996
Kenaf	157.7	0.9971
Rice husk	167.4	0.9953
Rice straw	176.2	0.9659
Wood-Maple	153.7	0.9905
Wood-Pine	159.3	0.9970
All fiber average[a]	161.8 (8.2)	0.9910 (0.0112)

[a] Values from ten types of fibers with mean value and standard deviation

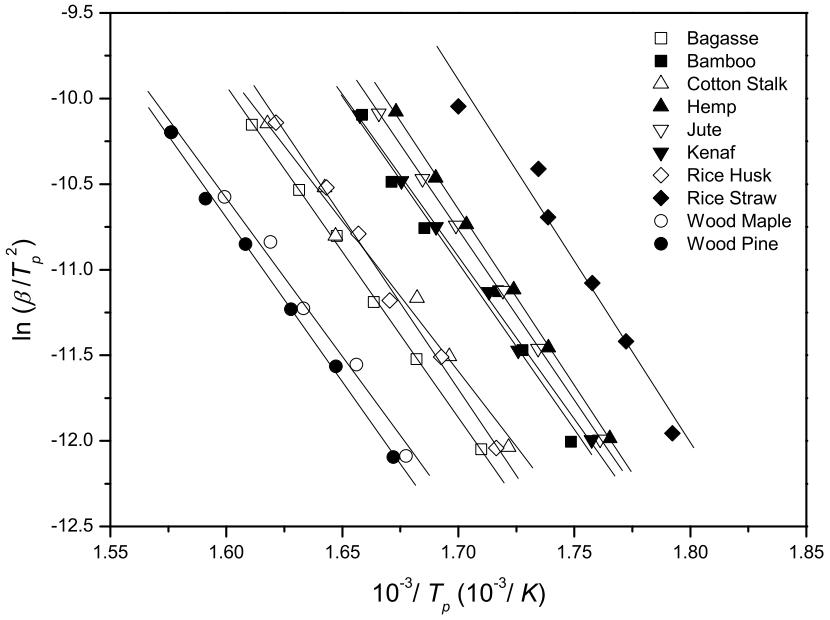

Fig. 2.5 Linear plots of $\ln(\beta/T_p^2)$ versus $1/T_p$ for various fibers in Kissinger methods.

kinetics analysis methods are *complementary* rather than *competitive*. Therefore, an appropriate apparent activation energy range should be obtained by combining all observations in Table 2.4 and Table 2.5 as well as Fig. 2.4 and, consequently, a general activation energy range of 160-170 kJ / mol is suggested for most fibers for needs of polymer composites processing. This general range might offer a comparatively narrower range of activation energy for understandingfiber decomposition for polymer composite with respect to previous reported values, e.g., 60-170 kJ / mol for wood decomposition (Di Blasi 2002). This general range might also help simplify the complexity of modeling decomposition behavior of natural fibers, e.g. modeling the global reactions of wood decomposition by superposing typical activation energies of 105-111, 195-213 and 35-65 kJ / mol for hemicelluloses, cellulose and lignin, respectively (Gronli et al. 2002). In deed, even though the thermal decomposition of main components in natural fibers might follow certain thermal decomposition reaction rules with certain activation energies, it might be difficult to distinguish and model the thermal decomposition behavior of each specific component in a natural fiber due to the complexity of growth of natural fibers which causes variance in component content, crystal structure or chemical composition from one species to another.

It should be noted that the activation energy alone cannot provide an integral prediction or modeling for thermal decomposition process. A satisfied degradation model must contain at least the whole set of activation energy, pre-exponential factor and reaction model (i.e., kinetic triplet) (Maciejewski 2000). As the energy barrier, the activation energy itself may provide the information of critical energy needed to start a reaction. The decomposition activation energy range obtained in this study can help understand thermal decomposition stability of natural fibers used in natural fiber reinforced polymer composite industry. From a modeling perspective a

narrow range of activation energy can help calculate other parameters of thermal kinetics, e.g., Malek approach.

2.5 CONCLUSIONS

The dynamic TG analysis was used to investigate the thermal decomposition process of ten kinds of natural fibers commonly used in polymer composite industry. These natural fibers included wood, bamboo, agricultural residue and bast fibers. Model free methods including Kissinger, Friedman, Flynn-Wall-Ozawa and modified Coats-Redfern methods were used to determine the apparent activation energy of these fibers.

Thermal decomposition process of selected natural fibers had the similar TG and DTG curves as a result of being lignincellulosic material. The common thermal decomposition curves of fibers showed a distinct DTG peak (cellulose) and high-temperature "tails" (lignin). The low-temperature "shoulder" could be seen in some fiber decomposition curves. The characteristics of all selected natural fibers showed that main thermal decomposition fraction (around 60%) happened in a temperature range of around 100°C (i.e., 215-310±10°C in terms of extrapolated temperatures) for most natural fibers. Weight loss fraction was probably the intrinsic property of natural fibers which was not affected by heating rate. The main decomposition period was overlapped with the processing temperatures of some thermoplastics. The result showed that a stable apparent activation energy range of 160-170 kJ / mol was suggested for the most of selected fiber throughout the polymer processing temperature range. The activation energy values allow developing a simplified approach to understand the thermal decomposition behavior of natural fibers in relation to polymer composite processing.

2.6 REFERENCES

Alvarez, V. A. and A. Vazquez (2004). "Thermal degradation of cellulose derivatives/starch blends and sisal fibre biocomposites." *Polymer Degradation and Stability* 84(1): 13-21.

Antal, M. J. and G. Varhegyi (1995). "Cellulose pyrolysis kinetics - The current state knowledge." *Industrial & Engineering Chemistry Research* 34(3): 703-717.

Antal, M. J., G. Varhegyi, et al. (1998). "Cellulose pyrolysis kinetics: Revisited." *Industrial & Engineering Chemistry Research* 37(4): 1267-1275.

Bilbao, R., A. Millera, et al. (1989). "Thermal-decomposition of lignocellulosic materials - Influence of the chemical-composition." *Thermochimica Acta* 143: 149-159.

Bledzki, A. K. and J. Gassan (1999). "Composites reinforced with cellulose based fibres." *Progress in Polymer Science* 24(2): 221-274.

Bledzki, A. K., V. E. Sperber, et al. (2002). "Natural and wood fiber reinforcement in polymers." *Rapra Review Reports* 13: 1-144.

Bradbury, A. G. W., Y. Sakai, et al. (1979). "Kinetic model for pyrolysis of cellulose." *Journal of Applied Polymer Science* 23(11): 3271-3280.

Brown, A. L., D. C. Dayton, et al. (2001). "A study of cellulose pyrolysis chemistry and global kinetics at high heating rates." *Energy & Fuels* 15(5): 1286-1294.

Brown, M. E., M. Maciejewski, et al. (2000). "Computational aspects of kinetic analysis Part A: The ICTAC kinetics project-data, methods and results." *Thermochimica Acta* 355(1-2): 125-143.

Capart, R., L. Khezami, et al. (2004). "Assessment of various kinetic models for the pyrolysis of a microgranular cellulose." *Thermochimica Acta* 417(1): 79-89.

Chen, H. X., N. A. Liu, et al. (2006). "Two-step consecutive reaction model and kinetic parameters relevant to the decomposition of Chinese forest fuels." *Journal of Applied Polymer Science* 102(1): 571-576.

Di Blasi, C. (2002). "Modeling intra- and extra-particle processes of wood fast pyrolysis." *Aiche Journal* 48(10): 2386-2397.

Diebold, J. P. (1994). "A unified, global-model for the pyrolysis of cellulose." *Biomass & Bioenergy* 7(1-6): 75-85.

Flynn, J. H. and L. A. Wall (1966). "General treatment of thermogravimetry of polymers." *Journal of Research of the National Bureau of Standards Section a-Physics and Chemistry A* 70(6): 487-&.

Friedman, H. L. (1964). "Kinetics of thermal degradation of char-forming plastics from thermogravimetry . Application to phenolic plastic." *Journal of Polymer Science Part C-Polymer Symposium* (6PC): 183-&.

Gronli, M. G., G. Varhegyi, et al. (2002). "Thermogravimetric analysis and devolatilization kinetics of wood." *Industrial & Engineering Chemistry Research* 41(17): 4201-4208.

Higuchi, T. (1957). "Biochemical studies of lignin formation .3." *Physiologia Plantarum* 10(4): 633-648.

Jackson, M. G. (1977). "Review article: the alkali treatment of straws." *Animal Feed Science and Technology* 2: 105-130.

Jakab, E., O. Faix, et al. (1995). "Thermogravimetry mass-spectrometry study of 6 lignins within the scope of an international round-robin Test." *Journal of Analytical and Applied Pyrolysis* 35(2): 167-179.

Kissinger, H. E. (1956). "Variation of peak temperature with heating rate in differential thermal analysis." *Journal of Research of the National Bureau of Standards* 57(4): 217-221.

Koufopanos, C. A., G. Maschio, et al. (1989). "Kinetic modeling of the pyrolysis of biomass and biomass components." *Canadian Journal of Chemical Engineering* 67(1): 75-84.

Liu, N. A. and W. C. Fan (1998). "Modelling the thermal decompositions of wood and leaves under a nitrogen atmosphere." *Fire and Materials* 22(3): 103-108.

Lu, J. Z., Q. L. Wu, et al. (2006). "The influences of fiber feature and polymer melt index on mechanical properties of sugarcane fiber/polymer composites." *Journal of Applied Polymer Science* 102(6): 5607-5619.

Maciejewski, M. (2000). "Computational aspects of kinetic analysis. Part B: The ICTAC Kinetics Project - the decomposition kinetics of calcium carbonate revisited, or some tips on survival in the kinetic minefield." *Thermochimica Acta* 355(1-2): 145-154.

Malek, J. (1992). "The kinetic analysis of nonisothermal data." *Thermochimica Acta* 200: 257-269.

Marti-Ferrer, F., F. Vilaplana, et al. (2006). "Flour rice husk as filler in block copolymer polypropylene: Effect of different coupling agents." *Journal of Applied Polymer Science* 99(4): 1823-1831.

Milosavljevic, I. and E. M. Suuberg (1995). "Cellulose thermal-decomposition kinetics - global mass-loss kinetics." *Industrial & Engineering Chemistry Research* 34(4): 1081-1091.

Mohan, D., C. U. Pittman, et al. (2006). "Pyrolysis of wood/biomass for bio-oil: A critical review." *Energy & Fuels* 20(3): 848-889.

Mohanty, A. K., M. Misra, et al. (2000). "Biofibres, biodegradable polymers and biocomposites: An overview." *Macromolecular Materials and Engineering* 276(3-4): 1-24.

Nada, A. M. A., N. A. El-Wakil, et al. (2006). "Differential adsorption of heavy metal ions by cotton stalk cation-exchangers containing multiple functional groups." *Journal of Applied Polymer Science* 101(6): 4124-4132.

Nada, A. M. A. and M. L. Hassan (2000). "Thermal behavior of cellulose and some cellulose derivatives." *Polymer Degradation and Stability* 67(1): 111-115.

Orfao, J. J. M., F. J. A. Antunes, et al. (1999). "Pyrolysis kinetics of lignocellulosic materials - three independent reactions model." *Fuel* 78(3): 349-358.

Ouajai, S. and R. A. Shanks (2005). "Composition, structure and thermal degradation of hemp cellulose after chemical treatments." *Polymer Degradation and Stability* 89(2): 327-335.

Ozawa, T. (1965). "A new method of analyzing thermogravimetric data." *Bulletin of the Chemical Society of Japan* 38(11): 1881-&.

Saheb, D. N. and J. P. Jog (1999). "Natural fiber polymer composites: A review." *Advances in Polymer Technology* 18(4): 351-363.

Sundstøl, F. (1984). "Straw and other fibrous by-products as feed." Amsterdam, New York: Elsevier.

Varhegyi, G., M. J. Antal, et al. (1989). "Kinetics of the thermal-decomposition of cellulose, hemicellulose, and sugar-cane bagasse." *Energy & Fuels* 3(3): 329-335.

Wollerdorfer, M. and H. Bader (1998). "Influence of natural fibres on the mechanical properties of biodegradable polymers." *Industrial Crops and Products* 8(2): 105-112.

Yang, Y. B., C. Ryu, et al. (2005). "Effect of fuel properties on biomass combustion. Part II. Modelling approach - identification of the controlling factors." *Fuel* 84(16): 2116-2130.

CHAPTER 3 THERMAL DECOMPOSITION KINETICS OF NATURAL FIBERS: KINETIC MODELING WITH DYNAMIC THERMOGRAVIMETRIC ANALYSIS

3.1 INTRODUCTION

Natural fiber fillers from agricultural residues and forest products processing are subjected to thermal degradation during polymer composite processing (Bledzki and Gassan 1999; Mohanty et al. 2000). It is therefore of practical significance to understand and model the decomposition process of the fibers. The model parameters obtained will help estimate the influence of the fiber decomposition on composite properties. Unfortunately, there is still a lack of research on suitable models for such a process as well as the model parameters for various fibers.

Thermal decomposition process and activation energy values of ten common natural fibers were investigated in the study presented in Chapter 2. It was found that thermal decomposition process of selected natural fibers had the similar TG and DTG curves as a result of being lignincellulosic material. The common thermal decomposition curves of fibers showed a distinct DTG peak (cellulose) and high-temperature "tails" (lignin). Also, the low-temperature "shoulder" can be seen in some fiber decomposition curves. The characteristics of all selected natural fibers showed that main thermal decomposition fraction (around 60%) happened in a temperature range of around 100°C (i.e., 215-310±10°C in terms of extrapolated temperatures) for most natural fibers. The calculation result from isoconversional methods showed that a stable apparent activation energy range of 160-170 kJ/mol was suggested for the most of selected fiber throughout the polymer processing temperature range. The objective of the study described in this chapter was to develop the modeling technique for the thermal decomposition process of the fibers. In particular, the model and related kinetic parameters were developed by employing a

comparatively reliable method (Malek 1992; 2000; Malek et al. 2001). Reaction mechanism and parameters of thermal decomposition process of natural fibers were described in details.

3.2 THEORETICAL APPROACH

The kinetics of solid-state process is generally complicated (Antal et al. 1998; Malek et al. 2001; Varhegyi et al. 1997). A method proposed by Málek, Šesták, and co-workers allows fairly reliable kinetic analysis and interpretation of non-isothermal TG-DTG data. This method has been described thoroughly in the cited literature (Malek 1992; Malek et al. 2001). A brief outline is shown below for consistence. Readers can refer to the original papers for details.

The fundamental expressions of analytical methods to calculate thermal decomposition kinetic parameters based on isothermal and/or non-isothermal TGA studies are generally described as:

$$\frac{d\alpha}{dt} = Ae^{-x} f(\alpha) \tag{3.1}$$

$$\frac{d\alpha}{dT} = \left(\frac{A}{\beta}\right) e^{-x} f(\alpha) \tag{3.2}$$

where α, t, T, A, β and x are conversion rate (%), time (s), absolute temperature (K), pre-exponential factor (s^{-1}), heating rate (°C/min) and reduced apparent activation energy $(x = E_a / RT)$, respectively. E_a and R are apparent activation energy (kJ / mol) and gas constant (8.314 $J / K \cdot mol$). The approach used to find a reliable and fairly accurate E_a of thermal degradation reaction is described in Section 2.2. Function $f(\alpha)$ is an analytical expression describing the kinetic model of a reaction, which depends on the actual reaction mechanism. The most frequently used $f(\alpha)$ functions with their symbols are summarized in Table 3.1.

Table 3.1 A summary of basic thermal kinetic models

Models	Symbol	$f(\alpha)$
Johnson-Mehl-Avrami	$JMA(n)$	$n(1-\alpha)[-\ln(1-\alpha)]^{1-1/n}$
Reaction order law	$RO(n)$	$(1-\alpha)^n$
Autocatalytic (Šesták-Berggren)	$SB(m,n)$	$(1-\alpha)^n \alpha^m$
2D-diffusion	D2	$-1/\ln(1-\alpha)$
Jander eqn.	D3	$3/2(1-\alpha)^{2/3}/[1-(1-\alpha)^{2/3}]$
Ginstling-Brounshtein	D4	$3/2[(1-\alpha)^{-1/3}-1]$
Prout-Tompkins	PT	$\alpha(1-\alpha)$

By integration of Eq. (3.2) in non-isothermal conditions, the following equation is obtained:

$$g(\alpha) = \int_0^{\alpha} \frac{1}{f(\alpha)} d\alpha = \int_0^{T} \frac{A}{\beta} e^{-x} dT = Ae^{-x}\left[\frac{T}{\beta}\pi(x)\right] \tag{3.3}$$

where $\pi(x)$ is an approximation of the temperature integral, which has various expressions in the literature (Malek et al. 2001). The rational expression performed by Senum and Yang (Senum and Yang 1977) gives sufficiently accurate approximation:

$$\pi(x) = \frac{x^3 + 18x^2 + 88x + 96}{x^4 + 20x^3 + 120x^2 + 240x + 120} \tag{3.4}$$

The combination of Eqs. (3.2) and (3.3) leads to one of two new functions, $z(\alpha)$, in non-isothermal conditions:

$$z(\alpha) = \left(\frac{d\alpha}{dt}\right)\left[\pi(x)\frac{T}{\beta}\right] = f(\alpha)g(\alpha) \tag{3.5}$$

Recently, it was found that the term $[\pi(x)T/\beta]$ in Eq. (3.5) is proportional to T^2. Therefore, a simplified expression for $z(\alpha)$ function is approximated as:

$$z(\alpha) \approx \left(\frac{d\alpha}{dt}\right) T^2 \tag{3.6}$$

One can easily transform experimental data to the $z(\alpha)$ function by using Eq. (3.6) and then normalize $z(\alpha)$ within the (0, 1) interval. Obviously, this can be done without the knowledge of any kinetic parameter in non-isothermal conditions. Another new function, $y(\alpha)$, is defined as:

$$y(\alpha) = \left(\frac{d\alpha}{dt}\right) e^x = Af(\alpha) \tag{3.7}$$

Therefore, the shape of the $f(\alpha)$ function can be obtained from the $y(\alpha)$ function even though the reaction rate, $d\alpha / dt$, is not directly proportional to $f(\alpha)$. The $y(\alpha)$ function is also usually normalized within (0, 1) interval. Two important parameters α_M and α_p^∞, at which the functions $y(\alpha)$ and $z(\alpha)$ have a maximum, respectively, are normally calculated by mathematic software. Then the function $f(\alpha)$ is determined through the schematic diagram introduced by Málek (1992; 2000).

1. If the parameter $\alpha_M = 0$, then $y(\alpha)$ can be convex, linear or concave. Convex dependence corresponds to $RO(n < 1)$ model, linear dependence to the $JMA(m = 1)$ or $RO(n = 1)$ model, and concave dependence corresponds to the $JMA(m < 1)$, D2, D3, D4 or $RO(n > 1)$ model depending on the value of α_p^∞.

2. If the parameter $\alpha_M \in (0, \alpha_p)$ (α_p is the fractional extent of reaction at the maximum $d\alpha / dt$), then it corresponds to the $SB(m, n)$ or $JMA(m > 1)$ depending on the value of α_M.

As discussed by Málek himself, the activation energy E_a is vital for the determination of function $y(\alpha)$ (Malek 1992). Several recommended "model-free" methods (isoconversional method) are presented in Chapter 2 to calculate the decomposition activation energy values of

selected fibers (Yao et al. 2008). Those E_a values were then used to calculate function $y(\alpha)$ and $z(\alpha)$ in this section. The experimental data, α, T and $d\alpha/dt$, related to calculation, were obtained from TG-DTG curves directly.

3.3 EXPERIMENTAL

The same ten natural fibers used in studies described in Section 2.2 were chosen for this investigation. The sample preparation and TG experiment procedure for the ten natural fibers were the same as those reported in Chapter 2. Readers can refer to Chapter 2 for the details. Universal Analysis 2000 software from TA Instruments Inc. and MS Excel were used for general calculation of parameters for the Málek Method. MATLAB 7.1 software was used to fit the curves of $[y(\alpha)-\alpha]$ and $[z(\alpha)-\alpha]$ in order to obtain the accurate values of α_M and α_p^∞.

3.4 RESULTS AND DISCUSSION

3.4.1 Determination of Kinetics Model and Parameters

The thermogravimetric curves of ten selected fibers in non-isothermal conditions are shown in Section 2.4 along with the activation energy values. The E_a value of most fibers was quite stable in a conversion range of 0.1-0.6 according to three isoconversional methods. According to Table 2.4, the variation of E_a in this range is within ca. 3% for every single selected fiber. Thus, the activation energy values obtained can be employed to calculate $y(\alpha)$ and $z(\alpha)$ function. As shown in Table 3.2, they were determined by averaging values from three isoconversional methods.

The dependence of function $y(\alpha)$ on conversion rate α for various fibers is shown in Fig. 3.1. Each individual function $y(\alpha)$ is concave and has a clear maximum α_M at $\alpha = 0$. This indicates that neither $JMA(n>1)$ nor $SB(m,n)$ will be the best kinetic model for thermal decomposition process of the selected fibers. Fig. 3.2 shows that each individual $z(\alpha)$ curve

Table 3.2 The kinetic parameters obtained by non-linear regression of non-isothermal data

Fiber	$E\ \ (kJ/mol)$	n	$\ln(A)\ \ (\ln s^{-1})$	α_M	α_p	α_p^{∞}	$fit(\%)$
Bagasse	168.6 (6.3)	3.25 (.11)	38.14(.08)	0	0.673 (.006)	0.685 (.007)	4.67 (.08)
Bamboo	160.9 (3.2)	3.85 (.07)	37.45 (.23)	0	0.570 (.015)	0.589 (.024)	3.57 (.04)
CottonStalk	171.8 (4.2)	3.77 (.05)	39.15 (.07)	0	0.611 (.022)	0.620 (.016)	4.32 (.13)
Hemp	178.6 (6.6)	3.18 (.26)	40.57 (.12)	0	0.508 (.014)	0.519 (.013)	3.73 (.18)
Jute	183.3 (9.0)	3.75 (.26)	42.17 (.10)	0	0.590 (.015)	0.595 (.017)	5.00 (.02)
Kenaf	169.9 (2.1)	3.23 (.17)	38.76 (.07)	0	0.550 (.012)	0.560 (.017)	3.60 (.07)
RiceHusk	165.4 (2.9)	4.03 (.19)	37.78 (.10)	0	0.600 (.007)	0.609 (.004)	3.64 (.07)
WoodMaple	153.3 (4.8)	3.04 (.08)	34.47 (.10)	0	0.694 (.003)	0.700 (.005)	4.79 (.05)
WoodPine	159.6 (3.9)	3.14 (.08)	35.65 (.05)	0	0.690 (.008)	0.697 (.008)	4.35 (.18)
RiceStraw	195.5 (2.5)	5.81 (.17)	46.57 (.12)	0	0.528 (.015)	0.543 (.017)	3.46 (.09)
Average	167.9 (9.4)	3.47 (0.37)	38.24 (2.34)	0	0.610 (.065)	0.619 (.063)	4.19 (.56)

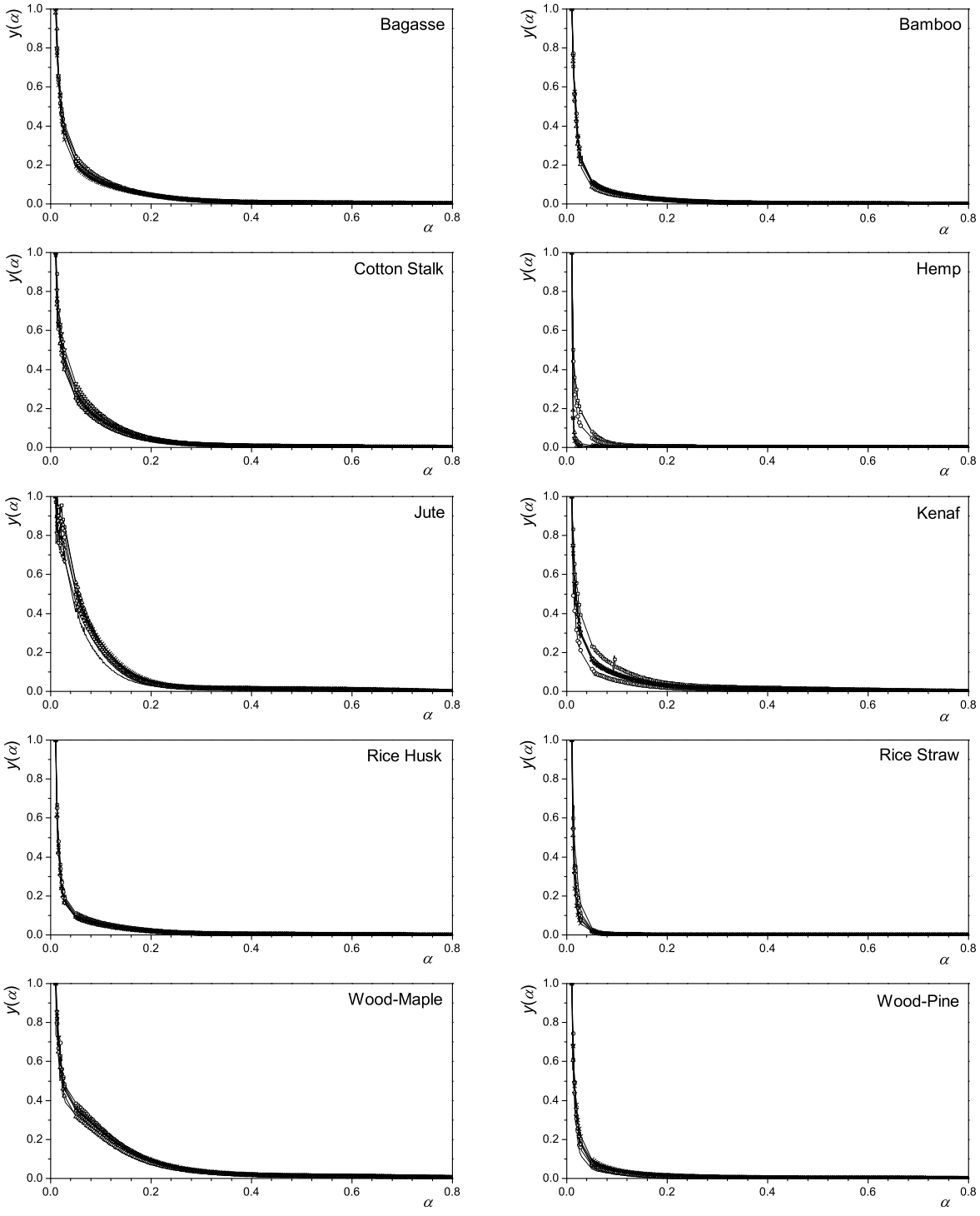

Fig. 3.1 Normalized $y(\alpha)$ function corresponding to fiber thermal decomposition kinetic data. The heating rates are shown in following symbols: 2°C/min (solid line); 3.5°C/min (-□-); 5°C/min (-○-); 7.5°C/min (-Δ-); 10°C/min (-∇-); 15°C/min (-×-).

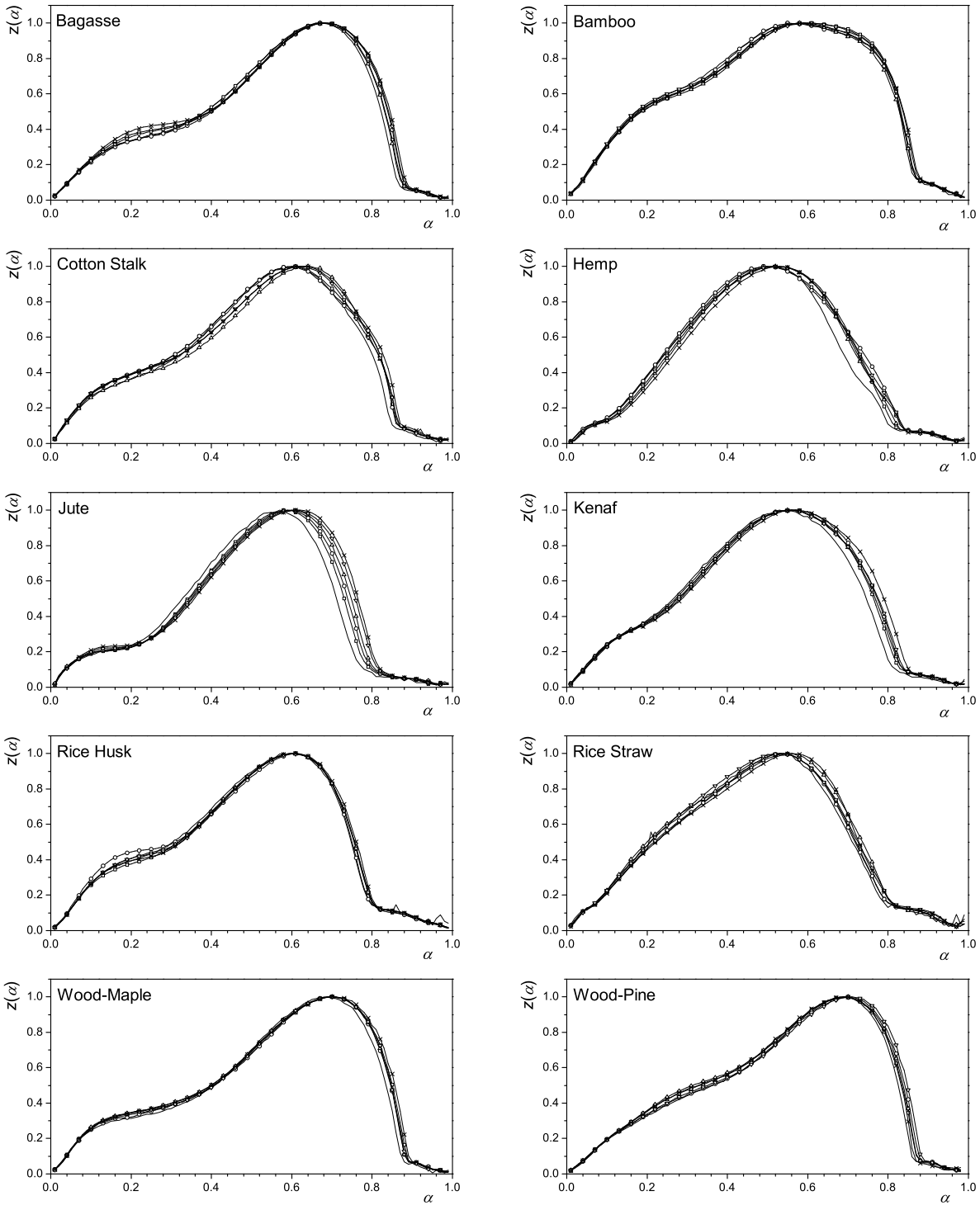

Fig. 3.2 Normalized $z(\alpha)$ function corresponding to fiber thermal decomposition kinetic data. The heating rates are shown in following symbols: 2°C/min (solid line); 3.5°C/min (-□-); 5°C/min (-○-); 7.5°C/min (-Δ-); 10°C/min (-▽-); 15°C/min (-×-).

from a certain fiber degradation process is practically invariant with respect to temperature. Each $z(\alpha)$ curve also exhibits a clear maximum which is consistent with the fact that $z(\alpha)$ function has a maximum at α_p^∞ for all kinetic models (Malek et al. 2001). MATLAB7.1 software was then carefully operated to fit each single $[z(\alpha)-\alpha]$ curve in order to obtain the accurate values of α_p^∞. During our practical fitting experience we can expect that the five-term polynomial fitting was accurate enough with acceptable R-square (normally >0.99). The fitting equations at various heating rates have general forms as described below:

$$y(\alpha), or, z(\alpha) = B_0 + B_1\alpha^1 + B_2\alpha^2 + B_3\alpha^3 + B_4\alpha^4 + B_5\alpha^5 \qquad (3.8)$$

where B_i (i = 0, 1, …, 5) is the coefficient of the polynomial. The values of α_p^∞ at various heating rates of each fiber can be further obtained by derivation of the above equations. However, this fitting process and related B_i values were omitted. The parameter α_p was easily obtained from the peak of $[(d\alpha/dt)-\alpha]$ curve plotted from experimental data.

All critical values are summarized in Table 3.2. It is clearly shown from α_M values (i.e., zero) and $y(\alpha)$ function shape (i.e., concave), as well as α_p^∞ values (i.e., not equal to 0.632, 0.704, 0.776 or 0.834), that the thermal degradation kinetic model of seven fibers (bagasse, bamboo, cotton stalk, hemp, jute, kenaf and rice husk fiber) can be described using $RO(n>1)$ model. The remaining two wood fibers, maple and pine, are possibly described as D3 model because their α_p^∞ values are close to 0.704. It is possible that $RO(n>1)$ model can also describe their thermal degradation processes since their α_p values are lower than their α_p^∞ values and consequently much lower than 0.704. This consideration is further discussed in Section 3.4.4. If the kinetic model is known, the equation for non-isothermal $\alpha(T)$ curve can be predicted from Eq. (3.3) as:

$$\alpha(T) = 1 - \left[1 - T\left(\frac{\pi(x)}{\beta} \right)(1-n)Ae^{-x} \right]^{1/(1-n)} \tag{3.9}$$

here, the $f(\alpha)$ function for $RO(n>1)$ model is employed, i.e.,

$$f(\alpha) = (1-\alpha)^n \tag{3.10}$$

and consequently,

$$g(\alpha) = \int_0^{\alpha} \frac{1}{f(\alpha)} d\alpha = \frac{1-(1-\alpha)^{1-n}}{1-n} \tag{3.11}$$

The temperature dependence of the reduced activation energy $(x = E_a / RT)$ can be calculated from average value of apparent activation energy obtained by isoconversional analysis. The key kinetic parameters A and n can be obtained by non-linear regression of experimental data using MATLAB 7.1 software because each part of an entire kinetic equation has been clearly defined. The parameter means are summarized in Table 3.2 along with standard deviations which were calculated from six different heating rates.

Comparison of experimental data (symbols) and prediction $\alpha(T)$ of $RO(n>1)$ (lines) for all fibers are shown in Fig. 3.3. These $\alpha(T)$ curves were calculated using Eq. (3.9) for the kinetic parameters shown in Table 3.2. There is quite good agreement between experimental data and prediction curves even though some discrepancies are observed at both very low and very high temperature (or, α) ranges. Those discrepancies were caused by the variability of activation energy and the strong dependence of the Málek method on activation energy values. However, if a good global agreement in the entire reaction process is reached, one can expect a reasonable model. Therefore, the model obtained must be evaluated to quantify the goodness of

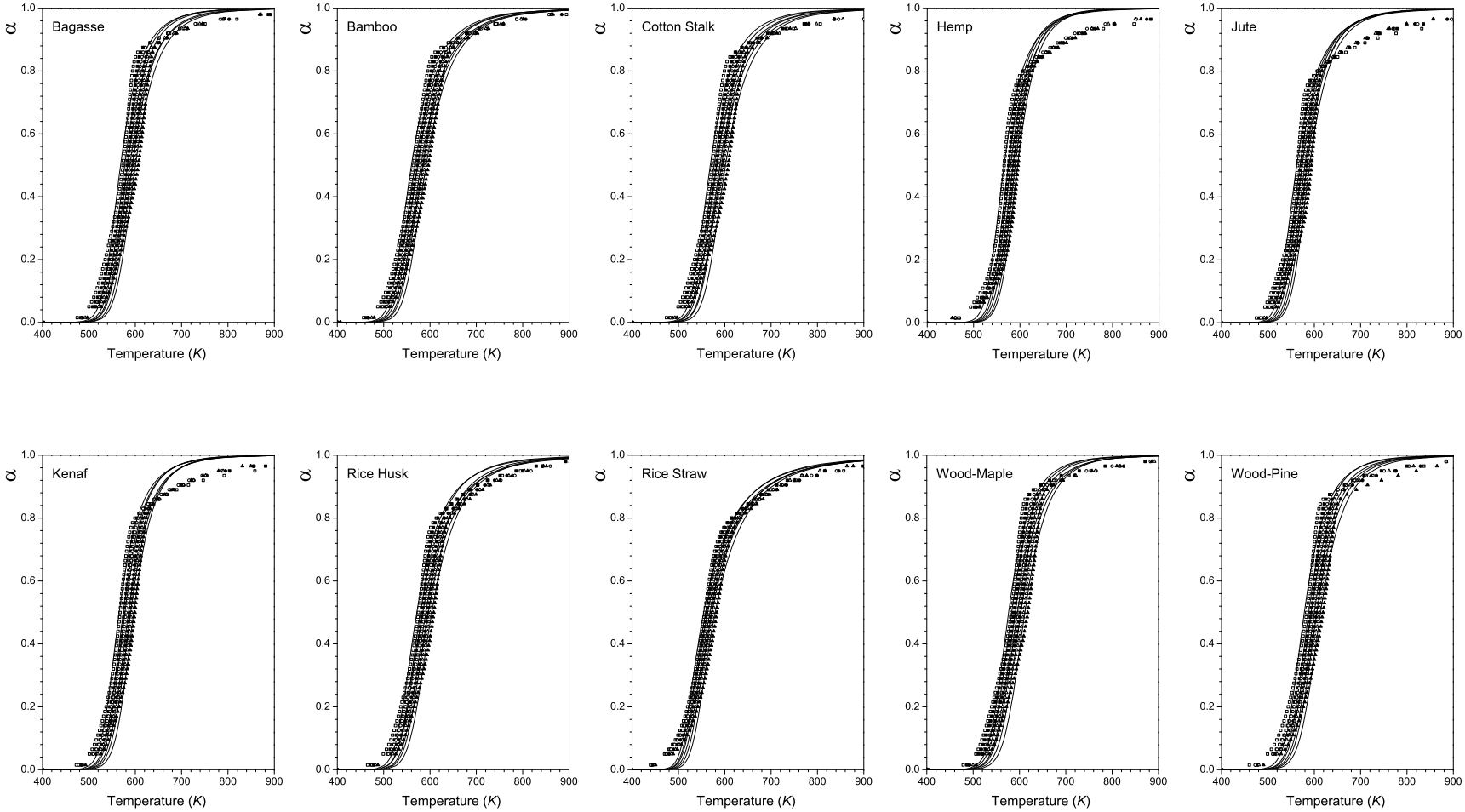

Fig. 3.3 Non-isothermal TG curves for select fibers measured at different heating rates: 2°C/min (□); 3.5°C/min (■); 5°C/min (○); 7.5°C/min (●); 10°C/min (Δ); 15°C/min (▲). Solid lines were calculated using Eq. (3.9) for the kinetic parameters shown in Table 3.2.

fit (GOF). Moreover, latent force-fitting caused by kinetic compensation effect (KCE) should also be evaluated (Brown et al. 2000; Vyazovkin 2000).

3.4.2 Evaluation of the Kinetic Parameters

GOF of model is evaluated by the method of least squares (LSQ). The sum S of squared error of all picked points is defined as:

$$S = \sum_{1}^{N} (y_i^{obs} - y_i^{calc})^2 \tag{3.12}$$

where y^{obs} is the experimental data and y^{calc} is the corresponding point of the calculated functions, subscript i indicates the discrete values of a given y, and the parameter N is the number of the data used in the curve fitting. The fit between the observed and calculated values at the obtained parameters is given in percentage of the highest observed y value, $y_{\max}^{obs}$:

$$fit(\%) = 100\% \frac{\sqrt{S/N}}{y_{\max}^{obs}} \tag{3.13}$$

The method actually tests the error between observed and calculated values. Therefore, the output $fit(\%)$ is also referred as $deviation(\%)$ in some literatures (Varhegyi et al. 1989). The fitted result is shown in Table 3.2. The good agreement, indicated by values less than 5%, was observed for all fibers. Shown in parentheses, the very small, neglectable standard deviation of each fiber indicates the invariant GOF at different heating rates. It consequently implies the reliability of obtained kinetic parameter n and A as well as $f(\alpha)$. On the other hand, the error of final fitting was expected as low as 5%.

GOF is necessary, but not sufficient, for the evaluation of a thermal model because it cannot evaluate latent force-fitting caused by KCE. KCE is caused by the exponent format of Arrehnius equation and refers to the fact that the co-variability of parameter E and A makes experimental data fit several different models well with different $f(\alpha)$ (Koga 1994; Vyazovkin

1992; Vyazovkin and Wight 1998). It was reported that one might obtain extreme perfect fitting using F1 model on artificially produced A3 model curves (Perez-Maqueda et al. 2006). A new approach proposed by Perez-Maqueda etc. (2006) helps offer a reliable evaluation in this situation with focusing more on physical aspect of thermal model.

In this technique, through algebraic transformation, any function $f(\alpha)$ can be simplified as:

$$f(\alpha) = c(1-\alpha)^n \alpha^m \tag{3.14}$$

using three constants c, n and m from the empirical Šesták-Berggren equation:

$$f(\alpha) = (1-\alpha)^n \alpha^m \left[-\ln(1-\alpha)\right]^p \tag{3.15}$$

A logarithm transformation of Eq. (3.1) leads to the following equation for fitting experimental data:

$$\ln\left(\frac{d\alpha/dt}{f(\alpha)}\right) = \ln cA - \frac{E}{RT} \tag{3.16}$$

Plotting the left hand side of Eq. (3.16) with respect to the reciprocal of corresponding temperature, one can get a single straight line with slope $(-E_a/R)$ and the intercept $(\ln cA)$ if an appropriate function $f(\alpha)$ is chosen. It is worth noting that the key to this evaluation is to get a single straight line even using data from different heating rates. It was pointed out in the literature (Perez-Maqueda et al. 2006) that sometimes an inappropriate model can also lead to perfect straight lines, but those lines are parallel to each other instead of superposing on to one single curve.

Using this method, the linear relationship between $\ln[(d\alpha/dt)/f(\alpha)]$ and $1/T$ is plotted in Fig. 3.4 after inserting obtained $f(\alpha)$ functions and experimental $d\alpha/dt$ and $1/T$ data into Eq. (3.16). As shown in the figure, for each fiber sample, six scatter lines corresponding to data

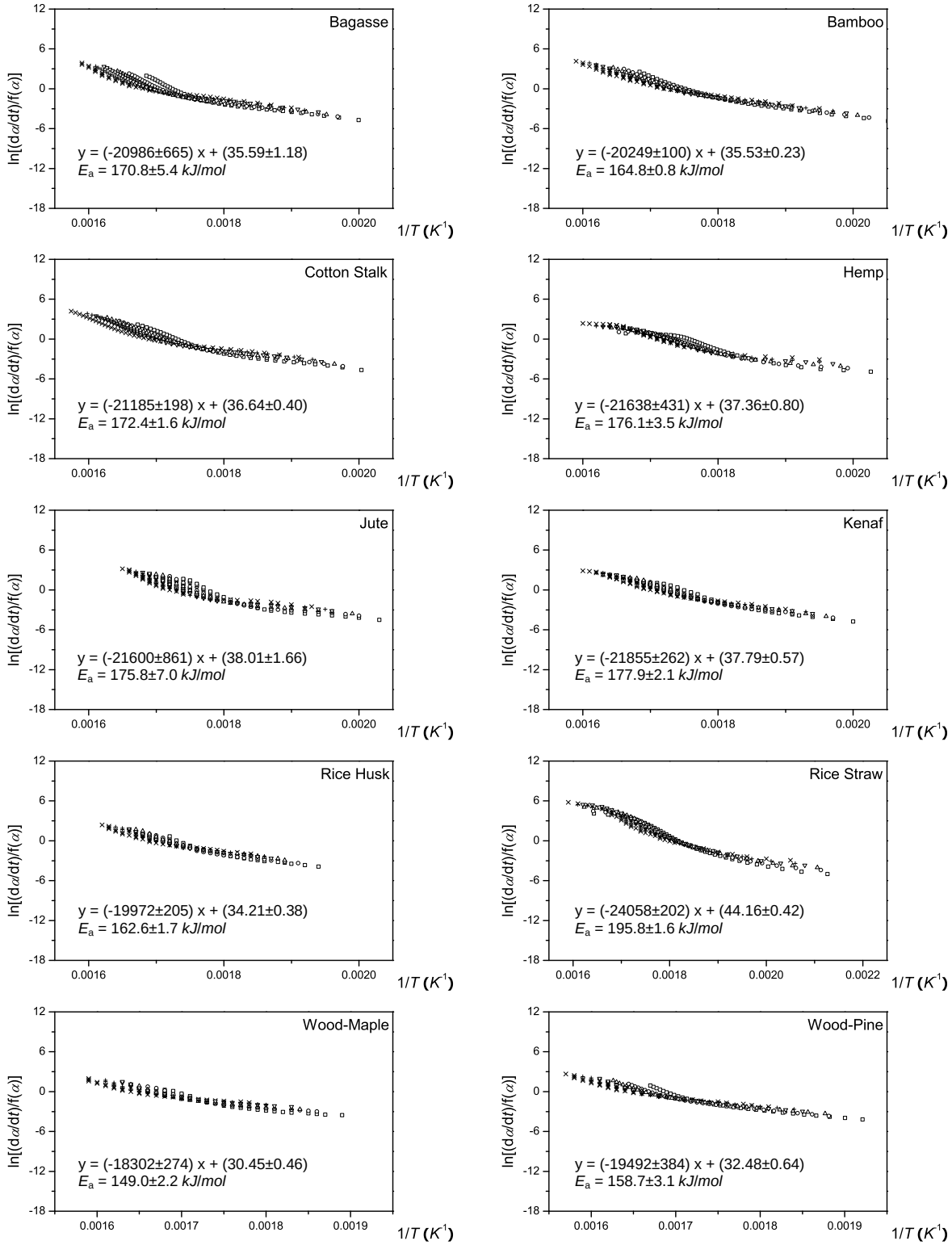

Fig. 3.4 Single linear relationship between $\ln(d\alpha/dt) - \ln f(\alpha)$ and $1/T$ for all fibers at six heating rates. The heating rates are shown in following symbols: 2°C/min (□); 3.5°C/min (○); 5°C/min (Δ); 7.5°C/min (∇); 10°C/min (+); 15°C/min (×).

from six different heating rates are overlapped with each other and yield a single straight line. The expression listed in each individual plot shows detailed slope and intercept. Here, the value followed by symbol "±" is the average value of six slopes while the value following "±" refers to standard deviation. Obviously, the superposition of six scatter lines is shown by a fairly small standard deviation (within 3% in most cases). The activation energy values listed in plots are calculated from the slope. They are quite comparable (error < 2%) with those shown in Table 3.2 except that in the cases of jute and kenaf fibers the error reaches around 5%. In conclusion, evaluation performed above shows that the model and relevant parameters obtained are appropriate for describing the degradation process of natural fibers.

3.4.3 Comparison of Kinetic Parameters of Different Fibers

Based on calculated parameters shown in Table 3.2, one can see a general trend of the degradation model for nine fibers (exclusive rice straw fiber which is specifically discussed in next Chapter). Degradation process has an activation energy range of 160-170 kJ/mol with an average of 168 kJ/mol; $f(\alpha)$ follows $RO(n) = (1-\alpha)^n$ model; parameter n has a range of 3-4 with an average of 3.5; while $\ln A$ is between 35 and 42 $\ln s^{-1}$ with an average of 38 $\ln s^{-1}$.

Based on these average values and specific parameters of individual fibers, overall $(\alpha - T)$ plots at a heating rate of 5 °C/min were obtained (Fig. 3.5). In this figure, the line with circles indicates the average degradation level of selected natural fibers which was plotted strictly using average values listed above, while nine solid lines corresponding to specific $(\alpha - T)$ curves of nine fibers (except rice straw fiber) give an interval. The predictive $(\alpha - T)$ curve of rice straw fiber (the focus of this dissertation) was specially marked with triangles in order to distinguish it with the others. Two arrows shown in the figure represent the positions, where potential deviation between real degradation and prediction might occur based on the observation in Fig. 3.3.

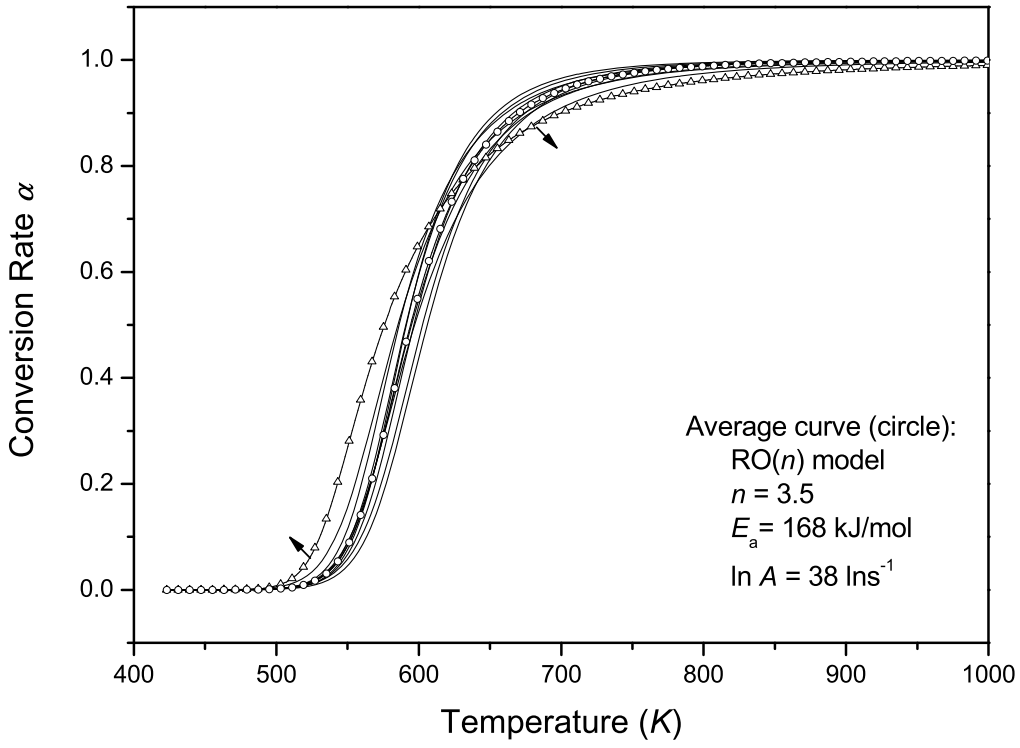

Fig. 3.5 Predictive $(\alpha - T)$ plot for thermal degradation process of natural fiber based on the modeling result of ten common fibers at a heating rate of 5 °C/min. Solid line: nine fibers exclusive rice straw fiber; line with triangle: rice straw fiber; and, line with circle: degradation curve calculated by average value shown in Table 3.2 with corresponding parameters. Arrows in the plots indicated the direction that the real degradation curve moves to.

As shown in Fig. 3.5, the interval is a fairly narrow one, which may indicate the similarity of natural fiber degradation process. This observation was first mentioned in Chapter 2, where a narrow range of activation energy for most of the natural fibers was seen. As the energy barrier, the activation energy itself may provide the information of critical energy needed to start a reaction. It implies the "difficulty" of starting a reaction. The similar activation energy values of various fibers indicated that critical energy of the decomposition reaction is similar among those fibers. However, only activation energy itself cannot be used to determine the "rate" of a

reaction. Once a reaction starts, the question of how fast the reaction is should be answered by the conversion function $f(\alpha)$ along with its parameters and pre-exponential factor A. Similar to the case of activation energy, close parameters n and A among various fibers offered a similar fiber degradation rate. The similarity of both "difficulty" and "rate" of fiber degradation reaction is associated with the similar elementary reactions of main components (cellulose, hemicelluloses, and lignin) of fibers. The elementary reaction is probably a melting, decrystallization or molecular-chain-related reaction, or the combination. Unfortunately, such elementary reaction is very complex and is still ambiguous so far.

The predictive TG curves can be obtained by some transitions. First, the adjusted conversion rate α_{WL} was introduced as:

$$\alpha_{WL}(T) = \alpha(T)(1 - residue) \tag{3.17}$$

The parameter α_{WL} actually reflects fractional weight loss. Therefore, secondly, the predictive weight percentage can be written as:

$$weight(\%) = 100\%[1 - \alpha_{WL}(T)] \tag{3.18}$$

Plotting the predictive weight percentages *vs.* temperatures led to the predictive TG curves. As shown in Fig. 3.6, the $[\alpha_{WL}(T) - T]$ and predictive TG curves at a heating rate of 5 °C/min for all fibers were obtained by inserting the residues shown in Table 2.3. The plot shown on the left hand side is predictive plot of adjusted conversion rate α_{WL} with respect to temperature, while the right hand plot shows the predictive TG curves for ten selected fibers. Arrows in the plots indicate the position where the deviation between model and experimental results exist. The direction of the arrow indicates the movement direction of the real degradation curve. Fig. 3.7 is plotted to validate the obtained predictive TG curves using bamboo, hemp, pine and rice straw fibers as examples. Also, a good agreement is obtained. Therefore, the kinetic

model obtained is valid for predicting weight percentage of fiber with respect to temperature during thermal degradation.

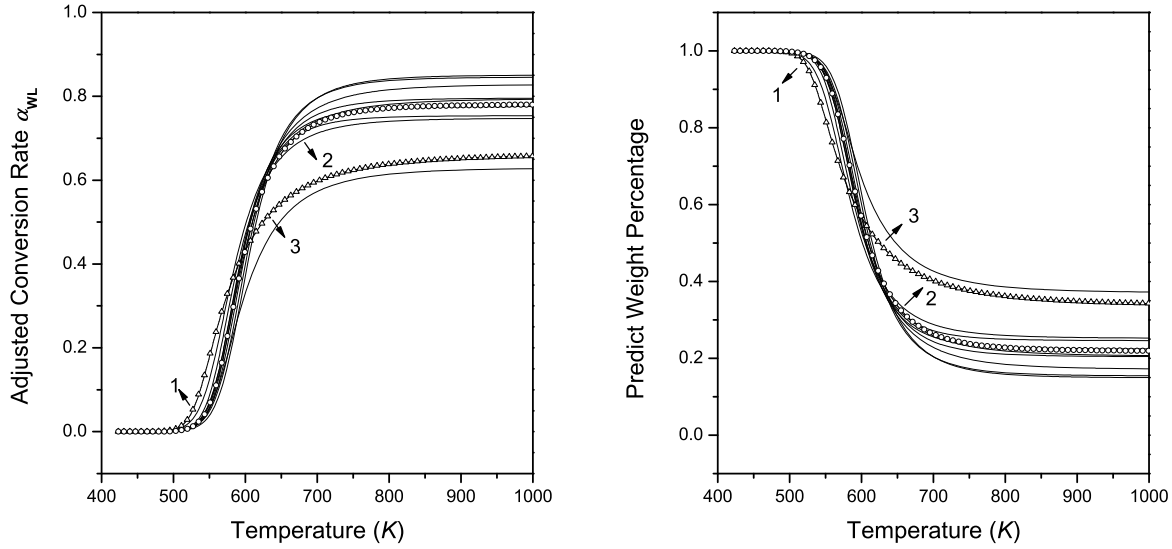

Fig. 3.6 Predictive plot of adjusted conversion rate α_{WL} (left) and weight percentage (right), respectively, with respect to temperature for ten selected fibers at heating rate of 5 °C/min. Solid line: nine fibers exclusive rice straw fiber; line with triangle: rice straw fiber; line with circle: degradation curve calculated by average value shown in Table 3.2 with corresponding parameters. Arrows indicated the direction that the real degradation curve moves to.

The degradation processes of various fibers can be modeled with close parameters, but fiber weight percentage curves (i.e., TG curves) are obviously different with each other (Fig. 2.1 and 3.6). It can be attributed to the different degradation residues of fibers. The residue is usually described as the first, tar or char generated during the degradation of fiber main components (Antal and Varhegyi 1995; Capart et al. 2004; Di Blasi 2008; Varhegyi et al. 1994) and the second, degradation products of minor components in fiber composition. However, it is still

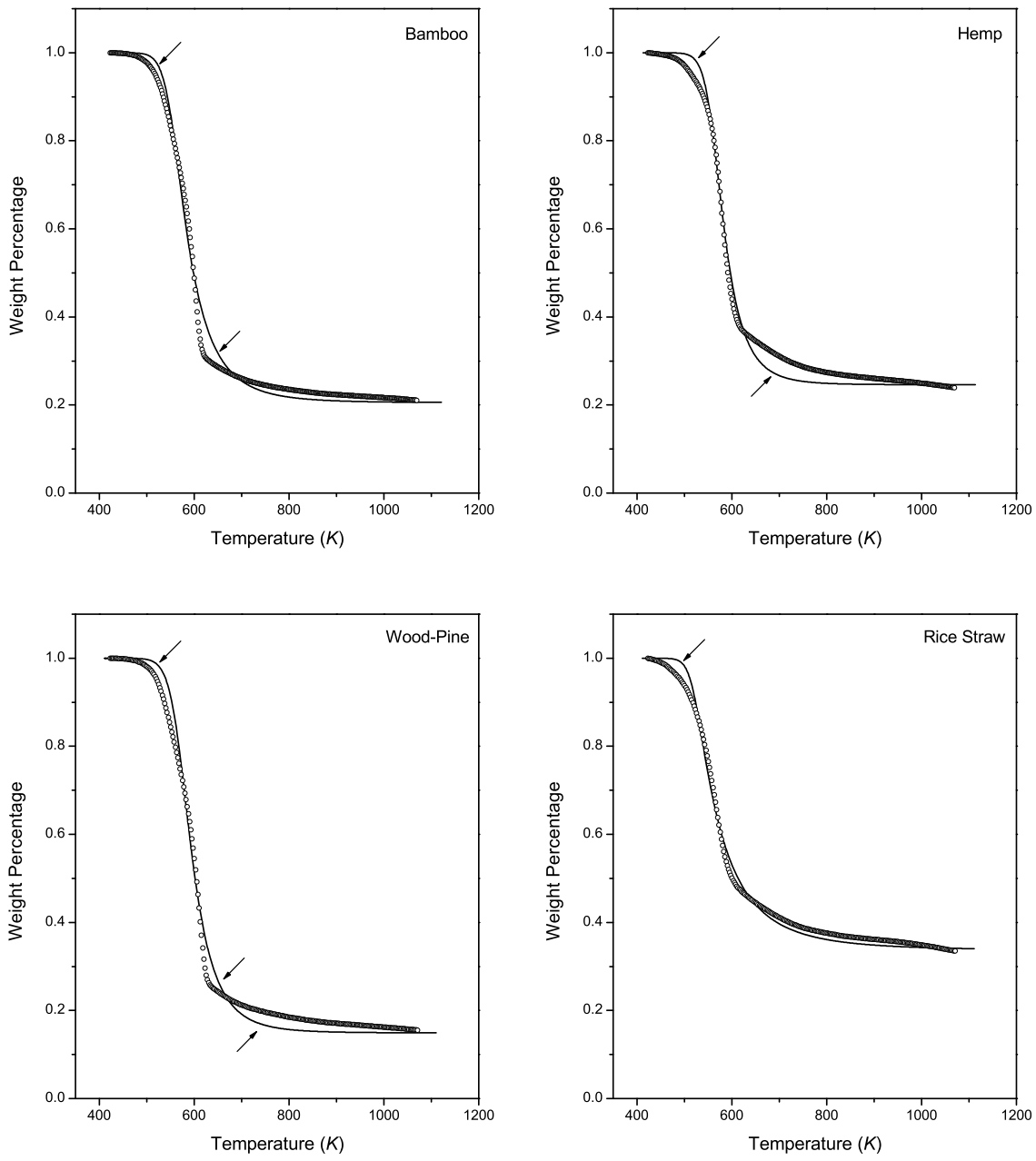

Fig. 3.7 The comparison of predictive and experimental TG curves using four fibers as examples. Circle: experimental curve; solid line: predictive curve. Arrows in the plots indicated the direction that the real degradation curve moves to.

ambiguous that when and how tar or char generate (Capart et al. 2004; Chen et al. 2006; Di Blasi 2008). Also, it is hard to clearly define the composition and structure of minor components of fibers (e.g., silicon in rice straw surface).

3.4.4 Discussions

3.4.4.1 Application of Málek Method on Fiber Decomposition Process

As mentioned in Section 3.4.1, two wood fibers (maple and pine) should possibly be described as D3 model because their α_p^∞ values are close to 0.704. However, the $RO(n>1)$ other than D3 model for the fibers was considered. In this case, the application of parameter α_p^∞ needs to be discussed. In the Málek method, the parameter α_p^∞ refers to the corresponding α value, at which the $z(\alpha)$ function has a maximum. According to this parameter, the model can be characterized and consequently parameter n can be calculated, if it is a $RO(n>1)$ model, based on the equation (Malek 1992; Malek et al. 2001; Montserrat et al. 1998).

$$\alpha_p^\infty = 1 - n^{1/(1-n)} \tag{3.19}$$

Using this equation, the parameter n can be calculated in an iterative manner. Therefore, $n \approx 0.63$ and $n \approx 0.64$ for maple and pine fiber respectively, can be easily obtained. However, these two values are obviously inappropriate due to failing to satisfy the condition $n > 1$ and model fitting. One will find that the parameter n of all fibers will not be possible to fit the parameter α_p^∞ and model fitting simultaneously if they are calculated using Eq.(3.19). The reason for the unsatisfactory result might be due to the existence of shoulder in fiber degradation DTG curve interpreted usually by the thermal degradation of hemicelluloses. As a result, the shoulder in DTG curves obviously brings shoulder to the $z(\alpha)$ curve (Fig. 3.2), while theoretically a standard reaction order law model (e.g., $RO(n>1)$) corresponding to the single degradation mechanism will only result in a smooth non-shoulder $z(\alpha)$ function curve (Fig. 3.8)

according to the combination of Eqs. (3.5), (3.10) and (3.11). Fig. 3.8 also shows the smooth non-shoulder global curves for $JMA(n)$ models (its calculation equation is not presented here). Since the model used assumes that only one pseudo-component with only one mechanism occurred during the whole degradation process, the discrepancies between theoretical and experimental $[z(\alpha)-\alpha]$ curves at the shoulder position is unavoidable. Therefore, in the case of fiber thermal degradation one cannot expect to get appropriate model parameter n if the calculation is only based on the theoretical Eq. (3.19).

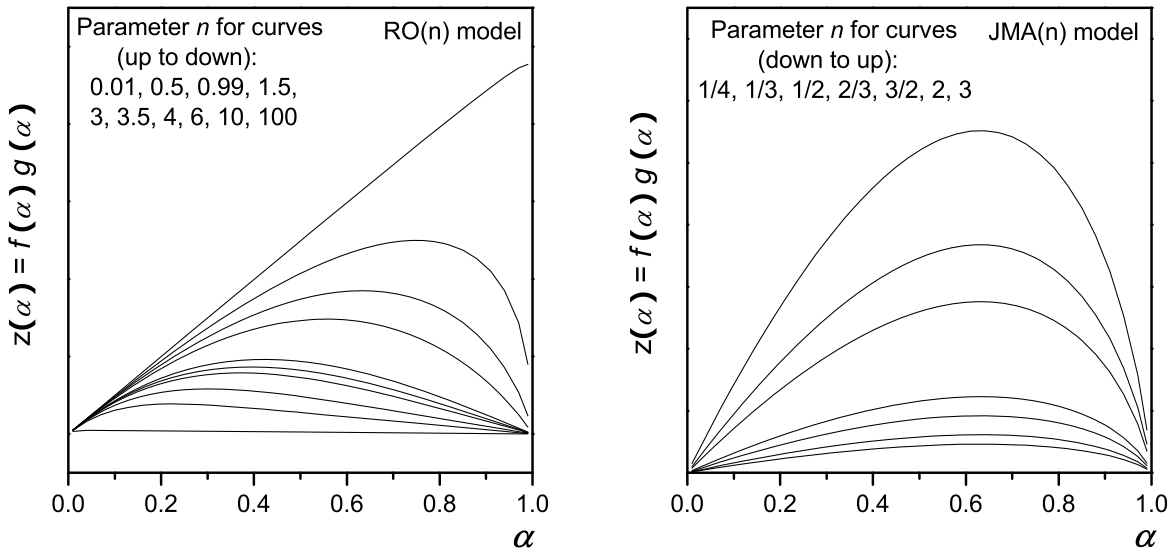

Fig. 3.8 The theoretic $z(\alpha)-\alpha$ curves calculated using $RO(n)$ and $JMA(n)$ model with different parameter n.

In order to avoid the discrepancies, a potential alternative is to perform mathematical peak separation to the DTG curve. Each peak should be calculated by isoconversional methods to obtain reliable activation energy value. Also $[y(\alpha)-\alpha]$ and $[z(\alpha)-\alpha]$ curves of each peak

should be determined to obtain appropriate $f(\alpha)$ and relevant parameters. However, this solution is sometimes self-contradictory because one has to determine what functions (e.g., Gauss, Weibull, Power or operator-defined functions) should be used before separating the peaks, while the determination is actually a pre-determination of the model and consequently force the data to fit the model. The parameter obtained later maybe meaningless because of the KCE. One can also perform peak separation directly to $[z(\alpha)-\alpha]$ plot. As shown in Fig. 3.9, separating the whole $[z(\alpha)-\alpha]$ curve into two peaks can lead to smooth non-shoulder curves, which is helpful for the evaluation of parameter n using Eq. (3.20). However, this operation usually needs to assume that two pseudo-reactions are independent and parallel because:

$$z(\alpha) = z_1(\alpha_1) + z_2(\alpha_2) = W_1 f_1(\alpha_1) g_1(\alpha_1) + W_2 f_2(\alpha_2) g_2(\alpha_2) \qquad (3.20)$$

where W_i refers to weighting function(%). Unfortunately, such assumption can be dogmatic.

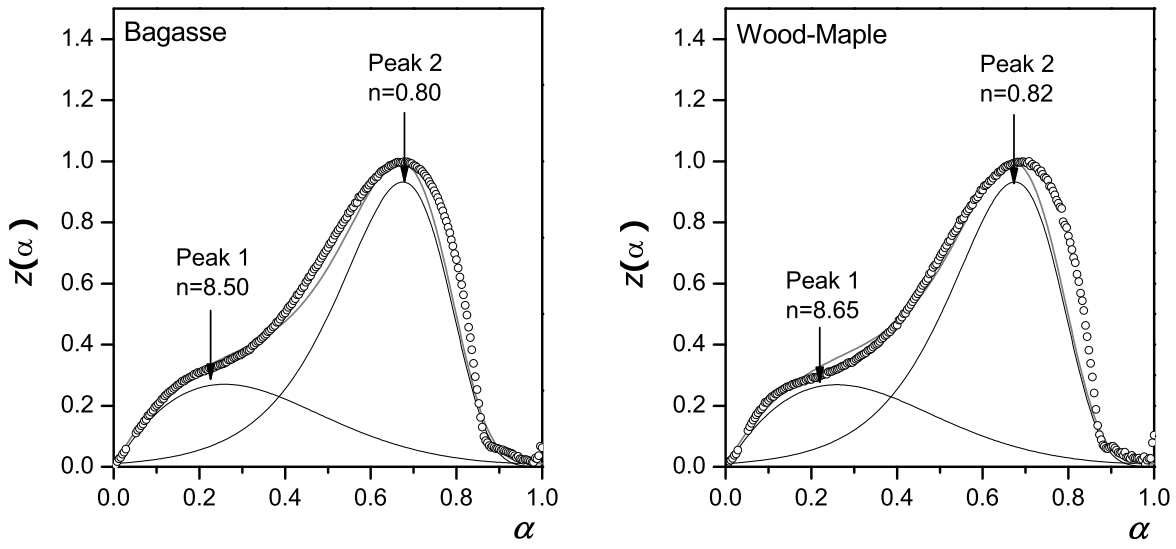

Fig. 3.9 Application of peaks separation (solid line) for experimental $z(\alpha)$ curve (circle) using bagasse and maple fibers as examples at heating rate of 2°C/min.

Peak separation, a mathematical operation, can be problematic not only to the application of Málek method but also to other fiber degradation modeling methods. First, additional errors maybe introduced during peak separation. The experience in peak separation operation shows that the fitting function (Gauss, Weibull, Power or operator-defined functions etc.), peak amount (2, 3 or more), initial peak position and its range, baseline determination, chi-square tolerance (depending on operator oneself) and weighting methods (weighting, statistical or non-weighting) etc. can all introduce errors into the final result. Consequently, the precision of the model maybe decreased. The second issue is the physical meaning. Many previous studies used three peaks to represent cellulose, hemicelluloses and lignin, and obtained some acceptable results (Branca and Di Blasi 2004; Calvo et al. 2004; Di Blasi 2008; Gronli et al. 2002). However, the pure hemicelluloses and lignin (usually represented by xylan) have not yet been separated individually due to the complexity of natural fiber composition. Therefore, controversy still occurred on physical meaning of the degradation process of these chemical components. This situation was discussed briefly in the Section 2.1. Therefore, peak separation maybe only useful in a mathematical sense so far. The last issue is that, in terms of practical utilization, the model should be as simple as possible based on reasonable assumption, simplification and evaluation. Since the operation of separating peaks may complicate the model, introduce new errors, and may not provide significantly improved interpretation on physical and chemical processes of degradation, peak separation was not performed in this case.

As mentioned in Section 3.4.1, Málek method depends on accurate activation energy value E. Therefore, applying the average value E_a within α of 0.2-0.8 (or 0.3-0.7) rather than the entire range was strongly recommended because most reactions, especially solid-state ones, are not stable at the beginning and ending periods. Different from solution reaction, solid-state reaction usually contains a diffusion process, the well-known mass and heat-transfer

phenomenon (Koga and Criado 1998a; b) at the beginning period. It generates temperature and partial pressure gradient. Consequently, it generates reaction gradient from the outer to the inner surface of the solid sample. This phenomenon is almost unavoidable even under strict sample size control (<1 mm). As a result, real activation energy values at this period are different from the ones at the middle period (0.1 or 0.2 to around 0.8). Thus, using apparent activation energy E_a to calculate the model parameters in this period will result in some discrepancies. In our case, the real conversion rates are correspondingly higher than model prediction shown in Fig. 3.3. About the ending period, the long tail was observed in most DTG curves of fiber degradation, which is normally interpreted by the long-term, low activation energy lignin decomposition process. The reactant that exists here does not likely include cellulose and hemicelluloses any more. Consequently, activation energy level changed sharply. Similar to the situation in the beginning period, using apparent activation energy E_a to model the decomposition process in this period will also cause some discrepancies. In our case, the real conversion rates are correspondingly lower than model prediction as indicated in Fig. 3.3. The fitting error obtained in this study was mostly caused by the mismatch in two periods mentioned above.

Despite some discrepancies, the Málek method is still recommended for global thermal degradation modeling of natural fiber due to providing fairly reasonable process and acceptable error limits. This method makes it possible to obtain the kinetic triplets step by step instead of simultaneously while the latter can cause KCE. It has also been successfully applied in several fields, including crystallization studies of various glasses and gels, phase-transition studies of calcium carbonate, and thermal decomposition of some epoxy resins and chemical complex. Moreover, this method can be applied in both non-isothermal and isothermal conditions (Montserrat et al. 1998; 1999).

3.4.4.2 Interpretation and Limitation of Obtained Model

The $RO(n>1)$ model obtained can be used to describe the degradation process of natural fiber with acceptable error limit. However, this does not indicate that the real degradation process completely follows the mechanism of reaction order law with $n>1$. Due to our assumption, the real degradation process of fiber was simplified to one reaction. However, it maybe composed of several parallel, consecutive or competitive reactions as mentioned in Section 2.1. Even if such an assumption can be made from a macroscopical perspective, it is necessary to avoid misleading readers in simply interpreting the mechanism as a reaction order law. Still, reaction order law is a possible choice. This is indicated by good fitting between experimental and simulative results from cellulose degradation research applying the first order model (Antal and Varhegyi 1995; Antal et al. 1998). As a conclusion, intensive research is strongly expected on linking interpretation of model with physical and chemical process of elementary reactions.

In order to obtain a reasonable and comparable kinetic model, the basic experimental conditions should be defined clearly and executed strictly during the entire experiment. These conditions are normally classified, but not limited to, as below:

(1) heating profile, e.g., isothermal, linear, stepped, modulated, or sample-controlled, etc.;
(2) heating or calculation range, e.g., low or high temperature range employed in isothermal analysis, and initial and final temperature used for calculation in non-isothermal analysis;
(3) heating rate, e.g., slow, rapid, or flash rate;
(4) atmosphere, e.g., inert, air or oxygen;
(5) sample loading rate, e.g., small (<1 mg, considered no mass and heat transfer phenomenon), medium (1-15 mg), or large amount (>15 mg);

(6) sample shape and size, e.g., sphere, cylinder, layer, line (has very high aspect ratio), or the most common situation, a combination of them which means irregular shape (may cause long tail in DTG curve), and small or large size;

According to the classification, the kinetic models obtained in Chapters 2 and 3 have to follow limitations: medium fiber loading of 20-28 mesh irregular samples under comparatively low linear heating rates (i.e., 2-15°C/min) within a temperature range of 423-1073 K in nitrogen atmosphere for ten selected natural fibers. Any change of conditions will cause a relevant change in final result, e.g., more round particles instead of irregular fiber will cause corresponding excursion of DTG peak (Perez-Maqueda et al. 2006). However, above conditions simulated the practical utilization conditions of fiber for polymer composite, i.e., suitable fiber type and sample size (as used usually in composites), comparative sample loading (simulate the dispersion of fiber in feeding process), and, reasonable temperature range (show overall view and cover polymer processing temperature). Therefore, the model obtained still has practical significance for introducing natural fiber to engineering thermoplastic.

3.5 CONCLUSIONS

The modeling of thermal decomposition process of ten natural fibers commonly used in polymer composite industry was performed by assuming a global model occurring within the entire degradation range with consideration of fiber as one pseudo-component. Málek method with activation energy values obtained from Chapter 2 was applied to the modeling process. Careful calculation and evaluation indicated that, within an acceptable error limit of 5%, $RO(n>1)$ model can be used to describe the degradation process of most selected fibers well. The other kinetic parameters used include activation energy range of 160-170 kJ/mol; parameter n in $RO(n)=(1-\alpha)^n$ of 3-4; and $\ln A$ between 35 and 42 $\ln s^{-1}$. Obtained predictive weight loss curves can simulate the thermal weight loss processes of natural fibers.

Due to strong dependence on accurate activation energy values of the Málek method, some discrepancies between predicted and experimental results at both very low and very high temperature ranges were observed. Therefore, the application of the Málek method to natural fiber system was discussed. Although it was pointed out that some condition limitation of the obtained model should be considered, the model still has the practical significance in predicting fiber weight loss when it is used in combination with engineering thermoplastics.

3.6 REFERENCES

Antal, M. J., and Varhegyi, G. (1995). "Cellulose pyrolysis kinetics - the current state knowledge." *Industrial & Engineering Chemistry Research*, 34(3), 703-717.

Antal, M. J., Varhegyi, G., and Jakab, E. (1998). "Cellulose pyrolysis kinetics: Revisited." *Industrial & Engineering Chemistry Research*, 37(4), 1267-1275.

Bledzki, A. K., and Gassan, J. (1999). "Composites reinforced with cellulose based fibres." *Progress in Polymer Science*, 24(2), 221-274.

Branca, C., and Di Blasi, C. (2004). "Global interinsic kinetics of wood oxidation." *Fuel*, 83(1), 81-87.

Brown, M. E., Maciejewski, M., Vyazovkin, S., Nomen, R., Sempere, J., Burnham, A., Opfermann, J., Strey, R., Anderson, H. L., Kemmler, A., Keuleers, R., Janssens, J., Desseyn, H. O., Li, C. R., Tang, T. B., Roduit, B., Malek, J., and Mitsuhashi, T. (2000). "Computational aspects of kinetic analysis Part A: The ICTAC kinetics project-data, methods and results." *Thermochimica Acta*, 355(1-2), 125-143.

Calvo, L. F., Otero, M., Jenkins, B. M., Moran, A., and Garcia, A. I. (2004). "Heating process characteristics and kinetics of rice straw in different atmospheres." *Fuel Processing Technology*, 85(4), 279-291.

Capart, R., Khezami, L., and Burnham, A. K. (2004). "Assessment of various kinetic models for the pyrolysis of a microgranular cellulose." *Thermochimica Acta*, 417(1), 79-89.

Chen, H. X., Liu, N. A., and Fan, W. C. (2006). "Two-step consecutive reaction model and kinetic parameters relevant to the decomposition of Chinese forest fuels." *Journal of Applied Polymer Science*, 102(1), 571-576.

Di Blasi, C. (2008). "Modeling chemical and physical processes of wood and biomass pyrolysis." *Progress in Energy and Combustion Science*, 34(1), 47-90.

Gronli, M. G., Varhegyi, G., and Di Blasi, C. (2002). "Thermogravimetric analysis and devolatilization kinetics of wood." *Industrial & Engineering Chemistry Research*, 41(17), 4201-4208.

Koga, N. (1994). "A review of the mutual dependence of arrhenius parameters evaluated by the thermoanalytical study of solid-state reactions - the kinetic compensation effect." *Thermochimica Acta*, 244, 1-20.

Koga, N., and Criado, J. M. (1998a). "The influence of mass transfer phenomena on the kinetic analysis for the thermal decomposition of calcium carbonate by constant rate thermal analysis (CRTA) under vacuum." *International Journal of Chemical Kinetics*, 30(10), 737-744.

Koga, N., and Criado, J. M. (1998b). "Kinetic analyses of solid-state reactions with a particle-size distribution." *Journal of the American Ceramic Society*, 81(11), 2901-2909.

Malek, J. (1992). "The kinetic-analysis of nonisothermal data." Thermochimica Acta, 200, 257-269.

Malek, J., Mitsuhashi, T., and Criado, J. M. (2001). "Kinetic analysis of solid-state processes." *Journal of Materials Research*, 16(6), 1862-1871.

Mohanty, A. K., Misra, M., and Hinrichsen, G. (2000). "Biofibres, biodegradable polymers and biocomposites: An overview." Macromolecular Materials and Engineering, 276(3-4), 1-24.

Montserrat, S., Malek, J., and Colomer, P. (1998). "Thermal degradation kinetics of epoxy-anhydride resins: I. Influence of a silica filler." *Thermochimica Acta*, 313(1), 83-95.

Montserrat, S., Malek, J., and Colomer, P. (1999). "Thermal degradation kinetics of epoxy-anhydride resins: II. Influence of a reactive diluent." *Thermochimica Acta*, 336(1-2), 65-71.

Perez-Maqueda, L. A., Criado, J. M., and Sanchez-Jimenez, P. E. (2006). "Combined kinetic analysis of solid-state reactions: A powerful tool for the simultaneous determination of kinetic parameters and the kinetic model without previous assumptions on the reaction mechanism." *Journal of Physical Chemistry A*, 110(45), 12456-12462.

Senum, G. I., and Yang, R. T. (1977). "Rational approximations of integral of arrhenius function." *Journal of Thermal Analysis*, 11(3), 445-449.

Varhegyi, G., Antal, M. J., Jakab, E., and Szabo, P. (1997). "Kinetic modeling of biomass pyrolysis." *Journal of Analytical and Applied Pyrolysis*, 42(1), 73-87.

Varhegyi, G., Antal, M. J., Szekely, T., and Szabo, P. (1989). "Kinetics of the thermal-decomposition of cellulose, hemicellulose, and sugar-cane bagasse." *Energy & Fuels*, 3(3), 329-335.

Varhegyi, G., Jakab, E., and Antal, M. J. (1994). "Is the broido-shafizadeh model for cellulose pyrolysis true." *Energy & Fuels*, 8(6), 1345-1352.

Vyazovkin, S. (1992). "Alternative description of process kinetics." *Thermochimica Acta*, 211, 181-187.

Vyazovkin, S. (2000). "Computational aspects of kinetic analysis. Part C. The ICTAC Kinetics Project - the light at the end of the tunnel?" *Thermochimica Acta*, 355(1-2), 155-163.

Vyazovkin, S., and Wight, C. A. (1998). "Isothermal and non-isothermal kinetics of thermally stimulated reactions of solids." *International Reviews in Physical Chemistry*, 17(3), 407-433.

Yao, F., Wu, Q. L., Lei, Y., Guo, W. H., and Xu, Y. J. (2008). "Thermal decomposition kinetics of natural fibers: Activation energy with dynamic thermogravimetric analysis." *Polymer Degradation and Stability*, 93(1), 90-98.

CHAPTER 4 IN-DEPTH INVESTIGATION OF THERMAL DECOMPOSITION KINETICS OF RICE STRAW FIBER BY ISOTHERMAL THERMOGRAVIMETRIC ANALYSIS

4.1 INTRODUCTION

Rice is one of the world's most widespread crops. Rice straw, a major by-product of the rice crop, is unfortunately treated as waste in many countries due to lacking efficient utilization technology. However, global ecology issues and energy shortage, biodegradability, and lignocellulosic characteristics of the straw have led to exploration on its utilization in recent decades. Two important directions are consequently developed: rice straw as bio-energy production (e.g., bio-oil, ethanol and methane) and as raw materials for composite (e.g., polymer composite, particleboard and fiberboard) (Bridgwater et al. 1999; Yaman 2004). Obviously, both of the two directions need a detailed characterization on thermal degradation process of rice straw. Therefore, fundamental work on thermal kinetics of rice straw degradation is greatly needed for practical utilization of the fiber.

Limited work has been done in this field. Nassar (1999) performed thermal analysis for rice straw using a heating rate of 5°C/min from room temperature to 800°C in both air and helium atmosphere. In his study, a dual mechanism concept was concluded and an activation energy value of 19.3 $Kcal/mol$ was obtained by assuming a pseudo first-order reaction. Calvo et al. (2004) focused more on the influence of different atmospheres of air and nitrogen on thermal behavior of rice straw using a single heating rate of 15°C/min from ambient to 923°C. Data were fitted by two models, one assuming first-order mechanism and the other assuming n th order, in a temperature range of 190-525°C. A comparatively lower activation energy value of 85 kJ/mol was obtained along with pre-exponential factor of $2.54\times105\ s^{-1}$ and n of 0.86 for rice straw under pure nitrogen atmosphere. Šimkovic and Csomorová (2006) compared several agricultural

residues including wheat straw using dynamic (single heating rate of 10°C/min) and isothermal methods in nitrogen and oxygen atmosphere. An activation energy value of 69 kJ/mol and relative rate constants for wheat straw were obtained only under the isothermal condition (temperature range of 220-260°C) with assumption of the first-order conversion function. Most recent research was carried out by Müller-Hagedorn and Bockhorn (2007) on barley and wheat straw using specific heating program up to 550°C. By assuming several parallel, independent n th order reactions, comparatively high activation energy values of 120, 170, 258 and 97 kJ/mol for cellulose, hemicelluloses 1 and 2, and lignin were obtained along with other relevant model parameters.

The previous research provided us some information about thermal degradation of rice straw. However, the information available is not sufficient for a comprehensive understanding of the mechanism involved. Moreover, some research was based on single heating rate and pre-assumption of certain kinetics. However, single heating rate method has not been recommended because of possible forced data fitting and kinetic compensation effect (KCE) according to recent research (Brown et al. 2000; Maciejewski 2000; Vyazovkin 2000). Therefore, more reliable methods are needed in investigating thermal degradation process of rice straw.

In Chapters 2 and 3, homogeneity of common natural fibers in relation to polymer composites is discussed and models under non-isothermal conditions are presented. There, some thermal properties of rice straw are listed as a part of natural fiber family without detailed analysis of rice straw itself. Therefore, the objective of the work presented in this chapter was to detail the thermal degradation process of rice straw under both isothermal and non-isothermal conditions in order to better understand its thermal behavior, and, consequently, better apply it in polymer composite systems.

4.2 THEORETICAL APPROACH

A theoretical approach regarding non-isothermal condition is introduced in the previous chapters. As a result, only basic procedures under isothermal condition are covered in the following.

Kinetic modeling procedure in isothermal condition is somewhat similar to that in non-isothermal condition. By integration of Eq. (3.1) in isothermal conditions, the following equation is obtained:

$$g(\alpha) = \int_0^{\alpha} \frac{1}{f(\alpha)} d\alpha = \int_0^{t} A e^{-x} dt = A e^{-x} \cdot t \qquad (4.1)$$

Under isothermal conditions, the apparent activation energy of the decomposition process can also be obtained by iso-conversional method using following the logarithmic form of Eq. (4.1):

$$\ln t = \ln[\frac{g(\alpha)}{A}] + \frac{E_a}{RT} \qquad (4.2)$$

The slope of $\ln t$ *vs.* $1/T$ for the same value of α gives the value of apparent activation energy. This procedure can be repeated for various values of α . Therefore, the method provides a check of invariance of E_a with respect to α in a selected range, which is one of the basic assumptions in kinetic analysis of the TG data.

Following the Málek method (Malek et al. 2001), $z(\alpha)$ function applied in the isothermal condition is defined by combining Eqs. (3.1) and (4.1) as:

$$z(\alpha) = \left(\frac{d\alpha}{dt} \right) t = f(\alpha) g(\alpha) \qquad (4.3)$$

Similar to the normalization procedure, this function is usually plotted within the (0, 1) interval for practical reasons. The maximum of this function, labeled α_p^{∞}, has characteristic

values for basic kinetic models. As mentioned in Chapter 3, this value is useful for basic classification of possible kinetic models, but it is not sufficient for an unambiguous determination of true kinetic model function $f(\alpha)$. Another defined function $y(\alpha)$ is proportional to $f(\alpha)$ in isothermal conditions because Ae^{-x} is constant (Eq. 4.4).

$$y(\alpha) = \left(\frac{d\alpha}{dt} \right) \approx f(\alpha) \tag{4.4}$$

It is convenient to normalize the $y(\alpha)$ within (0, 1) interval. The shape of this plot is characteristic for each kinetic model, and it can be used as a diagnostic tool for kinetic model determination using rules demonstrated by Málek (Malek 1992; Malek et al. 2001), which can also be found in Section 3.2.

4.3 EXPERIMENTAL

The same 20-28 mesh rice straw fiber as used in Section 2.2 was chosen for the isothermal investigation. Samples (8-10mg) were first heated to 100°C at a heating rate of 20°C/min and then kept in this temperature for 20 min to remove moisture before further heating to desired temperatures. A "jump" heating program associated with instrument was applied to make samples reach desired temperatures as fast and accurate as possible. Fourteen desired temperatures between 195 and 315°C were chosen to fulfill the request of the polymer processing temperature. This range was determined according to the onset and peak temperatures shown in Table 2.3. Outside the specific temperature ranges, it is quite difficult to obtain reliable TG data. At lower temperatures the thermal degradation becomes very slow, and it is not easy to determine correctly the relative mass loss corresponding to completely degraded samples. In contrast, at higher temperatures, the thermal degradation is so fast, which probably caused the initial part of the TG curve lost during the instrument setting period. Also, it is out of range for common engineering thermoplastic processing temperatures. The weight loss of all samples was

measured over 48h in order to find the stable final conversion rates. Experimental data were analyzed by the same experimental and mathematical software mentioned in previous chapters (i.e., Universal Analysis 2000, TA Instruments; and, MATLAB 7.1, the MathWorks, Inc.). Based on different degradation cases of samples under various temperatures, the time and conversion ranges used for calculation were different, which are specifically introduced in Section 4.4.

4.4 RESULTS AND DISCUSSION

4.4.1 Overall Isothermal Degradation Process of Rice Straw

A typical isothermal test under programmed heating procedure led to typical TG and DTG curves as shown in Fig. 4.1. The first degradation period (before 100°C) corresponded to loss of moisture and small molecular weight volatiles. In the programmed heating period (from 100°C to the stable target temperature), a sample usually suffered unavoidable non-isothermal degradation for about 5 min. It is noteworthy that this five-minute degradation must be taken into

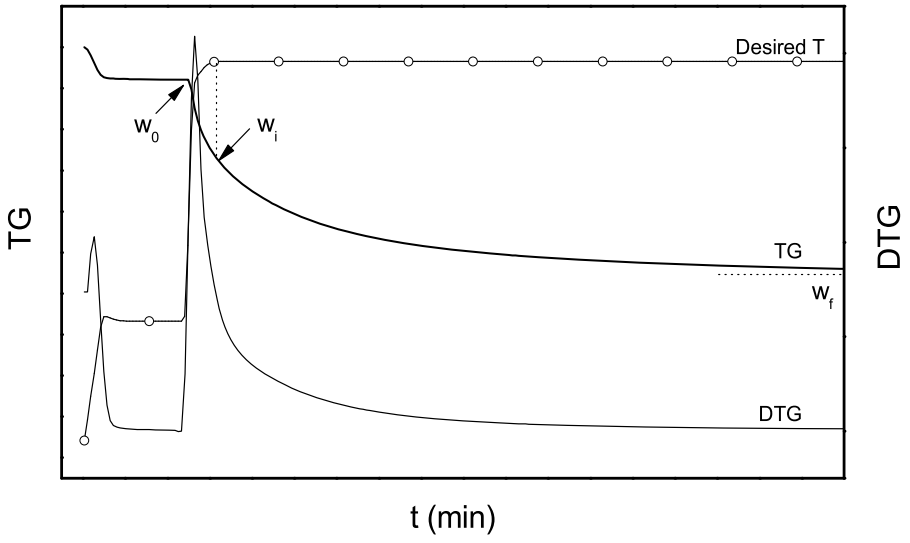

Fig. 4.1 Typical isothermal TG and DTG curves of sample under programmed heating profile (shown in red). Arrow points to the start point (w_0) used for calculation. Broken line indicating the final weight (w_f) when test ended.

account because it caused significant weight loss when high temperature was applied. This information is very important for practical processing. The arrow shown in Fig. 4.1 indicates the start point (w_0) of the whole isothermal experiment. Consequently, data were collected for calculation from this point. The broken line indicates the final weight (w_f) at the end of one certain time period of the isothermal degradation. Therefore, the conversion fraction at time t was obtained by Eq. (2.2) for this certain time period. Obviously, the initial actual isothermal conversion fraction w_i, which is the weight at the stable desired temperature, was not zero due to instrument setting process. However, this did not affect the process of obtaining accurate activation energy values of stable isothermal part by isoconversional method after appropriately choosing calculation segment.

The 48h-isothermal tests were carried out in a wide temperature range, i.e., from 195 to 315°C, to evaluate the variability of the degradation mechanism. Fig. 4.2 shows part of the results by normalizing fractional weight loss to the starting sample weight w_0 using experimental data at five temperatures as examples. As shown in Fig. 4.2, five curves did not exhibit the same trend, which gave a strong implication that degradation mechanism changed with experimental temperatures. Also, degradation reaction still actively occurred at the end of the 48h degradation process and seemed not to reach a stable residue value, especially in some low temperature cases. The latter phenomenon caused extra difficulty and error in calculation and interpretation of modeling parameters. Therefore, extrapolation was performed to pursue a stable final weight loss. Here, the basic requirements for extrapolated curve are (1) having good agreement with obtained experimental data; (2) satisfying the essential of degradation process, i.e., both entire weight loss percentage and fractional conversion rate α in isothermal period between 0 and 1; and (3) having *stable* extrapolated final point. Two-parameter power function

was found to satisfy the requirements for all cases in this study after appropriate adjustment shown below:

$$y = WL_t = (1 - WL_i)[1 - (1 + ax)^b] + WL_i; (a > 0, b < 0) \quad (4.5)$$

where, x is the degradation time (min) while WL_t and WL_i are weight loss at time t and initial point defined by $(w_0 - w_t)/w_0$ and $(w_0 - w_i)/w_0$, respectively. The expression in square brackets is two-parameter power function with parameter limitation, which satisfies the numerical essential of $\alpha(t)$ function, i.e., monotone increase when x increasing, $\alpha = 0$ when $x \to 0$, and $\alpha = 1$ when $x \to \infty$. The whole equation also satisfies the numerical essential of weight loss curve.

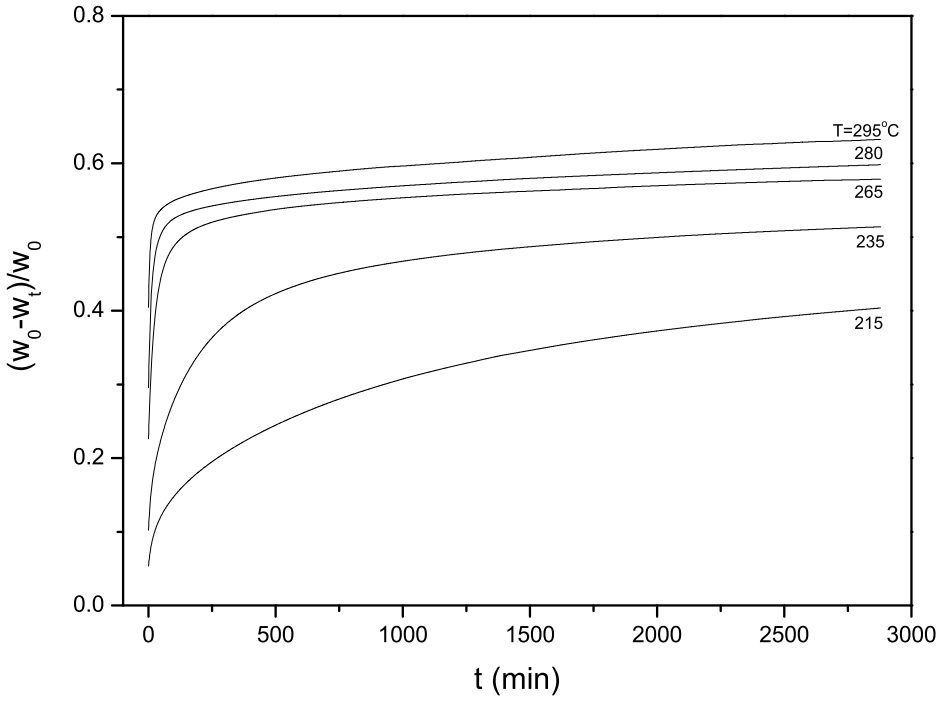

Fig. 4.2 Overall view of rice straw over a 48h isothermal degradation period normalized to the starting sample weight w_0 in a wide temperature range using experimental data at five temperatures as examples.

The application of Eq. (4.5) to obtain extrapolated final weight loss is plotted in Fig. 4.3 using isothermal data at 215°C as an example. The time point of 6000 min was chosen as the final time because after this time the weight loss was less than 0.1% within any one-hour degradation period, which can be considered reaching a stable state. This time point satisfied all cases in this study.

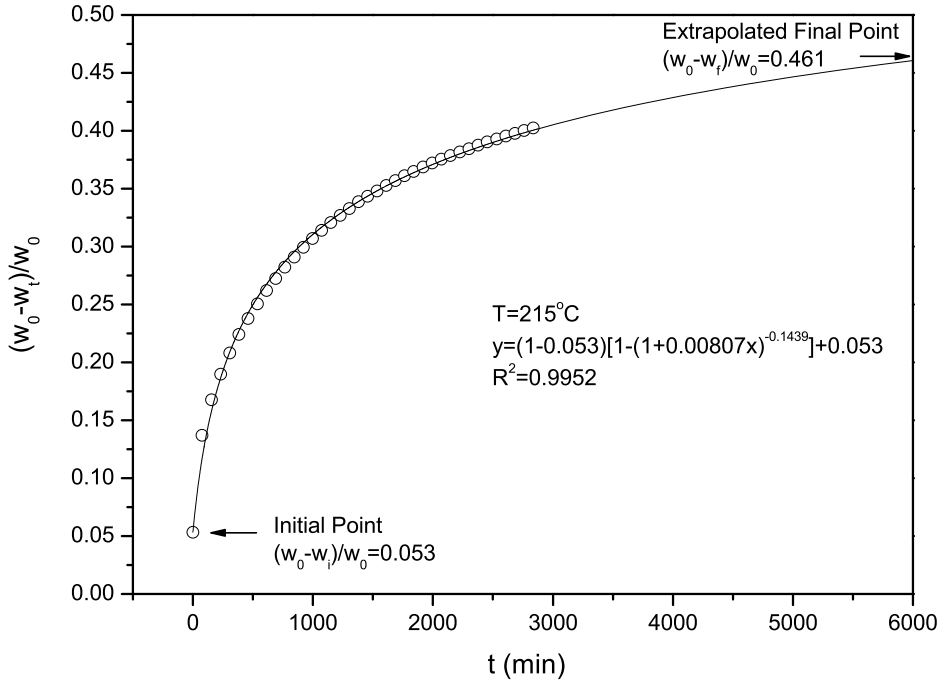

Fig. 4.3 Extrapolating degradation to 6000 min to determine the final degradation weight loss using isothermal experiment at T=215°C as an example. Circle: experimental data; line: extrapolated line generated by the function shown in the middle with coefficient of determination R^2.

Collecting all extrapolated final as well as other experimental characteristic weight loss values and normalizing them to the starting sample weight w_0, an overall view of weight loss at different experimental temperatures is plotted in Fig. 4.4, which offers a trend view of weight loss process. Then, a special "American football" shape was observed in this figure with the

center line located at about 260°C. It was observed that, below 260°C (temperature sub-range one), degradation showed comparatively low initial weight loss but increasing reaction rate, which was concluded from increasing the gap between initial weight loss and either 48h or extrapolated final weight loss. The increasing gap implied that the degradation of some important component was involved in the reaction. On the contrary, in cases of temperatures above 260 °C (temperature sub-range two), degradation showed comparatively high initial weight loss but decreasing reaction rate concluded from the decreasing gap. This observation implied that the degradation peak of some important component possibly passed through. This phenomenon may be associated with the degradation of two main components, hemicelluloses and cellulose. Hemicelluloses was considered as the first degraded component of natural fiber and happened in a temperature range of 200-260°C usually, while most cellulose degraded in a comparatively higher degradation temperature of 240-350°C (Antal et al. 1998; Branca and Di Blasi 2003; Di Blasi 2008; Varhegyi et al. 1997). Therefore, in temperature sub-range one, hemicelluloses were the primary degradation components. With temperature increasing, more cellulose degradation was involved and finally yielded a high initial weight loss in temperature sub-range two. From Fig. 4.4, extrapolated final weight showed a comparatively flat change after 270°C, which indicated that the cellulose in straw fiber was completely degraded in this temperature range. This result confirmed the observation shown in Table 2.3, where extrapolated DTG peak and shift temperatures under various heating rates to 274 and 311°C, respectively, at a heating rate of zero are shown. Based on the common knowledge, the degradation of cellulose causes significant strength loss of fiber, and a processing temperature above this range should be avoided in terms of natural fiber reinforced polymer composites. However, the question of what degree of strength the fiber will loss due to the degradation of cellulose along with hemicelluloses still remains unanswered.

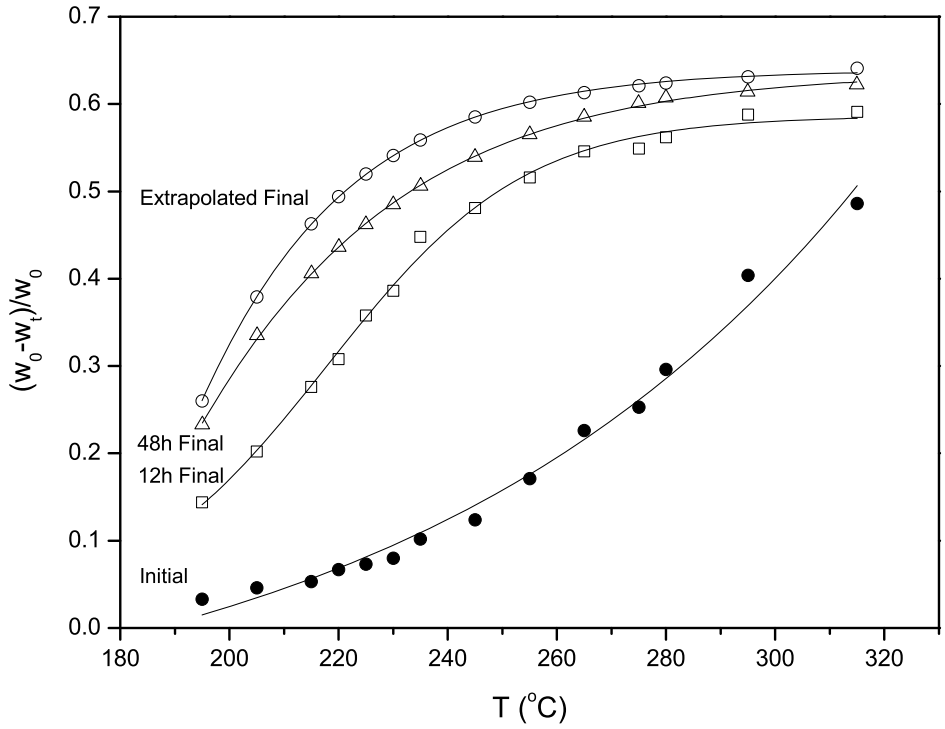

Fig. 4.4 All critical weight loss values of rice straw isothermal degradation normalized to the starting sample weight w_0 in the whole experimental temperature range. Among them, initial (●), 12h final (□), 48h final (Δ) and extrapolated final (○), respectively, referred to the weight loss values at the time of actual isothermal run start point after instrument setting period, after 12h degradation, after 48h degradation, and after 6000 min degradation which are extrapolated instead of real measurement following method defined in text.

4.4.2 Modeling of Isothermal Degradation of Rice Straw

Even though the influence of degradation of cellulose and hemicelluloses on mechanical properties of natural fiber is still unclear, the weight loss of two temperature sub-ranges can be modeled to yield useful information. It is noteworthy to point out that a separated modeling for two temperature sub-ranges is necessary because they obviously have different main reactants.

4.4.2.1 Temperature Sub-Range One

The modeling procedure was quite similar with the procedure introduced in Chapters 2 and 3. For temperature sub-range one, the isothermal experiments involved are: 195, 205, 215, 220, 225, 230, 235, 245, 255, and 265°C with their $\alpha - t$ plots shown in Fig. 4.5. The α in this figure was calculated using Eq. (2.2), and w_f here was defined as the extrapolated final value at 6000 min degradation time point. From this figure, one can observe a fairly similar trend between these low temperature isothermal curves.

For the calculation of the apparent activation energy in this temperature sub-range, four $\alpha - t$ curves, from 235 to 265°C, were chosen because they are of interest in terms of polymer composite processing, and they have comparatively wide α range. The calculated $E_a - \alpha$ results are plotted in Fig. 4.6 with an average R^2=0.9714. Generally, the apparent activation energy should be invariant with respect to α in the $0.3<\alpha<0.7$ range. In fact, the value of E_a increased, then kept invariant, and finally decreased as α increased within this range. However, the variant is considerably insignificant and, therefore, the average value here was $116\pm5\, kJ/mol$ taken in the $0.30 < \alpha < 0.70$ range.

Using apparent activation energy value and experimental data, the normalized $y(\alpha)$ and $z(\alpha)$ curves are plotted in Fig. 4.7. From Fig. 4.7, one can easily find that $y(\alpha)$ functions had concave shape, and all α_p^∞ of $z(\alpha)$ functions were less than 0.6. Both characteristics led to a conclusion that $RO(n>1)$ model is suitable to describe the degradation curve of rice straw fiber under isothermal condition. Therefore, the fractional conversion is written in the following form:

$$\alpha(t) = 1 - \left[1 - t(1-n)Ae^{-x}\right]^{1/(1-n)} \tag{4.6}$$

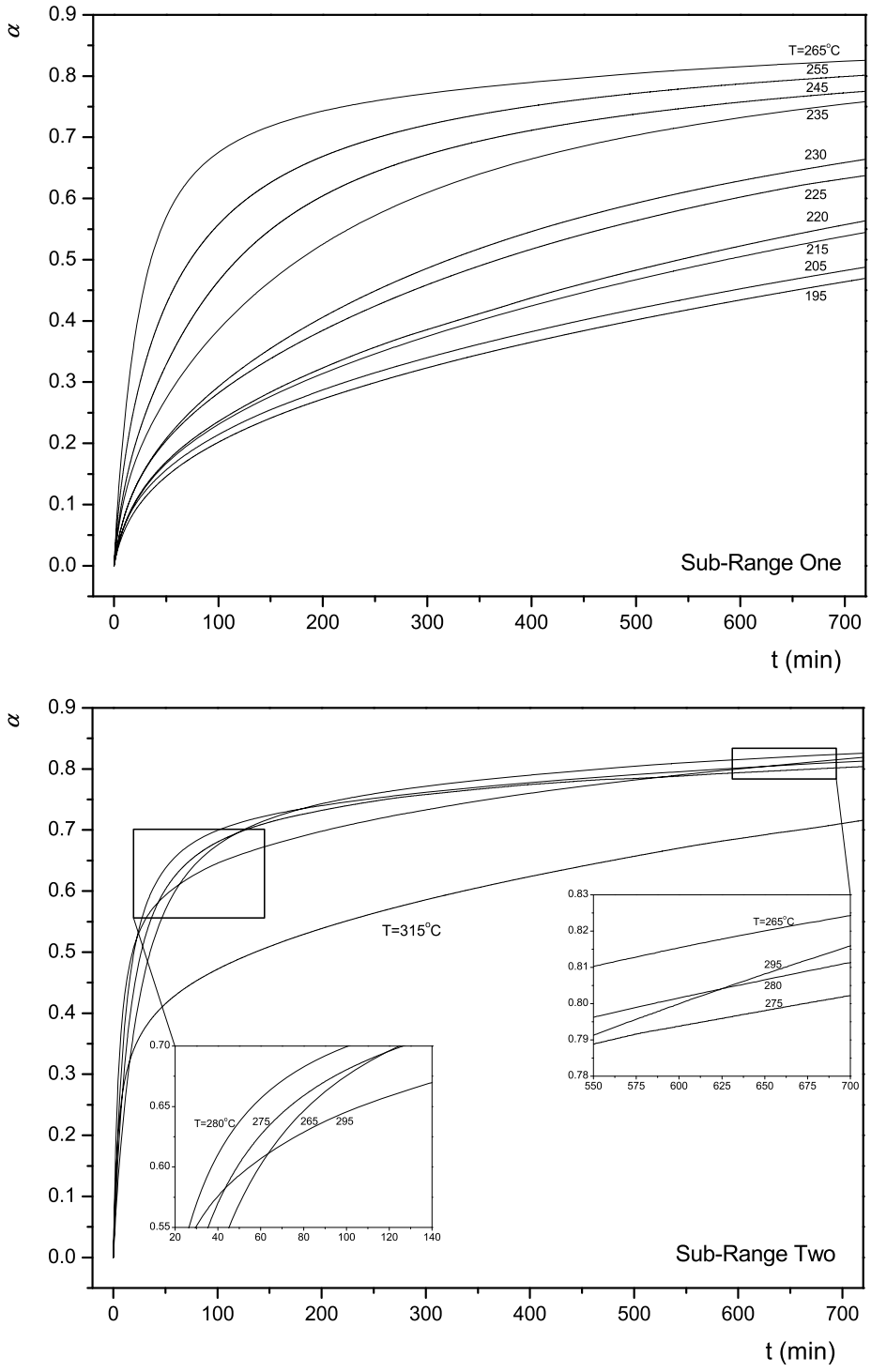

Fig. 4.5 The conversion dependence on time for two temperature sub-ranges.

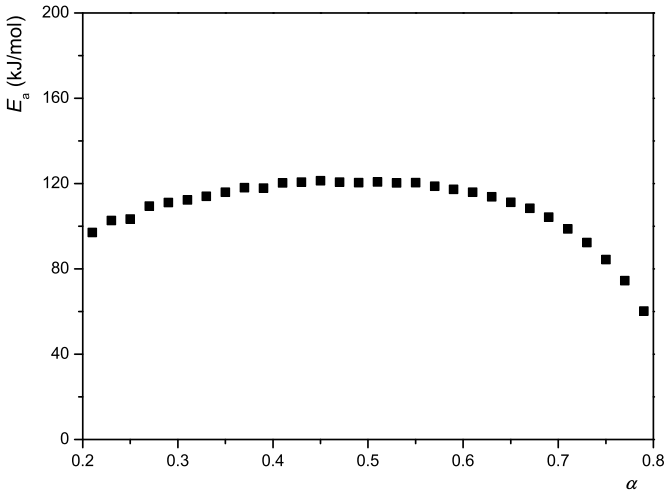

Fig. 4.6 The apparent activation energy calculated from isothermal TG data of four temperatures (from 235 to 265°C) plotted as a function of fractional conversion (α) for the temperature sub-range one.

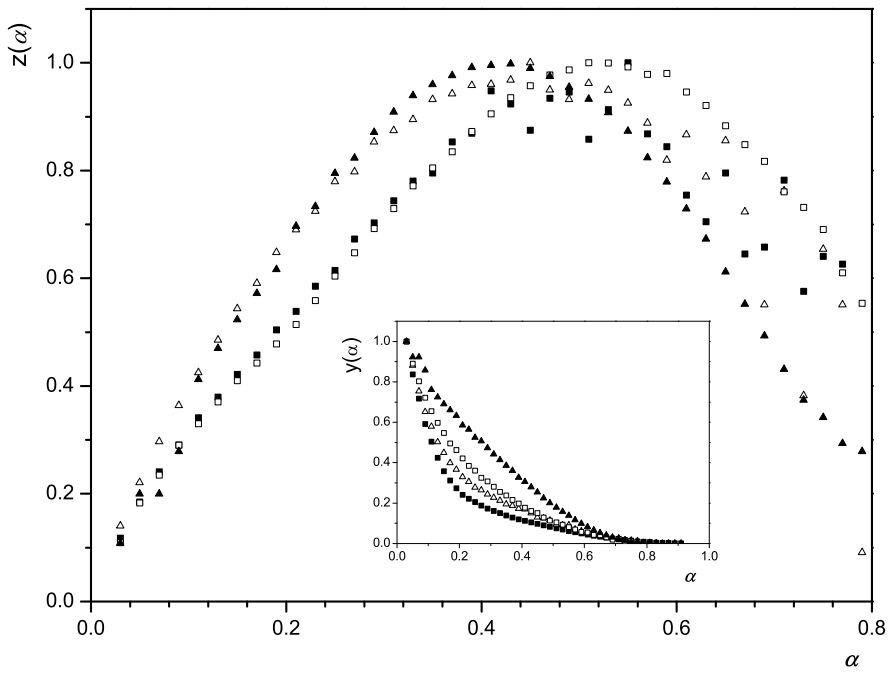

Fig. 4.7 The $z(\alpha)$ function for temperature sub-range one using various isothermal experiments: 235°C (□); 245°C (■); 255°C (Δ); 265°C (▲). The inset shows concave shape of $y(\alpha)$ function curves for the same experiments.

The value of reduced activation energy is constant in isothermal condition $(x = E_a / RT)$ and it can easily be calculated from the average value of apparent activation energy obtained by isoconversional analysis previously shown. Using the same procedure of non-linear regression of experimental data, the values of n and A can be obtained later. Shown in Table 4.1, these values are fairly close to each other in a temperature range of 235-265°C. Parameter n had a slightly increased trend with respect to the temperature selected, which might be associated with the initial degradation of another main component of fiber – cellulose. As mentioned in Section 4.4.1, the temperature sub-range one mainly involved degradation of hemicelluloses. However, noticing that cellulose has a low initial degradation temperature, 240°C, the change of parameter n from 235°C may be promoted by this factor. In other words, initial degradation of cellulose possibly added a parallel reaction to the main hemicellulose degradation and yielded the parameter change. But this change is not very significant. Using calculated parameters, the result of curve fitting is also calculated (Table 4.1). It shows a fairly good agreement between experimental and simulated curves.

Table 4.1 The kinetic parameters obtained by non-linear regression of isothermal data in temperature sub-range one

T (°C)	n	$\ln(A)$ $(\ln s^{-1})$	$fit(\%)$
235	2.77	18.68	2.06
245	2.95	18.57	1.27
255	3.14	18.60	0.54
265	3.17	18.76	1.86
Average	3.01 (.19)	18.65 (.09)	1.43 (.68)

The comparison of experimental data (symbols) and prediction $\alpha(t)$ of $RO(n > 1)$ (solid lines) for all selected fibers is shown in Fig. 4.8. These $\alpha(t)$ curves were calculated using

Eq. (4.6) for the kinetic parameters shown in Table 4.1. There is a quite good agreement between experimental data and prediction curves even though some discrepancies are observed. Evaluation of single linear relationship between $\ln(d\alpha/dt) - \ln f(\alpha)$ and $1/T$ for modeling results at different α is also plotted in Fig. 4.9. Superposition of the data points makes a single straight line, which indicates the model and relevant parameters obtained are appropriate for the real degradation process. The activation energy values listed in the plot are calculated from slope, which are quite comparable (error < 7%) with the one obtained from isoconversional method, i.e., $116 \pm 5\ kJ/mol$.

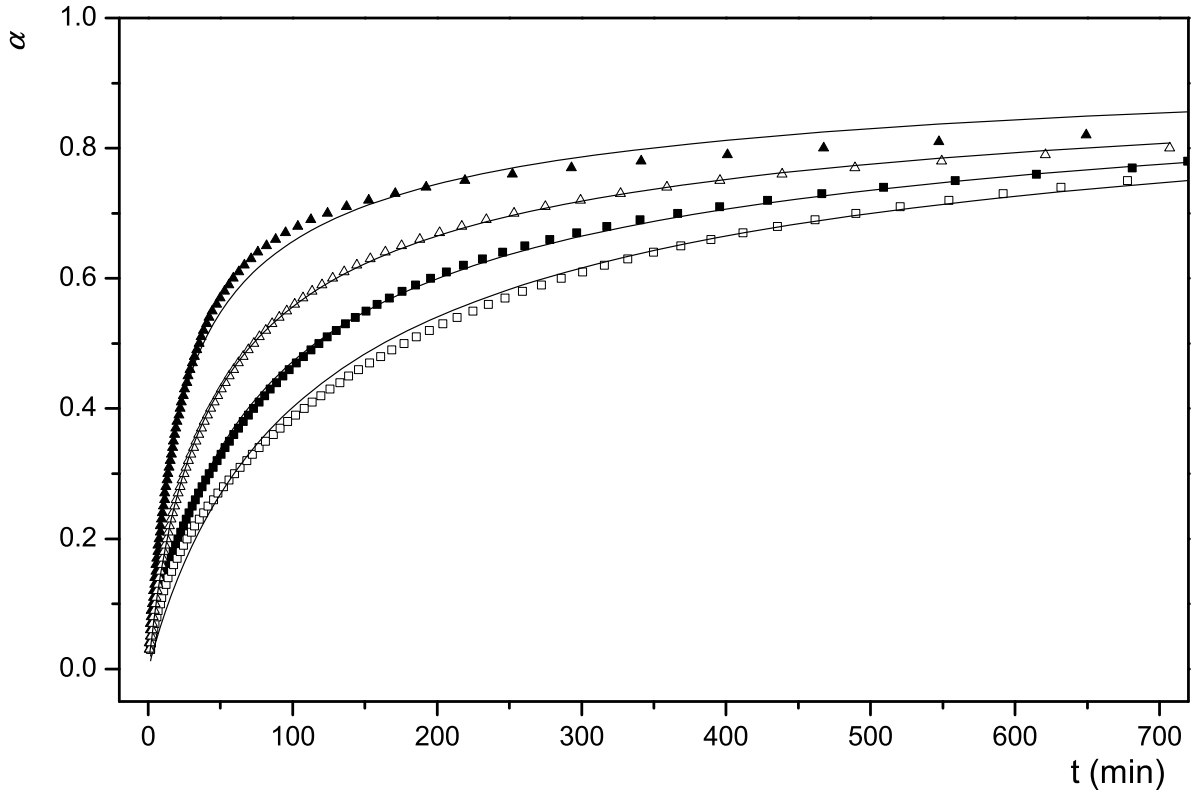

Fig. 4.8 Experimental (symbols) and simulated (solid line) isothermal $\alpha - t$ curves for sub-range one at different temperatures: 235°C (□); 245°C (■); 255°C (Δ); 265°C (▲). Simulated curves are calculated using Eq. (4.6) for the kinetic parameters shown in Table 4.1.

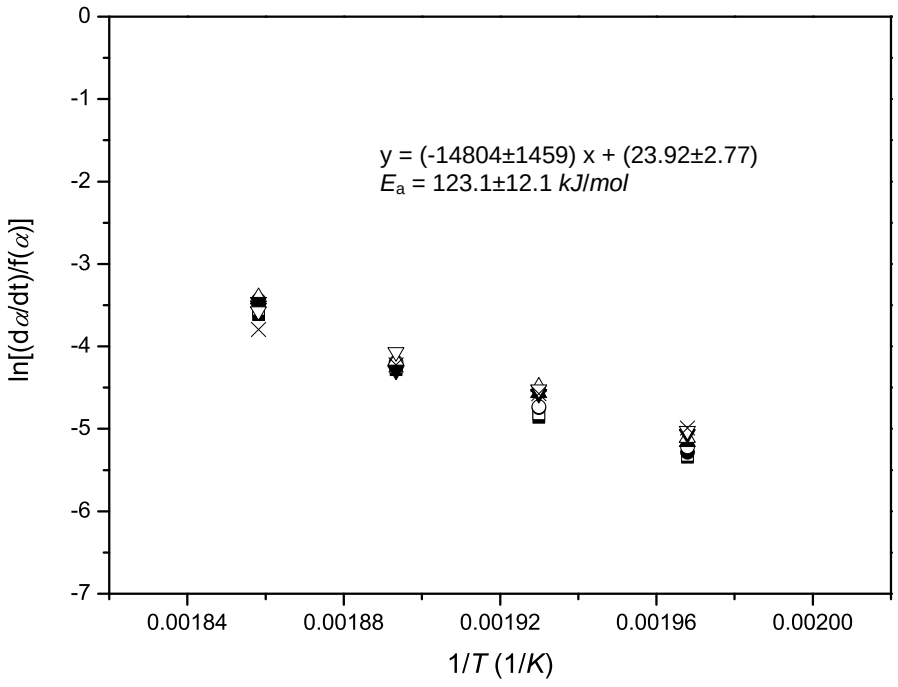

Fig. 4.9 Evaluation of single linear relationship between $\ln(d\alpha/dt) - \ln f(\alpha)$ and $1/T$ for modeling of temperature sub-range one at different α (different symbols).

4.4.2.2 Temperature Sub-Range Two

The isothermal experiments involved in sub-range two are: 265, 275, 280, 295, and 315°C. Unfortunately, as shown in Fig. 4.5, the $\alpha - t$ curves had different trends, which are quiet different with the situation in temperature sub-range one. Generally, if under the same degradation mechanism with similar reactant, reactions should exhibit parallel curves. However, curves shown in Fig. 4.5 are crossed with each other, indicating that different mechanisms or reactants were involved. Consequently, curves cannot be compared and used to calculate activation energy value. Such calculation will cause negative activation energy values. Therefore, a modeling cannot be performed in this case.

In fact, the reactions under 275 and 280°C may involve some degradation process similar with the case in the temperature sub-range one concluded by parallel curves at the most beginning period. But degradation reaction at 315°C is definitely different due to cellulose degradation during instrument setting period.

4.4.3 Discussion on Rice Straw Degradation Kinetics

Non-isothermal modeling was performed in Chapter 3. It was found that $RO(n>1)$ model can describe the degradation process of rice straw fiber along with other kinetic parameters: activation energy value of 196±3 kJ/mol; parameter n in $RO(n)=(1-\alpha)^n$ of 5.8±0.2; and, $\ln A$ of 46.6±0.1 $\ln s^{-1}$. Those parameters are obviously higher than the average level of modeling parameters of other fibers listed in Table 3.2. The result hinted that the degradation of rice straw is actually different with common fibers such as wood and bast fiber. Generally, the higher activation energy means a higher energy barrier of starting a chemical reaction, which indicates, in this case, that the elementary reactions of rice straw thermal degradation need more energy to start. It might be associated with the microstructure of cellulose crystal or some special components such as silica in straw fiber. Those elementary reactions are very difficult to define individually so far, and the information we obtained is actually the combination of multiple elementary reactions. On the other hand, the combination of n and $\ln A$ gave higher $d\alpha/dt$ for straw fiber, which means that the degradation will be faster in a unit time. Three parameters, E_a, n and $\ln A$, determined why rice straw had a higher offset temperature but a lower DTG peak temperature compared to other fibers in Table 2.3. Therefore, the thermal stability of rice straw is somewhat worse than other fibers if they are introduced in engineering plastic composites. However, appropriately controlling processing temperature to an acceptable range such as aforementioned temperature sub-range one, where the degradation is somewhat

slow (no significant strength loss), the rice straw can be considered as a possible filler for some engineering plastics with relatively low melting temperatures.

All kinetic results obtained in both isothermal and non-isothermal experiments are consistent with a thermal degradation described by a "reaction-order" model. However, comparing Table 4.1 to Table 3.2, it is found that the parameters obtained in both conditions are different, which is not a surprising result. Generally, results from two different experimental methods cannot be directly compared unless strictly the same reactants and mechanism are involved (Brown et al. 2000; Vyazovkin 2000). However, limited case was proven to satisfy this limitation. In addition, in terms of the kinetic model expressions themselves, the transition from isothermal to non-isothermal expressions was very simple (changing $d\alpha/dt$ to $d\alpha/dT$ by simply inserting heating rate $\beta = dT/dt$). However, it implies a very important physical assumption that linear heating profile does not affect reactions. Actually, this assumption is too ideal to be achieved. Therefore, results from isothermal conditions only reflect certain points of a continuous degradation process and cannot be used to interpret the entire process. Non-isothermal kinetic result will miss some specific information at certain temperature due to introducing multiple parallel or competition reactions, though it leads to a better macroscopical interpretation. However, the results from two experiment techniques based on the global reaction assumption, the reaction-order model can offer an acceptable description for the degradation process of rice straw. With obtained parameters, we can offer a global prediction on straw degradation for future application of composite processing. It is also found in this study that Málek method provides a satisfactory procedure for isothermal degradation of rice straw.

The main limitation of the obtained isothermal model is the temperature range, i.e., lower than approximately 265°C. In addition, irregular fiber shape and 20-28 mesh fiber size are also a limitation. Considering this temperature range can cover some engineering plastics, such as

nylon-6 (melting temperature <235°C normally), the model obtained still has some practical significance. In the last chapter of this dissertation, we discuss a specific application example – rice straw reinforced HDPE/nylon-6 based composite.

4.5 CONCLUSIONS

The modeling of isothermal thermal decomposition of rice straw fibers was performed by assuming a global reaction model that considers fiber as one pseudo-component. Málek method with activation energy values obtained from iso-conversional method was applied to modeling.

Within acceptable error limit of less than 3%, $RO(n>1)$ model can describe the degradation process of rice straw fiber fairly well in a temperature range of less than about 265°C along with other kinetic parameters: activation energy value of $116\pm5\,kJ/mol$; parameter n in $RO(n)=(1-\alpha)^n$ of 3.0±0.2; and, $\ln A$ of $18.7\pm0.1\ln s^{-1}$. For temperature range higher than 265°C, modeling cannot be well performed due to pre-degradation during instrument setting period. The model obtained has the practical significance for introducing straw fibers into some engineering plastics with comparatively lower melting temperature.

4.6 REFERENCES

Antal, M. J., Varhegyi, G., and Jakab, E. (1998). "Cellulose pyrolysis kinetics: Revisited." *Industrial & Engineering Chemistry Research*, 37(4), 1267-1275.

Branca, C., and Di Blasi, C. (2003). "Kinetics of the isothermal degradation of wood in the temperature range 528-708 K." *Journal of Analytical and Applied Pyrolysis*, 67(2), 207-219.

Bridgwater, A. V., Meier, D., and Radlein, D. (1999). "An overview of fast pyrolysis of biomass." *Organic geochemistry*, 30(12), 1479-1493.

Brown, M. E., Maciejewski, M., Vyazovkin, S., Nomen, R., Sempere, J., Burnham, A., Opfermann, J., Strey, R., Anderson, H. L., Kemmler, A., Keuleers, R., Janssens, J., Desseyn, H. O., Li, C. R., Tang, T. B., Roduit, B., Malek, J., and Mitsuhashi, T. (2000). "Computational aspects of kinetic analysis Part A: The ICTAC kinetics project-data, methods and results." *Thermochimica acta*, 355(1-2), 125-143.

Calvo, L. F., Otero, M., Jenkins, B. M., Moran, A., and Garcia, A. I. (2004). "Heating process characteristics and kinetics of rice straw in different atmospheres." *Fuel Processing Technology*, 85(4), 279-291.

Di Blasi, C. (2008). "Modeling chemical and physical processes of wood and biomass pyrolysis." *Progress in Energy and Combustion Science*, 34(1), 47-90.

Maciejewski, M. (2000). "Computational aspects of kinetic analysis. Part B: The ICTAC Kinetics Project - the decomposition kinetics of calcium carbonate revisited, or some tips on survival in the kinetic minefield." *Thermochimica acta*, 355(1-2), 145-154.

Malek, J. (1992). "The kinetic-analysis of nonisothermal data." *Thermochimica Acta*, 200, 257-269.

Malek, J., Mitsuhashi, T., and Criado, J. M. (2001). "Kinetic analysis of solid-state processes." *Journal of Materials Research*, 16(6), 1862-1871.

Muller-Hagedorn, A., and Bockhorn, H. (2007). "Pyrolytic behaviour of different biomasses (angiosperms) (maize plants, straws, and wood) in low temperature pyrolysis." *Journal of analytical and applied pyrolysis*, 79(1-2), 136-146.

Nassar, M. M. (1999). "Thermal analysis kinetics of bagasse and rice straw." *Energy Sources*, 21(1-2), 131-137.

Simkovic, I., and Csomorova, K. (2006). "Thermogravimetric analysis of agricultural residues: Oxygen effect and environmental impact." *J. Appl. Polym. Sci.*, 100(2), 1318-1322.

Varhegyi, G., Antal, M. J., Jakab, E., and Szabo, P. (1997). "Kinetic modeling of biomass pyrolysis." *Journal of Analytical and Applied Pyrolysis*, 42(1), 73-87.

Vyazovkin, S. (2000). "Computational aspects of kinetic analysis. Part C. The ICTAC Kinetics Project - the light at the end of the tunnel?" *Thermochimica acta*, 355(1-2), 155-163.

Yaman, S. (2004). "Pyrolysis of biomass to produce fuels and chemical feedstocks." *Energy Conversion and Management*, 45(5), 651-671.

CHAPTER 5* RICE STRAW FIBER REINFORCED HIGH DENSITY POLYETHYLENE COMPOSITE: EFFECT OF FIBER TYPE AND LOADING

5.1 INTRODUCTION

Natural fiber reinforced thermoplastic composites have recently gained importance in various applications as building materials and automotive components. The fibers offer advantages of large quantity, annual renewability, low cost, light weight, competitive specific mechanical properties, reduced energy consumption, and environmentally friendliness. The natural fibers used to reinforce thermoplastics mainly include wood, cotton, flax, hemp, jute, sisal, and sugarcane fibers (Wollerdorfer and Bader, 1998; Bledzki and Gassan, 1999, 2002).

Rice straw fiber can also be considered as important potential reinforcing filler for thermoplastic composite because of its lignocellulosic characteristics. Global paddy production reached 628 million tons in 2005 with an additional one percent increase in 2006 (FAO, 2006). The U.S. rice production in 2006/07 is projected at 10 million ton (USDA, 2006). With an approximate rice-to-straw ratio of 1.0, an equivalent amount of rice straw (i.e., 10 million tons) is produced. Chemically, lignocellulosic rice straw fiber has similar compositions as other natural fibers used in thermoplastics (Table 5.1). The whole rice straw fiber is composed of rice husk, leaf sheath, straw leaf blade, straw stem and knot, and straw root (Sundstøl, 1984). Various fiber components have different chemical constituents, especially cellulose and residual ash contents (Table 5.1), which may contribute differently to the properties of rice straw fiber reinforced thermoplastic composites. However, these different contributions have not yet been established.

Previous research has mainly focused on rice-husk and whole-rice-straw fiber reinforced thermoplastic composites. Ishak et al. (2001) and Premalal et al. (2002) studied the hygrothermal

* Reprint in part with permission from Industrial Crops and Products, Volume 28, Issue 1, Pages 63-72. Yao, F., Wu, Q. L., Lei, Y. & Xu, Y. J. 2008. Rice straw fiber-reinforced high-density polyethylene composite: Effect of fiber type and loading.

Table 5.1 The ranges of the chemical constituents in cell wall

Constituent (%)	Wood		Others			Rice straw			
	Softwood	Hardwood	Flax	Jute	Sisal	Husk	Whole straw	Leaf	Stem
Cellulose	40-45	45-50	64	64	66	35-45	41-57	37-41	24-46
Hemicellulose	25-30	21-36	17	12	12	19-25	33	22-25	24-28
Lignin	26-34	22-30	2	12	10	20	8-19	7-8	4-6
Residual ash	-	-	7	2	2	14-17	8-38	26-33	8-16

Sources: Jackson, 1977; Sundstøl, 1984; Mohanty et al., 2000; Bledzki et al., 2002; Martı′-Ferrer et al., 2006.

aging and mechanical properties of rice-husk/polypropylene. Panthapulakkal et al. (2005) and Martı′-Ferrer et al. (2006) presented the effect of coupling agents on properties of rice-husk/HDPE composites and rice-husk/block-copolymer-polypropylene, respectively. For whole-rice-straw/polymer composites, Grozdanov et al. (2006) studied the rice-straw/maleated-polypropylene composite containing 20 and 30 wt% rice straw by extrusion and compression molding. Higher tensile moduli were obtained for composites containing higher rice straw content. Kamel (2004) studied rice-straw/PVC composite with bagasse lignin as a coupling agent. The obtained composite showed superior properties, and the extent of improvement in mechanical properties and dimensional stability of composites depended not only on the pretreatment of rice straw, concentration of PVC and lignin, but also on pressure and pressing temperature. Few comparative studies have been so far conducted using various rice straw components to reinforce polymer composites. Thus, composite properties and individual contribution of various rice-straw components are of the primary research interest in this study.

Material recycling appears to be one of the important future routes for sustainable development in the polymer related industries. The recycling process generally consists of waste collection, separation, cleaning, drying, grinding, and repelletizing. Due to difference in their composition of recycled plastics and recycling process itself, the properties of composites from recycled plastics are expected to be significantly different from those of the corresponding virgin plastics. However, only limited work on natural fiber reinforcement of recycled PE has been done so far (Oksman and Lindberg, 1998; Viksne et al. 2004; Lei et al. 2007).

The objective of this study was to investigate the influence of various rice straw fiber components on mechanical, thermal, and crystalline properties of the reinforced HDPE composites using both virgin and recycled HDPE materials. Untreated rice straw was used in this study to obtain the elementary properties of rice-straw based HDPE composites. Future

publications in this series will deal with effect of chemical treatments (i.e., fiber surface modification with coupling agent) on the rice-straw-fiber/HDPE composites.

5.2 EXPERIMENTAL

5.2.1 Raw Material Preparation and Testing

Five kinds of reinforcing materials, including rice husk fiber (RHF), rice straw leaf fiber (SLF), rice straw stem fiber (SSF), rice whole straw fiber (WSF), and wood fiber (WF), were used in this study. Rice husk and whole rice straw were obtained from Louisiana State University (LSU) Ag Center's Crowley Rice Research Station in Crowley, LA. The harvested whole rice straw, consisting of stem, leaf blade, and leaf sheath, was divided into two parts. One part was milled directly to obtain the WSF. The second part was used to obtain rice straw leaf and stem as follows. Flexible leaf blades were removed from internodes first. Leaf sheath (i.e., the outmost layer of the stem fraction) was then separated by hand. SLF used in this study was composed of both leaf blade and sheath. The solid stem portion was considered as SSF. All rice fibers obtained were milled to pass through a 20-mesh screen. Pine (*Pinus sp.*) flour with a nominal 20-mesh particle size from American Wood Fibers Company (Madison, WI) was used as control. Virgin HDPE (VHDPE) 6761 and recycled HDPE (RHDPE) resin were purchased from Avangard Industries (Houston, TX). The resins are in the form of free-flowing granules and with the melt flow index (MFI) of 6.1 g/10 min and 0.7g/10 min (190°C, 2.16 kg), and density of 952 and 940 kg/m^3., respectively.

An imaging system was used for the fiber dimension measurement. The system consists of a Leica MZFIII microscope (Leica Microsystems, Wetzlar, Germany), a CCD digital camera (Diagnostic Instruments, Sterling Heights, MI), a u-Lux 1000 optical lighter (Volpi MFG USH Co., Auburn, NY), a RT SP402-115 power supply (Diagnostic Instruments), and a computer. For the measurement, about 100 mg fibers of each fiber type were randomly selected before

compounding. Each fiber sample was evenly placed on a glass dish under the microscope. The optical light was adjusted to achieve the best focusing alignment and image resolution. The fiber images were taken with a CCD digital camera and recorded with Spot Advanced imaging software (Diagnostic Instruments). Then, the Image-ProPlus 6.0 software (Media Cybernetics, Silver Spring, MD) was used to measure the length and diameter of individual fibers. The aspect ratio was described as the ratio of the fiber length and width for each fiber.

5.2.2 Compounding and Compression Molding

Prior to blending, all fiber was dried to 1–2% moisture content at 80°C. HDPE was used as received. Blend formulation included five fiber types (RHF, SLF, SSF, WSF, and WF), two plastics (VHDPE and RHDPE), and two fiber-plastics loading ratios (30 and 50 wt%), leading to a total of 20 blends. A two-roll rheomixer (Haake Rheomix 600) was used in blending with a typical mixing history of 3-minute HDPE loading/melting, 6-minute HDPE mixing, 1-minute fiber loading, and 5-minutes whole blend mixing. The blending was made at 165°C with a rotor speed of 60 rpm. Both mixing torque and temperature were monitored and recorded during compounding.

Each blend was removed from mixing chamber, cooled, and cut into smaller pieces suitable for feeding three-piece stainless steel compression molds to make 1- and 5-mm thick test sample plates. Compression molding was done with a Wabash V200 hot press (Wabash, ID) for 3- and 5-minute melting (for 1 and 5-mm thick specimens, respectively) under controlled pressure of 30 tons at 175°C temperature. Each sample was then cooled to room temperature under the pressure before being removed from the press. The sample plates were used to machine individual test samples as outlined below. Prior to sample testing, all specimens were conditioned for 72 h at a temperature of 23 ± 2°C and a relative humidity of 50 ± 5%.

5.2.3 Composite Property Testing

Compression-molded specimens were tested following ASTM standard D638-03 for tensile properties and D256-05 for notched Izod impact strength. An INSTRON machine (Model 1125, Boston, MA) and A TINIUS 92T impact tester (Testing Machine Company, Horsham, PA) were used for tensile strength and Izod impact strength, respectively. Six replicates were tested for each property under each formulation. Storage modulus E′ and loss modulus E″ of samples were determined by TA Instruments DMA Q800 (New Castle, DW) using dual cantilever mode. Six replicates were cut from each compressed test plate (100 × 60 × 1 mm) for each blend. The measurements were carried out at a frequency of 1 Hz at room temperatures.

Wide angle X-ray diffraction (XRD) analysis was carried out to investigate the effect of the fiber on crystallization behavior of HDPE. A 2θ range from 5º to 35º in reflection mode was scanned at a 2º/min. A computer-controlled wide angle goniometer coupled to a sealed-tube source of $Cu-K_a$ radiation (λ =1.54056Å) was used. The $Cu-K_a$ line was filtered electronically with a usual thin Ni filter. Usual diffraction parameters, such as 2θ, full width at half-maximum (FWHM), and integral intensity were measured and analyzed using Rigaku software. The average size of the crystals (crystalline thickness) and crystallinity level of composites were calculated from both (110) and (200) plane diffraction peaks using Bragg's law and Scherrer formula with the instrument width of 0.16º. A differential scanning calorimeter (DSC, TA Q100) was used to study the crystallization and melting behavior of composites. Each blended composite sample (4.5±0.3 mg) was heated in a DSC pan from room temperature to 180°C and maintained at the temperature 10 min before being cooled to room temperature. The sample was then underwent a second heating from room temperature to 180°C. All scans were carried out at a heating rate of 10°C/min. The first heating run was used to erase the thermal history of composites. The data of cooling run were used to analyze the crystallization

information. The second heating run was conducted to prove the accuracy of results from cooling run after comparing their melting enthalpy with crystallization enthalpy from cooling run.

5.2.4 Statistics Method

Duncan's multiple range tests for pair-wise comparison were used to test the effect of various treatments on the composite properties using SAS (SAS Institute Inc., NC).

5.3 RESULT AND DISCUSSION

5.3.1 Fiber Dimension Distribution

Typical fiber images are shown in Fig. 5.1, and Table 5.2 lists the average dimension parameters (i.e., length, width, and aspect ratio) of various fibers. Among the five fibers, WF had the smallest average dimension (i.e., 0.57 and 0.15 mm for length and width respectively) and relatively low average aspect ratio (4.38). RHF had the largest average width (i.e., 0.49 mm) and smallest average aspect ratio (3.41). The other three fibers had values in the between. Fiber dimension distribution (Fig. 5.2) offered a complementary view of average fiber size. For fiber length (Fig. 5.2a), around 50% WFs were less than 0.5 mm long, while 50% SSFs were longer than 1.5 mm. However, WF had the narrowest range while SSF had the widest range with respect to the other fibers. Therefore, WF was more uniform in fiber length, while SSF was the most inhomogeneous. RHF and SLF had the similar length distribution. The dimension distribution curve of WSF, which was the mainly composed of SLF and SSF as well as some awn and auricle fibers, was consequently between SLF and SSF curves. For aspect ratio (Fig. 5.2b), obvious left shift curve of RHF indicated the "square-like" feature of RHF compared with other fibers. SSF and SWF had better fiber configuration with half of them reaching 5 and one-fifth of them exceeding 10 on aspect ratio. SLF was similar with WF on aspect ratio distribution. However, SLF had more fibers with aspect ratio greater than 5 compared with WF.

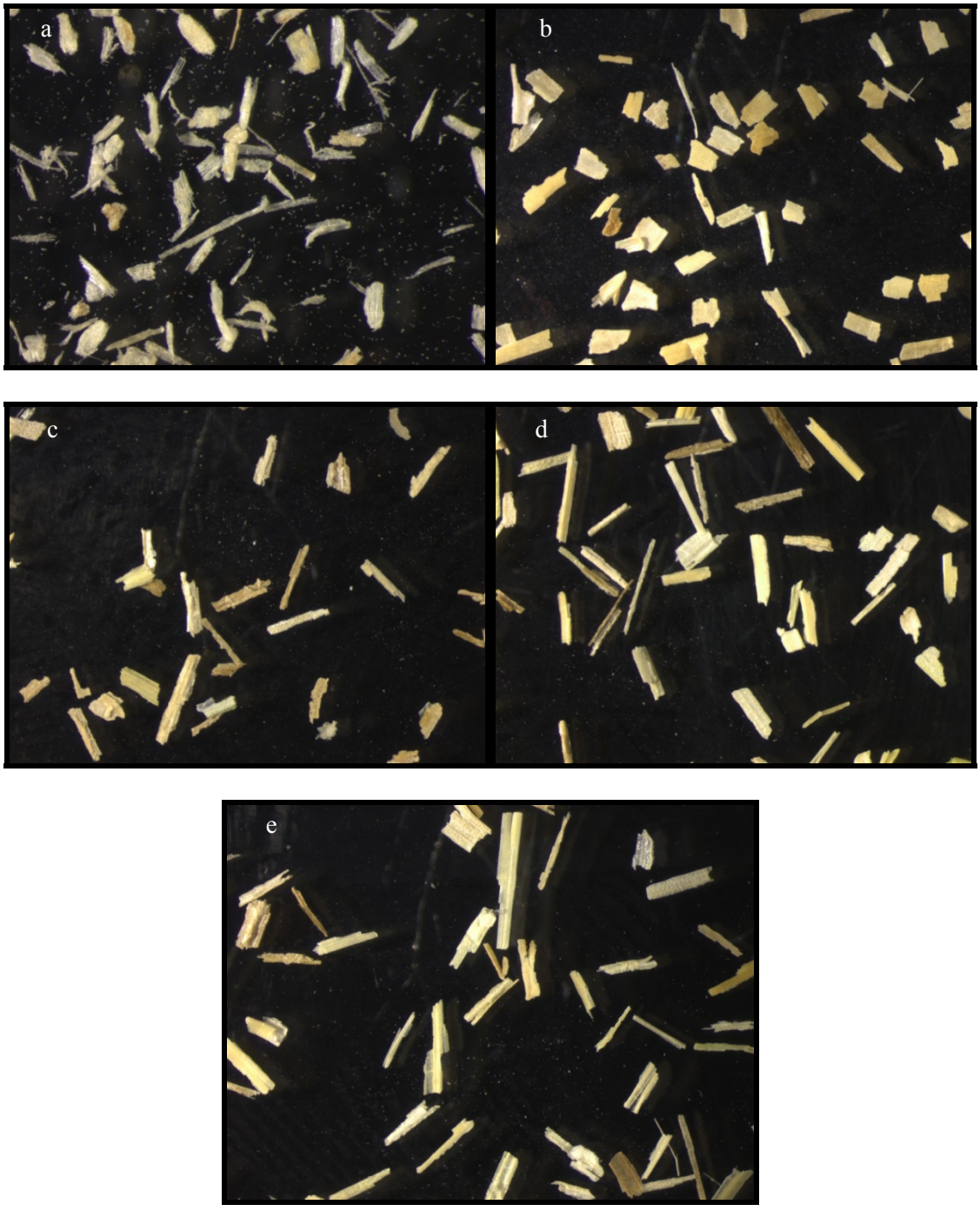

Fig. 5.1 Photographs of selected fibers: (a) Wood, (b) Rice husk (c) Rice straw leaf, (d) Rice straw stem, and (e) Rice straw whole straw. Magnification: (a) = 16x; (b) to (e) = 8x.

Table 5.2 Comparison of the fiber dimension of selected fiber types

Fiber Type	Number of Fiber Samples	Average Length (mm)	Average Diameter (mm)	Average Aspect Ratio
Wood	1635	0.57 (.01) E[1]	0.15 (.09) D	4.38 (2.50) C
Rice husk	651	1.21 (.40) D	0.49 (.19) A	3.41 (3.74) D
Straw leaf	743	1.30 (.46) C	0.36 (.15) B	4.52 (3.62) C
Straw stem	842	1.71 (.76) A	0.34 (.17) C	6.81 (6.66) A
Whole straw	787	1.53 (.70) B	0.35 (.16) BC	5.93 (6.27) B

[1]The values in parentheses are standard deviation. Means with the same letter for each property were not significantly different at the 5% significance level.

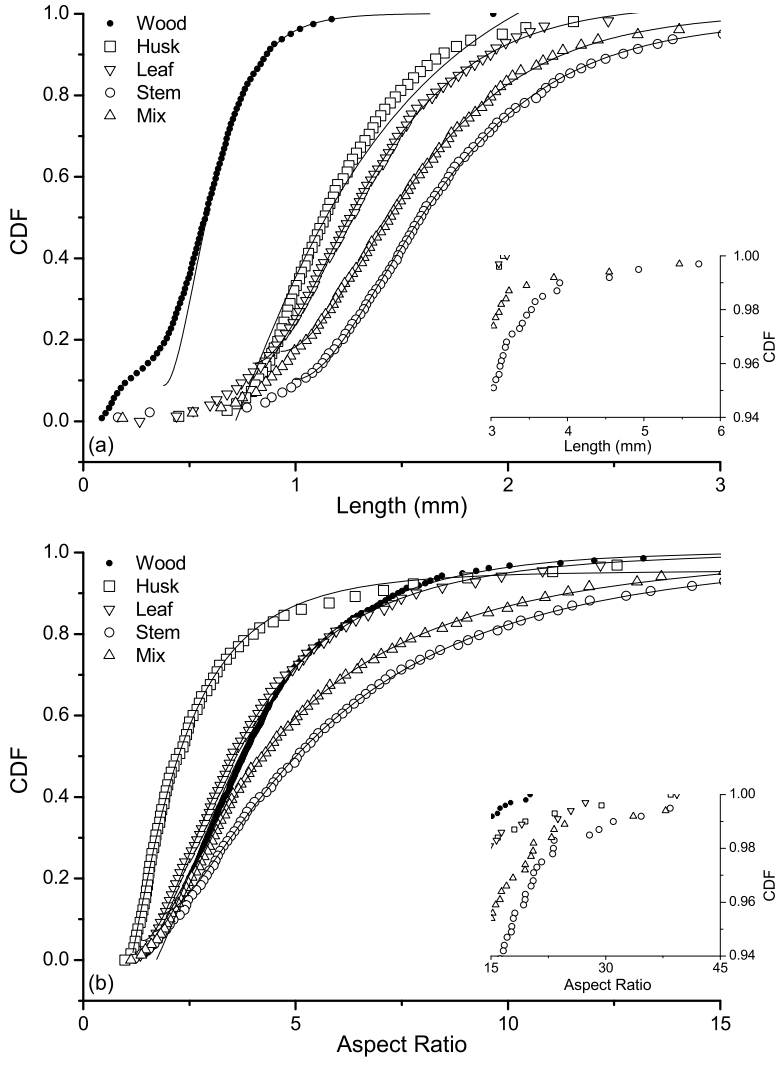

Fig. 5.2 Lognormal fit on dimension distribution of selected fibers after milling: (a) Length distribution; (b) Aspect ratio distribution. Solid lines: fitting curves.

As shown in Fig. 5.2, the cumulative distribution function (CDF) of various fibers fitted a lognormal distribution well (Lu et al. 2006):

$$f(X \mid \mu, \sigma) = \frac{1}{X\sqrt{2\pi\sigma^2}} \exp\left[-\frac{(\ln X - \mu)^2}{2\sigma^2}\right] \quad (5.1)$$

where, $f(X)$ is the probability density function (PDF) of X. The independent variable, X, is the fiber length or diameter with the unit of millimeter ($X \geq 0$). In addition, μ and σ are the location and shape parameters, respectively.

5.3.2 Mechanical Properties of the Composites

Compared with properties of neat VHDPE, fiber reinforced VHDPE composites had relatively larger storage modulus (E') and loss modulus (E''), but reduced tensile and impact strength. The trend was more obvious at the higher fiber loading level (Table 5.3). However, the influences of fiber on mechanical properties of resultant composites varied with fiber type. For instance, VHDPE/RHF composites had the lowest moduli at both fiber loading rates with respect to the other four composites. In addition, no significant differences were observed for other four composites with 30 wt% fibers loading (Table 5.3). However, when 50 wt% fibers were used, the difference was significant. VHDPE/WSF composites had the most increment on moduli compared to other composites (Fig. 5.3a). SLF and SSF showed a similar reinforcement effect for composites. For tensile strength of the VHDPE composites, the VHDPE/SSF composites showed the lowest tensile strength compared to other four composites under both fiber loading rates (Table 5.3 and Fig. 5.3b). In addition, no significant difference was noticed among all other four composites. For impact strength (Fig. 5.3c), RHF showed the best reinforcement effect compared to the other fibers at the 30 wt% fiber loading, but the effect of RHF was not reduced at the 50% fiber loading level.

Table 5.3 Effect of fiber type and fiber loading on mechanical properties of VHDPE/fiber and RHDPE/fiber composites

Composite type		Fiber loading (%)	Storage modulus (GPa)	Loss modulus (GPa)	Tensile strength (MPa)	Impact strength (kj/m^2)
Matrix	Fiber					
Virgin HDPE	none	0	1.61 (0.07) [1,2]	0.14 (0.00)	29.5 (0.9)	3.89 (0.15)
	WF	30	2.17 (0.17) A	0.17 (0.01) A	19.0 (1.0) A	3.25 (0.14) C
	RHF		1.67 (0.15) B	0.14 (0.01) B	19.0 (1.2) A	3.95 (0.05) A
	SLF		2.10 (0.21) A	0.18 (0.01) A	19.3 (0.9) A	3.26 (0.11) C
	SSF		2.13 (0.18) A	0.18 (0.01) A	18.0 (1.3) B	3.61 (0.17) B
	SWF		2.11 (0.14) A	0.17 (0.01) A	19.0 (1.3) A	3.60 (0.30) B
	WF	50	3.63 (0.40) B	0.25 (0.03) B	17.3 (0.9) A	2.45 (0.11) B
	RHF		2.64 (0.29) D	0.18 (0.02) D	17.1 (1.1) A	2.41 (0.13) B
	SLF		2.88 (0.18) C	0.21 (0.01) C	17.0 (1.6) A	2.32 (0.13) B
	SSF		2.95 (0.19) C	0.23 (0.02) C	13.9 (1.6) B	2.79 (0.23) A
	SWF		4.02 (0.28) A	0.28 (0.02) A	16.5 (0.8) A	2.76 (0.21) A
Recycled HDPE	none	0	1.55 (0.12)	0.15 (0.00)	32.4 (1.6)	13.19 (0.85)
	WF	30	2.51 (0.17) A	0.19 (0.01) A	23.1 (1.6) A	5.60 (.39) C
	RHF		1.98 (0.08) C	0.15 (0.01) C	19.7 (1.4) C	7.42 (.78) A
	SLF		2.13 (0.13) BC	0.17 (0.01) B	21.7 (0.9) B	5.99 (.34) B
	SSF		2.48 (0.21) A	0.19 (0.02) A	21.2 (0.7) B	7.56 (.57) A
	SWF		2.24 (0.21) B	0.18 (0.01) AB	21.5 (1.9) B	6.62 (.25) B
	WF	50	3.88 (0.32) A	0.25 (0.02) A	21.0 (2.6) A	3.63 (.39) C
	RHF		2.60 (0.11) D	0.19 (0.01) C	17.3 (1.2) C	4.37 (.15) B
	SLF		2.98 (0.35) C	0.23 (0.02) B	19.1 (1.6) B	3.60 (.19) C
	SSF		3.31 (0.15) B	0.24 (0.01) B	19.3 (1.0) B	4.85 (.28) A
	SWF		2.97 (0.20) C	0.22 (0.01) B	19.4 (1.6) B	4.24 (.65) B

[1]The values in parentheses are standard deviation.
[2]Means with the same letter for each property were not significantly different at the 5% significance level.

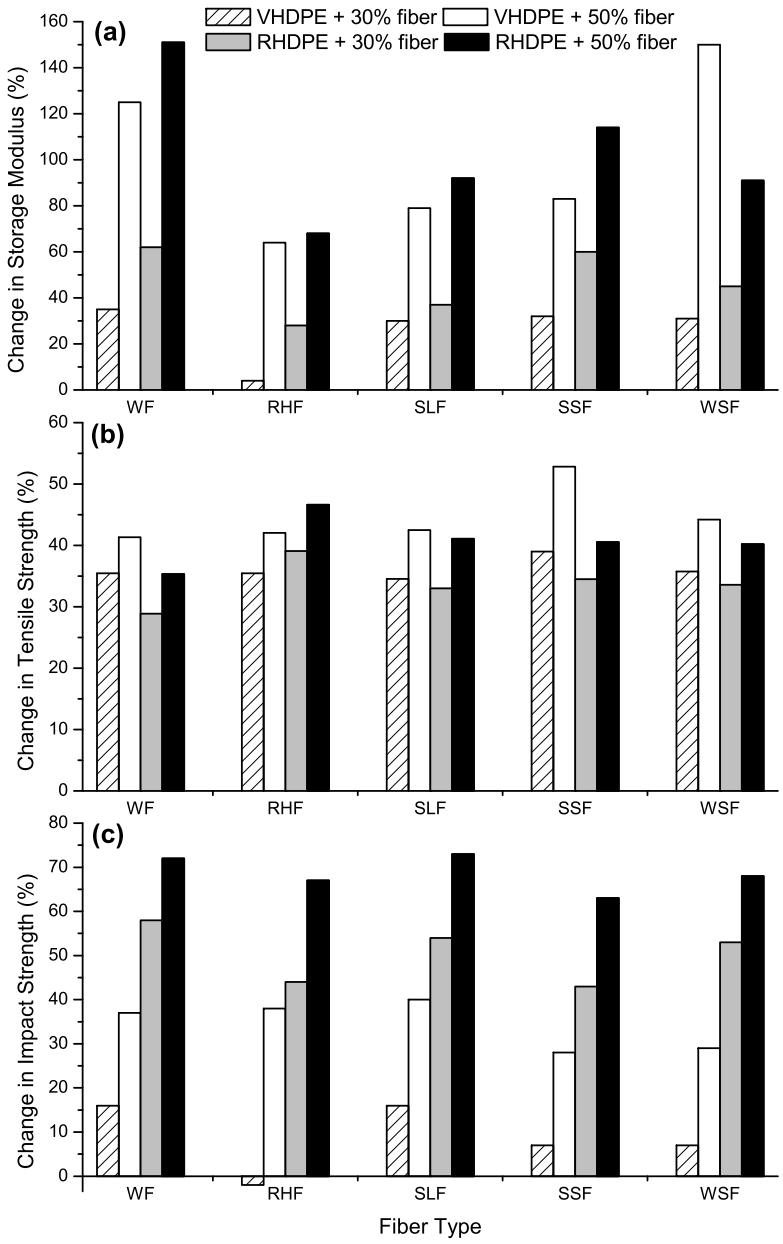

Fig. 5.3 Comparison of the influence of composite type and fiber loading rate on (a) Storage modulus, (b) Tensile strength, and (c) Impact strength of resultant composites. Property change (%) = (Composite property – Neat polymer property)/Neat polymer property. Numbers: (1) VHDPE/fiber composites with 30 wt% fiber loading, (2) VHDPE/fiber composites with 50 wt% fiber loading, (3) RHDPE/fiber composites with 30 wt% fiber loading, (4) RHDPE/fiber composites with 50 wt% fiber loading.

Similar to VHDPE/fiber composites, fiber reinforced recycled-HDPE (RHDPE) composites also had relatively better storage modulus (E') and loss modulus (E''), but reduced tensile and impact strength (Table 5.3) compared with neat RHDPE. In addition, the influences of different types of fiber on mechanical properties of RHDPE/fiber composites were different. For E' and E'', WF reinforced RHDPE composites showed the highest values compared to other composites under both fiber loading rates, while RHDPE/RHF composites presented a lowest E' and E''. This was probably caused by their different cellulose and residual ash contents. In addition, the "square-like" shape of RHF, indicated by their lowest aspect ratio, also made RHF to contribute less on stress dispersion than those "higher respect ratio" fibers. For the same reason, VHDPE/SSF composites presented a second better E' and E'' value benefiting from relative "higher" aspect ratio of SSF. Moreover, it is observed that moderate aspect ratio of SLF and SWF led to moderate E' and E''.

The tensile strength of RHDPE/fiber composites was worse than that of neat RHDPE and decreased with fiber content increase (Table 5.3). Especially, RHF had the most negative effect on the tensile strength of resultant composites with a value of 19.7 MPa, only approximately half of neat RHDPE strength value (Fig. 5.3b). WF presented better performance compared with other three rice-straw fibers. Also, no significant difference among three rice-straw reinforced composites was observed. For impact strength, however, SSF and WSF showed better performance than SLF under both fiber loading rates (Fig. 5.3c). The result also showed that adding 30 wt% RHF had no influence on impact strength of composites. However, increasing RHF from 30 to 50 wt% decreased the impact strength dramatically (40% down).

5.3.3 Crystallization Behavior from XRD

Typical XRD curves of the neat VHDPE and RHDPE as well as two composites in the 2θ range of 5º to 35º spectra are shown in Fig. 5.4. The characteristic sharp peaks appearing at

2θ between 20 to 25º correspond to HDPE. The strongest peak presented at the position of 21.43º corresponds to (110) reflection crystalline plane, which has a d -spacing of 4.15 nm according to the Bragg's Law:

$$2d\sin\theta = n\lambda \qquad (5.2)$$

where d is the distance between crystallographic planes, and θ is half of the angle of diffraction, n is an integer, and λ is the wavelength of the X-ray. The second strongest peak presented at the position of 23.80º corresponds to (200) reflection crystalline plane which has a d -spacing of 3.74 nm.

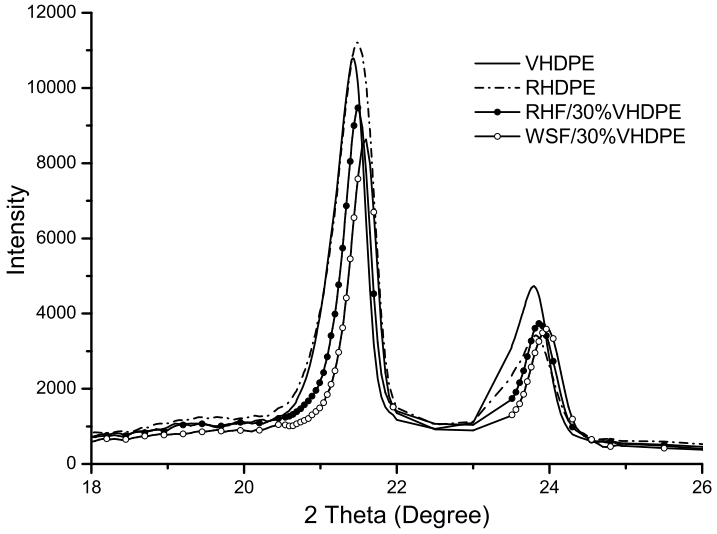

Fig. 5.4 XRD curves of the neat VHDPE and RHDPE at a scan rate of 2º/min for 2θ angles from 5° to 35°.

Peak positions of the major reflection crystalline planes, (100) and (200) planes, of VHDPE are listed in Table 5.4. As shown in Table 5.4, no obvious changes on characteristic

peak position of VHDPE systems were observed after introducing the fiber. The crystalline thickness, however, was found changing remarkably according to the Scherrer formula:

$$L_{hkl} = \frac{K\lambda}{\beta_0 \cos\theta} \tag{5.3}$$

where L_{hkl} is the crystalline thickness perpendicular to the reflection plane; β_0 is line broadening (rad) by reference to a standard using the formula $\beta_0^2 = \beta_m^2 - \beta_s^2$, where β_s is the half width of the standard material in radians; K is the shape factor of crystalline thickness, related to β_0 and L_{hkl}. When β_0 is defined as the half-height width of diffraction peaks, K = 0.9.

The crystalline thickness perpendicular to the crystal plane of neat VHDPE are 18.76 nm for the (110) plane and 16.07 nm for the (200) plane. As shown in Table 5.4, the introduction of fiber increased the crystalline thickness obviously. A 7-24% increase was gained for (110) plane and a 17-22% increase for (200) plane with 30 wt% fiber loading. Moreover, when fiber content increased to 50 wt%, the crystalline thickness of VHDPE on (100) and (200) planes increased more, 21-36% and 26-34%, respectively. The reason for this result might be that adding natural fiber to the system can increase the crystallization rate of the VHDPE partially because a single fiber can act as an effective heterogeneous nucleation agent for VHDPE crystallization. The crystalline thickness of VHDPE in VHDPE/SLF, VHDPE/SSF and VHDPE/WSF composites was larger than that in VHDPE/WF and VHDPE/RHF composites (Table 5.4) probably contributing to more long fibers in their system which might help crystals grow. Particularly, WF had the smallest fiber dimension and consequently led to the obviously smallest crystalline thickness of VHDPE among the four other composites on both (110) and (200) planes.

The crystalline thickness perpendicular to the crystal plane of neat RHDPE are 15.85 nm for the (110) plane and 15.11 nm for the (200) plane (Table 5.4). No obvious changes on

Table 5.4 Crystalline peaks position and crystal thickness of VHDPE/fiber and RHDPE/fiber hybrids

Composite Type		Fiber loading (%)	Peak position 2θ (°)		Crystal thickness (nm)	
Matrix	Fiber		(110)	(200)	L_{110}	L_{200}
Virgin HDPE	none	0	21.43	23.80	18.76	16.07
	WF	30	21.17	23.52	20.04	18.87
	RHF		21.49	23.87	22.68	19.27
	SLF		21.37	23.76	23.33	19.22
	SSF		21.46	23.83	23.11	19.67
	SWF		21.60	23.96	23.11	18.98
	WF	50	21.43	23.80	22.75	20.35
	RHF		21.44	23.83	23.71	20.30
	SLF		21.42	23.83	24.26	19.56
	SSF		21.60	23.92	25.54	20.64
	SWF		21.38	23.76	24.92	21.52
Recycled HDPE	none	0	21.48	23.82	15.85	15.11
	WF	30	21.50	23.88	21.94	19.12
	RHF		21.46	23.80	23.94	21.70
	SLF		21.40	23.76	23.63	21.10
	SSF		21.47	23.84	23.27	20.41
	SWF		21.55	23.89	22.75	20.47
	WF	50	21.30	23.68	22.13	18.60
	RHF		21.48	23.83	26.48	20.25
	SLF		21.12	23.52	24.16	21.39
	SSF		21.22	23.56	26.97	19.92
	SWF		21.15	23.50	24.91	19.91

characteristic peak position of RHDPE were observed after introducing the fiber. However, the introduction of fiber increased the crystalline thickness of RHDPE in composites obviously with respect to neat RHDPE. With 30 wt% fiber loading, RHDPE/WF composites had the smallest crystalline thickness on both (110) and (200) planes while RHDPE/RHF composites had the largest thickness. Surface feature of fibers probably contributed to this result. WF had a fusy surface structure, which might interfere with the crystallization of RHDPE, whereas RHF had a relatively smooth surface, which could benefit for crystallization. Due to long fibers, RHDPE/SLF and RHDPE/SSF composites as well as RHDPE/WSF composites had also larger crystalline thickness compared with RHDPE/WF composites. When fiber loading increased to 50 wt%, similar to VHDPE, the crystalline thickness of RHDPE on (110) plane increased in each kind of composite. However, the crystalline thickness of RHDPE on (200) plane significantly decreased in RHDPE/WF, RHDPE/SSF and RHDPE/WSF composites.

5.3.4 Crystallization and Melting Behavior from DSC

The DSC curves are shown in Fig. 5.5 using VHDPE/fiber composites as example, and DSC results of all neat matrix and composites are summarized in Table 5.5. T_o and T_m are peak temperatures of crystallization and melting, respectively. Peak heat flow of cooling run, H_p, presented peak crystallization rate of polymer. The normalized crystallization degree, X_R, was determined as follows (Ganan and Mondragon, 2003),

$$X_R = (\Delta H / \Delta H_M) \times 100\% \qquad (5.4)$$

where ΔH is the melting or (crystallization enthalpy) for composite sample and ΔH_M is the melting (or crystallization) enthalpy of neat matrix.

Generally, the introduction of fiber increased the crystallization and melting temperature of VHDPE at both fiber loading rates (Table 5.5). However, this influence was not significant,

especially when 50wt% fibers were added (≤ 1 ºC). The influence of added fiber on crystallization degrees of VHDPE was significant (Fig. 5.6a). For example, introducing WF and SSF in the matrix, the X_R increased dramatically (16 and 11%) and the increment reached 19 and 17% when 50wt% fibers were added. Also, introducing RHF and SLF, the X_R increased slightly at 30wt% fiber loading. However, different fibers influenced X_R differently. For instance, WF and SSF/VHDPE composites not only had higher X_R, but also had higher H_p (1.61 and 1.63 W/g at 50wt% fiber loading, respectively). The higher H_p indicated that both of them had higher crystallization rates which caused by more prominent nucleation in interfaces between fibers and matrix. However, VHDPE/WF composite had a small crystal thickness,

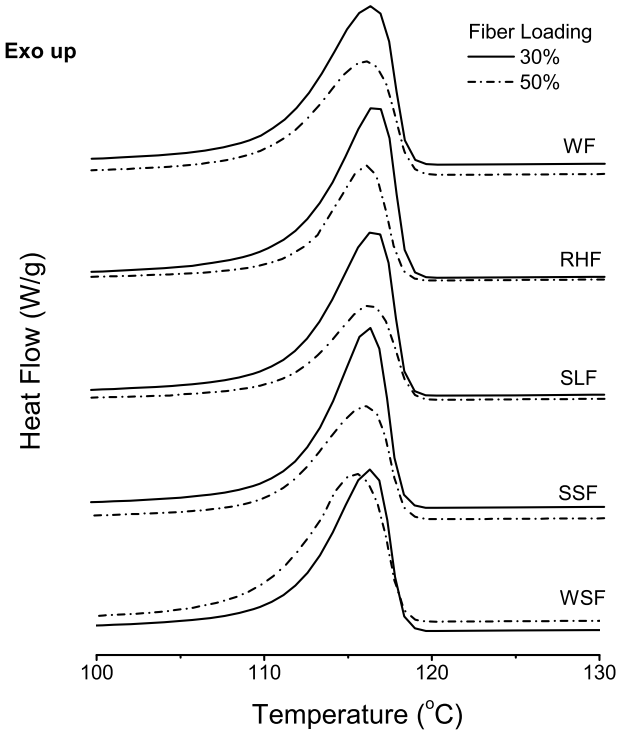

Fig. 5.5 DSC curves of the VHDPE/fiber composites.

Table 5.5 DSC result of VHDPE/fiber and RHDPE/fiber composites

Composite Type		Fiber loading	Cooling			2nd Heating	
Matrix	Fiber	(%)	T_c (ºC)	X_R (%)	H_p (W/g)	T_m (ºC)	X_R (%)
Virgin HDPE	none	0	115.6	100	3.41	130.5	100
	WF	30	116.4	116	2.74	132.3	118
	RHF		116.7	102	2.56	132.2	102
	SLF		116.6	105	2.66	131.7	105
	SSF		116.2	111	3.12	131.5	112
	SWF		116.3	100	2.61	131.8	101
	WF	50	116.1	119	1.61	132.3	115
	RHF		116.1	96	1.73	131.9	97
	SLF		116.4	97	1.37	132.0	97
	SSF		116.6	117	1.63	131.2	118
	SWF		115.5	94	1.43	133.3	95
Recycled HDPE	none	0	114.0	100	0.85	136.4	100
	WF	30	113.9	98	0.72	135.3	97
	RHF		115.8	82	0.48	133.3	80
	SLF		114.9	108	0.94	134.2	108
	SSF		115.5	92	0.76	133.3	92
	SWF		115.0	91	0.67	133.3	91
	WF	50	115.0	94	0.54	133.3	94
	RHF		114.9	87	0.41	134.1	88
	SLF		115.2	103	0.53	133.4	102
	SSF		117.7	108	1.03	130.5	106
	SWF		116.1	128	0.92	131.2	128

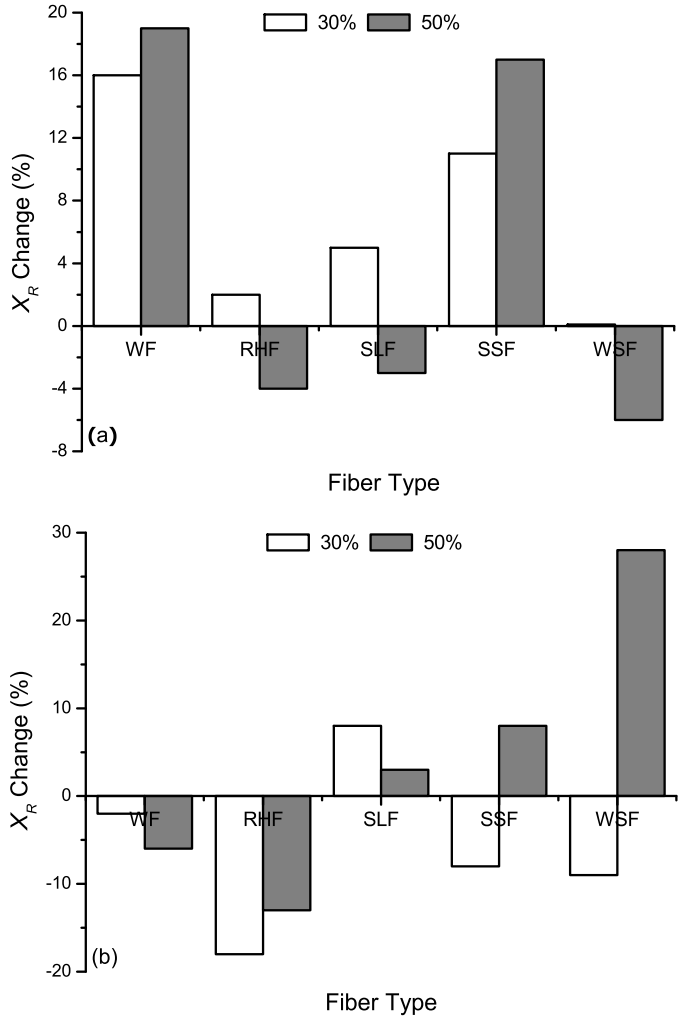

Fig. 5.6 The trend of X_R change of (a) VHDPE/fiber and (b) RHDPE/fiber composites with both fiber loading (30 and 50 wt%). Property change (%) = (Composite property – Neat polymer property)/Neat polymer property.

which was observed from XRD study, while VHDPE/SSF composite had a large thickness on both (110) and (200) crystalline phase (Table 5.4). Therefore, the crystallization of VHDPE in VHDPE/WF composites was caused by fast nucleation from "small" nucleate agents while the crystallization of VHDPE/SSF composites was by "big" ones. The introduction of RHF, SLF and

WSF changed X_R slightly (0-6%). Also, with 50wt% fiber loading, the X_R showed a moderate decrease with respect to 30wt% fiber loading. It indicated less nucleation compared to WF and SSF composites, especially at higher fiber loading. Noticeably, though mainly composed of SLF and SSF, WSF did not impose an average effect of these two on crystallization of VHDPE – lower than both two at a certain fiber loading rate. It was probably because of the low fibrous and miscellaneous awn and auricle fibers in WSF which might resist the crystal growth of polymer. Therefore, the X_R decreased when more WSF was added.

Different with VHDPE, the introduction of fiber increased the crystallization temperature but decreased the melting temperature of RHDPE composites (Table 5.5). It implies an improvement on the processing temperature of RHDPE after filling selected fibers. Based on peak temperature changes, SSF presented the best improvement especially at 50wt% fiber loading (5.9 and 3.7ºC change on T_o and T_m, respectively). Also, other paddy-based fibers (SLF and WSF) showed better performance than WF. WF had the smallest dimension but did not benefit for this improvement due to their strong hydrogen bond.

Fiber type influenced crystallization degree of RHDPE dramatically (Fig. 5.6b). Introducing 30wt% fiber in matrix, for instance, SLF was observed to increase the crystallization degree of RHDPE around 8%. However, other four fibers all presented negative influences on X_R of RHDPE. Particularly, RHF composites had an 18% decrement on X_R after introducing RHF in matrix. Associated with the lowest H_p of RHF composite, the RHF might decrease the crystallization rate of RHDPE and consequently resist the re-crystallization of RHDPE strongly. Comparatively, WF did not influence crystallization behavior of RHDPE significantly (only change 2% on X_R and 0.1ºC on T_o, respectively). SSF and WSF presented a moderate influence

on X_R (8-9% change). Results also showed that, with 50wt% fiber loading, rice-straw-based fibers (SLF, SSF and WSF) increased X_R of RHDPE while WF and RHF decreased X_R.

5.4 CONCLUSIONS

Composites based on virgin and recycled high density polyethylene and five types of natural fibers were made and their properties characterized. The cumulative percentage distribution of length and aspect ratio of various fibers after milling fitted a lognormal distribution well with two parameters defining the curve location and shape. The mechanical properties of both VHDPE and RHDPE rice straw fiber composites were comparable with these of wood composites. Increased moduli and decreased tensile and impact strength of composites were observed when increasing fiber loading. Particularly, rice husk HDPE composites had the smallest storage moduli, but their impact strength was comparable or better than that of other straw fiber composites. Very little difference in mechanical properties existed among rice straw leaf, stem, and whole straw fiber composites. The particular recycled HDPE resin and its composites had significantly better moduli and strength properties compared to the virgin HDPE systems probably due to additives used during initial processing. XRD and DSC experiments were carried out to investigate the effect of the fiber on crystallization behavior of HDPE in composites. The results showed that introducing fiber to HDPE matrix did not change characteristic peak position, but the fiber increased crystalline thickness of HDPE system. DSC experiments showed higher crystallization rates for VHDPE than RHDPE indicated by their significantly larger peak heat flow during cooling run. The use of fiber in both resin systems led to the reduced peak heat flow rate.

This study showed that rice straw fibers can work well with both VHDPE and RHDPE as reinforcing filler. Also, different components of rice straw had no significant influence on mechanical properties of composites. This might imply the application prospect of conveniently

introducing rice straw into thermoplastic composite industry. However, it also implied that special attention should be paid to rice husk composites due to their different mechanical behavior with composites made by other straw components.

5.5 REFERENCES

Bledzki, A. K. and J. Gassan (1999). "Composites reinforced with cellulose based fibres." *Progress in Polymer Science* 24(2): 221-274.

Bledzki, A.K., Sperber, V.E., Faruk, O, (2002). Natural and wood fibre reinforcement in polymers. *Rapra Review Reports*, 13, 152.

Ganan, P. and I. Mondragon (2003). "Thermal and degradation behavior of fique fiber reinforced thermoplastic matrix composites." *Journal of Thermal Analysis and Calorimetry* 73(3): 783-795.

Grozdanov, A., A. Buzarovska, et al. (2006). "Rice straw as an alternative reinforcement in polypropylene composites." *Agronomy for Sustainable Development* 26(4): 251-255.

FAO, (2006). "Rice market monitor." June, Volume IX - Issue No. 2

Ishak, Z. A. M., B. N. Yow, et al. (2001). "Hygrothermal aging and tensile behavior of injection-molded rice husk-filled polypropylene composites." *Journal of Applied Polymer Science* 81(3): 742-753.

Jackson, M.G., (1977). Review article: the alkali treatment of straws. *Animal Feed Science and Technology*, 2, 105-130.

Kamel, S. (2004). "Preparation and properties of composites made from rice straw and poly(vinyl chloride) (PVC)." *Polymers for Advanced Technologies* 15(10): 612-616.

Lei, Y., Q. Wu, et al. (2007). "Preparation and properties of recycled HDPE/natural fiber composites." *Composites Part A: Applied Science and Manufacturing* 38(7): 1664-1674.

Lu, J. Z., Q. L. Wu, et al. (2006). "The influences of fiber feature and polymer melt index on mechanical properties of sugarcane fiber/polymer composites." *Journal of Applied Polymer Science* 102(6): 5607-5619.

Marti-Ferrer, F., F. Vilaplana, et al. (2006). "Flour rice husk as filler in block copolymer polypropylene: Effect of different coupling agents." *Journal of Applied Polymer Science* 99(4): 1823-1831.

Mohanty, A. K., M. Misra, et al. (2000). "Biofibres, biodegradable polymers and biocomposites: An overview." *Macromolecular Materials and Engineering* 276(3-4): 1-24.

Oksman, K. and H. Lindberg (1998). "Influence of thermoplastic elastomers on adhesion in polyethylene wood flour composites." *Journal of Applied Polymer Science* 68(11): 1845-1855.

Panthapulakkal, S., M. Sain, et al. (2005). "Effect of coupling agents on rice-husk-filled HDPE extruded profiles." *Polymer International* 54(1): 137-142.

Premalal, H. G. B., H. Ismail, et al. (2002). "Comparison of the mechanical properties of rice husk powder filled polypropylene composites with talc filled polypropylene composites." *Polymer Testing* 21(7): 833-839.

Sundstøl, F., (1984). Straw and other fibrous by-products as feed. Amsterdam, New York: Elsevier.

USDA, (2006). "World agricultural supply and demand estimates." July 12, WASDE-436-2

Viksne, A., L. Rence, et al. (2004). "The effect of paraffin on fiber dispersion and mechanical properties of polyolefin-sawdust composites." *Journal of Applied Polymer Science* 93(5): 2385-2393.

Wollerdorfer, M. and H. Bader (1998). "Influence of natural fibres on the mechanical properties of biodegradable polymers." *Industrial Crops and Products* 8(2): 105-112.

CHAPTER 6 RICE STRAW FIBER REINFORCED HIGH DENSITY POLYETHYLENE COMPOSITE: EFFECT OF COUPLED COMPATIBILIZATING AND TOUGHENING TREATMENT

6.1 INTRODUCTION

The use of compatibilizers in natural fiber reinforced polymer composites (NFPC) is to improve poor interphase between hydrophilic fiber and hydrophobic polyolefin matrix. Among numerous compatibilizers, maleic anhydride (MA) grafted PE and PP (PE-g-MA or PP-g-MA) are considered to be some of the most effective interphase modifiers for polyolefin/wood/natural fiber composite due to the polar interaction and covalently link between anhydride carbonyl and hydroxyl groups of the fiber surfaces (Kazayawoko et al. 1999a; Kazayawoko et al. 1999b; Kazayawoko et al. 1997; Matuana et al. 2001), as well as their good compatibility with matrix (Lai et al. 2003; Li and Matuana 2003; Lu and Wu 2005; Lu et al. 2005; Wang et al. 2003).

Various polyolefinic elastomers, including styrene/ethylene-butylenes/styrene triblock copolymer (SEBS) (Lai et al. 2003; Oksman 1996; Oksman and Lindberg 1998; Oksman et al. 1998; Wang et al. 2003) and ethylene/propylene/diene terpolymer (EPDM) (Oksman and Clemons 1998; Park and Balatinecz 1997), have also been of interest because of enhanced performance on impact strength of pure HDPE and PP matrix. However, the addition of elastomers alone fails to effectively improve the strength and modulus of final composites. Their use even weakens composite strength and modulus properties, although the impact toughness is more or less improved depending on the nature and content of elastomers used. To optimize the balance between stiffness/strength and toughness of NFPC, combination of elastomers with maleated polyolefins as combined modifiers has been reported (Oksman and Clemons 1998; Rana et al. 2003; Sombatsompop et al. 2005). For instance, Oksman and Clemons (1998) studied mechanical properties and morphology of impact modified PP/wood-flour composites, and

observed that adding combined 10phr SEBS-g-MA and 2phr PP-g-MA into the system exhibited more superior impact strength improvement than adding either 10phr SEBS-g-MA or 2phr PE-g-MA individually. The tensile strength of system was less decreased even by the incorporation of 10phr SEBS-g-MA. However, the same improvement was not observed in the EPDM/PP-g-MA or EPDM-g-MA/PP-g-MA modified system. Sumbatsompop et al. (2005) investigated the effect of combining both PP-g-MA and other impact modifiers into PP/wood-sawdust system, and suggested that 2.0wt% PP-g-MA concentration into the composites containing 11.1wt% total impact modifier could optimize overall mechanical properties. Although some work has been done, there is a lack of understanding on how the ratio of the combined modifiers affects various mechanical properties of the resultant composites.

Ethylene/propylene copolymer (EPR) is one of the polyolefin-based thermoplastic elastomers. It offers excellent thermal/oxidative stability and weatherability compared with conventional EPDM due to its fully saturated backbone. MA functionalized EPR (EPR-g-MA) could further increase both filler-matrix adhesion and impact strength by promoting the favorable core-shell encapsulation (Dubnikova et al. 2002; Wang et al. 1996). Moreover, EPR copolymers are generally classified into semi-crystalline and amorphous ones depending on stereoregularity and composition of the monomer sequence. The former is considered somewhat better for improving various properties of matrix than the latter in some research (Okada et al. 2001).

The study described in previous chapters showed that rice straw (RS) fibers can be successfully used as reinforcement filler for high density polyethylene (HDPE) matrix. It also showed that different components of rice straw had no significant influence on the mechanical properties of composites. Thus, the whole rice straw fiber can be conveniently used for the composite process. Some work has been done in this field. Beyond the studies (Grozdanov et al. 2006; Kamel 2004) reviewed in the last chapter, Habibi et al. (2008) recently reported

mechanical, thermal and morphology properties of various lignocellulosic fiber including RS filled low density polyethylene (LDPE) or LDPE-g-MA composites using extrusion-molding. They found that better compatibility and enhanced mechanical properties were obtained when using LDPE-g-MA as compatibilizer. However, rice-straw has not been widely used as reinforced filler for polymer system compared to wood. Moreover, there is a lack of detailed investigation on the effect of various compatibilizers on HDPE/RS system at this point. The objective of the study described in this chapter was to investigate the influence of various compatibilizers, including PE-g-MA, EPRs, and their combinations on mechanical and thermal properties, as well as morphologies of the rice straw reinforced HDPE composites.

6.2 EXPERIMENTAL

6.2.1 Material and Experimental Design

Rice straw (RS) was obtained from Louisiana State University (LSU) Ag Center's Crowley Rice Research Station in Crowley, LA. The harvested whole rice straw was washed with water to remove the impurity and then dried in an oven at 85°C for 24 h. Dried materials were ground with a Wiley mill, and then screened. The samples with particle size between 20 and 28 meshes were collected for composite manufacturing.

Related information of the polymer and various compatibilizers used in the study is listed in Table 6.1 (Liu et al.). Exxelor^{TM} VA1801, designated as EPR-g-MA, is a medium viscosity, semi-crystalline ethylene copolymer functionalized with maleic anhydride. Vistalon^{TM} 722, designated as uEPR, is a high viscosity ethylene-propylene copolymer without MA group functionalization.

Experiment design included three factorial experiments. The first experiment was to investigate the effect of individual compatibilizer, consisting of nine blends covering three compatibilizers (PE-g-MA, uEPR, and EPR-g-MA) and three loading rates (1.5, 2.9 and 4.3wt%

based on the total composite weight). The second experiment was designed to study the effect of combined compatibilizers, consisting of twelve blends covering two combined compatibilizer systems (PE-g-MA/uEPR and PE-g-MA/EPR-g-MA), two compatibilizer contents (1.5 and 4.3%), and three PE-g-MA/EPR ratios (2:1, 1:1, and 1:2). The third experiment intended to research the total content of combined compatibilizers under the optimum PE-g-MA/EPR ratio obtained from the second experiment. This part consisted of eight blends covering four total combined compatibilizers contents (1.5, 2.9, 4.3 and 5.7wt%) and two optimum ratios (2:1 for PE-g-MA/uEPR system and 1:1 for PE-g-MA/EPR-g-MA system). The virgin HDPE and HDPE/RS composite without any compatibilizer were used as control. The weight ratio of HDPE/RS was fixed at 60/40 for all experiments.

Table 6.1 Characteristics of polymeric resins used in this study

Polymer	Commercial designation	Property	Manufacturer
HDPE	HD6706.17	MFR(190°C/2.16kg) = 6.1g/10min, density = 0.952 g/cm^3	ExxonMobil Chemical Co. (Houston, TX)
PE-g-MA	Epolene™ G2608	MFR(190°C/2.16kg) = 6~10g/10min, M_w = 65,000g/mol, acid number = 8 mgKOH/g	Eastman Chemical Co. (Kingsport, TN)
uEPR	Vistalon™ 722	MFR = 1g/10min (manufacturer method), 72% ethylene	ExxonMobil Chemical Co. (Houston, TX)
EPR-g-MA	Exxelor™ VA1801	MFR(230°C/10Kg) = 9g/10min, density = 0.87g/cm^3, ethylene: propylene: MA = 43:53:1.21	ExxonMobil Chemical Co. (Houston, TX)

6.2.2 Sample Preparation

Rice straw fiber was oven-dried at 80°C for 12h prior to compounding. Melt compounding was performed using an intermesh, counter-rotating Brabender twin-screw

extruder (Brabender Instruments Inc., Hackensack, NJ) with a screw speed of 40rpm. The temperature profile of barrels ranged 150-175-175-175-175°C. The extrudates were quenched in a cold water bath and then pelletized into granules. After being oven-dried at 100°C for 12h, the granules were injection molded into standard mechanical test specimens using a Batenfeld Plus 35 injection molding machine (Batenfeld Inc, NJ). The injection temperatures were 190 and 180°C for HDPE/RS composites and virgin HDPE, respectively. All specimens were then conditioned for 72 h at a temperature of 23 ± 2°C and a relative humidity of 50 ± 5% for later characterization.

6.2.3 Characterization

6.2.3.1 Static Mechanical Tests

Tensile strength and modulus of type-I dumbbell-shape specimens with a typical dimension of 165×12.5×3mm were measured using an Instron 5582 testing machine (Instron Co, Norwood, MA) following ASTM D638. A crosshead speed of 5 mm/min and a gauge length of 50mm were used for the test. Using the same testing machine, flexural strength and modulus of 80×13×3mm specimens were determined under three-point bending mode with a crosshead speed of 1.3mm/min and a span length of 50mm according to ASTM D790. Izod impact strength of 63.5×12.5×3mm specimens with a notch angle of 45° and a "V"-type notch depth of 2.5mm was measured using a Tinius Olsen Mode 1892 impact tester (Tinius Olsen Inc., Horsham, PA) following ASTM D256. Five replicates were carried out for each test and each blend. The average values along with corresponding standard deviations were reported.

6.2.3.2 Scanning Electron Microscopy (SEM) Analysis

The scanning electron microscope (Hitachi S-3600N VP-SEM, Japan) was employed to analyze the morphology of impact-fractured surfaces of resultant composites. Prior to

observation, the fractured surfaces of the impact specimens were coated with gold to improve the surface conductivity. The acceleration voltage used was 15 KV.

6.2.3.3 Dynamic Mechanical Analysis (DMA)

Storage modulus E' and loss modulus E'' as well as $\tan\delta$ of the specimens (63.5×12.5×3mm) were determined by TA Instruments DMA Q800 (New Castle, DW) using a dual cantilever mode with a span of 35mm. The measurements were carried out in a temperature range of 25-100°C at a frequency of 1 Hz.

6.2.3.4 Differential Scanning Calorimetry (DSC) Analysis

Crystallization and melting behaviors were investigated using a TA Q100 differential scanning calorimeter (TA Instruments, New Castle, DE). Each sample (4.5±0.3 mg) was heated in a DSC pan from room temperature (25±3°C) to 180°C and maintained at the temperature 10 min to eliminate previous thermal history before being cooled to 30°C. The sample was then underwent a second heating from 30 to 180°C. All scans were carried out at a heating rate of 10°C/min. The crystallization and melting temperatures were determined as the peak temperatures of cooling and second heating cycles respectively. The normalized crystallization degree of HDPE, X_R, was determined using the relationship (Ganan and Mondragon 2003):

$$X_R = (\Delta H / \Delta H_M) \times 100\% \qquad (6.1)$$

where ΔH is the melting (or crystallization) enthalpy of composite sample and ΔH_M is the melting (or crystallization) enthalpy of neat matrix.

6.2.3.5 Thermogravimetric Analysis (TGA)

The thermal stability of resultant composites was analyzed by a TA Q50 thermal gravimetric analyzer (TA Instruments, New Castle, DE). Oven-dried samples with an initial amount of 8-10 mg were scanned from room temperature to 800°C at a heating rate of 10°C/min

in a nitrogen atmosphere. A high purity nitrogen stream (99.5% nitrogen, 0.5% oxygen content) was continuously passed through the furnace at a flow rate of 60 mL/min at room temperature and atmospheric pressure. Before starting each run, the nitrogen was used to purge the furnace for 30 min to establish an inert environment in order to prevent any unwanted oxidative decomposition.

6.2.4 Statistics Method

Duncan's multiple range tests for pair-wise comparison were used to test the effect of various treatments on the composite properties using Statistical Analysis Software (SAS Institute Inc., NC).

6.3 RESULTS AND DISCUSSION

6.3.1 Effect of Individual Compatibilizer Type and Loading Level

6.3.1.1 Composite Static Mechanical Strength

Experiment one was designed to investigate the effect of individual compatibilizer and its content on properties of the resultant composites. Their mechanical strength and modulus properties are summarized in Table 6.2 along with statistical comparison information for each category. The mechanical properties of virgin HDPE and HDPE/RS composite without compatibilizer are also listed in the table as a control group.

In general, three compatibilizers showed different influences on various properties due to their different reinforcement mechanisms. For tensile strength, PE-g-MA led to the maximum enhancement effect. When 1.5wt% PE-g-MA was added, the tensile strength of composites was increased by 19 and 11% with respect to pure HDPE and unmodified binary composites respectively. Further increasing PE-g-MA content to 4.3%, the increase of tensile strength reached 38 and 28%, respectively. Though not as effective as PE-g-MA, EPR-g-MA (the semi-crystalline ethylene/propylene elastomer functionalized with MA group) also showed moderate

Table 6.2 Summary of mechanical properties of virgin HDPE and resultant HDPE/RS composites modified by individual compatibilizer

System[a]	Compatibilizer Content (wt%)[d]	Strength property			Modulus property	
		Tensile strength (MPa)	Flexura strength (MPa)	Impact strength (KJ/m^2)	Tensile modulus (GPa)	Flexural modulus (GPa)
Control group						
Virgin HDPE		18.9(.2)G [b,c]	21.3(.1)G	8.12(.21)A	0.26(.02)D	0.80(.01)H
HDPE/RS w/o compatibilizer		20.3(.4)E	31.7(.8)E	3.20(.14)FG	3.36(.10)B	2.72(.06)A
HDPE/RS/PE-g-MA						
	1.5	22.5(1.2)C	38.8(.6)B	4.62(.29)C	2.72(.26)C	1.78(.04)E
	2.9	24.2(.5)B	41.7(.7)A	4.68(.14)C	2.70(.39)C	1.87(.07)E
	4.3	26.0(.5)A	41.3(.7)A	5.34(.13)B	2.75(.25)C	1.68(.05)F
HDPE/RS/uEPR						
	1.5	19.3(.6)FG	33.0(.8)D	3.01(.18)G	4.26(.35)A	2.59(.11)B
	2.9	18.7(.3)G	31.5(.7)E	3.27(.12)F	3.46(.15)B	2.54(.11)B
	4.3	19.8(.6)EF	30.1(.9)F	4.74(.17)C	2.72(.38)C	1.59(.07)G
HDPE/RS/EPR-g-MA						
	1.5	22.4(.4)C	33.7(.5)D	3.60(.10)E	3.32(.18)B	2.24(.02)C
	2.9	21.5(.1)D	35.6(.3)C	4.31(.18)D	3.30(.05)B	2.17(.07)CD
	4.3	22.9(.6)C	38.1(.4)B	5.12(.32)B	2.92(.20)C	2.14(.09)D

[a] HDPE/RS=60:40 (wt%) fixed for all composites;
[b] Mean values with the same capitalized letter for each property are not significantly different at the 5% significance level;
[c] Numbers in the parenthesis are standard deviation based on five specimens;
[d] The content of each compatibilizer was based on the total composite weight.

improvement effect on tensile strength of composite with 21 and 13% increase observed, respectively, when 4.3% EPR-g-MA was added. It was also found that, in both compatibilizer systems, tensile strength values were all higher than those of the control group. Taking into account that the improved tensile strength usually benefits from enhanced adhesion between the components and the improvement of the nature of the matrix-filler interface, it is therefore concluded that both PE-g-MA and EPR-g-MA promoted interfacial bonding between hydrophilic RS fiber and hydrophobic HDPE matrix and, consequently, improved tensile strength. Similar results on tensile strength by functionalized polyolefin elastomers have also been observed in previous researches on wood flour filled SEBS-g-MA modified PE (Lai et al. 2003; Oksman 1996; Oksman and Lindberg 1998; Wang et al. 2003), PP systems (Oksman and Clemons 1998; Wu et al. 2000), and on EBAGMA modified PP systems (Kaci et al. 2006). Different from PE-g-MA and EPR-g-MA, unfunctionalized EPR failed to show positive effect on tensile strength. As shown in Table 6.2, tensile strength of HDPE/RS/uEPR composite was significantly lower than that of the composite with other two compatibilizer systems, which may attribute to very poor interphase between matrix and filler. Since the uEPR has no effective function group, such as MA, it cannot provide an interphase as strong as that by PE-g-MA and EPR-g-MA for stress transfer despite its possibly better compatibility with matrix due to higher ethylene content (72wt%) than EPR-g-MA (43 wt%). Moreover, compared to the binary pure-HDPE/RS system, the uEPR modified HDPE/RS composites are actually ternary systems due to containing propylene inside. Therefore, it may have worse matrix-RS interphase than pure-HDPE/RS system.

For the influence of the three compatibilizers on flexural strength of composites (Table 6.2), similar effect was found. PE-g-MA led to the maximum enhancement effect to composites when compatibilizer content level was fixed, while uEPR still failed to show positive effect on

the bending strength. Within individual compatibilizer, the loading level showed significant effect based on statistical ranking results. For both PE-g-MA and EPR-g-MA systems, more compatibilizers usually meant higher strength when the content level varied from 1.5 to 4.3wt%. In addition, the fact that only 1.5wt% compatibilizer already led to significant improvement implied the importance of improving matrix-RS interphase bonding. For uEPR system, due to lack of effective interphase adhesion, negative effect of ternary systems was more obvious as indicated by decreased strength when uEPR content level increased. For a given modified composite system, flexural strength was much higher than corresponding tensile strength.

Impact strength is the major concern in natural fibers reinforced polymer composite research since the composites are mainly used in structural applications. In general, as shown in Table 6.2, the improvement in impact toughness with respect to unmodified HDPE/RS composite was clearly observed in modified composites regardless of types of compatibilizers. Specifically, analyzing influence of compatibilizer type on impact strength, one can find that PE-g-MA still showed the best enhancement effect among the three. However, increasing compatibilizer content to 4.3wt%, the strength of the EPR-g-MA system was fairly close to that of the PE-g-MA system and, actually, they had no statistically significant difference. At this compatibilizer content, uEPR modified composite also showed fairly remarkable improvement (increase 48%) with respect to unmodified HDPE/RS system. Furthermore, for individual compatibilizer, it was obvious that the impact strength increased significantly when more compatibilizers were added. Therefore, it is concluded that all three compatibilizers can provide good improvement for impact strength of HDPE/RS composite if their loading level are well controlled.

However, it is worth noting that the sources of enhanced toughness were probably different for three compatibilizer systems if the variation of tensile and flexural strength between

them is taken into account. PE-g-MA is a well-known interphase compatibilizer, while elastomers or rubbers can toughen either matrix or interphase around fillers. It is known that the toughening of matrix tends to reduce ultimate strength of composites due to inferior bulk modulus of added elastomers, while strengths of the final composites in the case of interphase toughening might be either decreased or increased, depending on interphase nature. Recalling the observation that tensile and flexural strength increased with increasing EPR-g-MA concentration from 1.5 to 4.3wt%, the increased toughness in the case of EPR-g-MA modified system should be primarily associated with the formation of more flexible interphase around rice straw fiber and, consequently, resulting in more energy absorption during impact fracture (Oksman and Clemons 1998; Oksman and Lindberg 1998; Wu et al. 2000). In the case of uEPR composites, however, the lower strength compared to the unmodified one implied that the enhanced impact strength could mainly result from toughening of HDPE matrix.

6.3.1.2 Composite Static Modulus

Generally, the introduction of individual compatibilizer led to a universal decrease in modulus as shown in Table 6.2. The composites modified by PE-g-MA exhibited the most reduction in tensile modulus compared to that of two EPR modified systems. However, the reduction appeared in PE-g-MA system was not dependent on PE-g-MA content, while the other two EPR systems led to more decreased tensile strength when more compatibilizers were used. It is well-known that tensile modulus is not as sensitive to interfacial interaction as tensile strength is (Danyadi et al. 2006; Li and Matuana 2003; Matuana et al. 1998). Therefore, the reduction appeared in both EPR systems can be associated with the stiffness loss caused by elastomer as one of their intrinsic characteristics. Highly similar to tensile modulus, the flexural modulus of the composites decreased after introduction of individual compatibilizer compared to unmodified HDPE/RS system. In addition, more reduction was observed when compatibilizer content was

increased. This suggested that the excessive addition of EPRs had an adverse effect on stiffness of the final composites.

6.3.1.3 Composite Morphology

The SEM images taken from impact fractured surfaces of various HDPE/RS composites can provide additional information related to interfacial adhesion and impact energy dissipation mechanisms involved during impact testing. Those images are shown in Figs. 6.1 and 6.2. Without the addition of any compatibilizers (Fig. 6.1a), fiber bundles (circle 1) had fairly smooth, clean surfaces and were devoid of HDPE matrix. Also, typical pulled-out traces (circle 2) are remarkably visible everywhere on fracture surface. These characteristics indicate poor interfacial adhesion between the filler and the matrix. With the addition of 4.3wt% PE-g-MA (Fig. 6.1b), pulled-out trace is very unusual and the broken fibers are normally embedded in the matrix without evident gap in the interfacial area (circles 1 and 2) evidencing good interface bonding (solid arrows). In addition, plastic deformation of the surrounding matrix involved is not obvious, which suggests that the fracture of RS itself instead of debonding is the main energy dissipation mode in this case. As shown in Fig. 6.2a, the introduction of 4.3wt% uEPR usually generated a very coarse fracture surface, which is fairly similar to that in the unmodified system, indicating formation of weak bonding between HDPE and filler. However, it should be pointed out that the signs for plastic deformation (dashed arrows) of local matrix (circles 1 and 2) appeared more evident in this case than unmodified one, indicating the toughening of matrix brought by uEPR. The situation in the case of EPR-g-MA (Fig. 6.2b) is more like the combination of that in Figs. 6.1a and 6.1b. At the matrix-RS interphase (circles 1 and 2), both good matrix coverage and obvious matrix deformation can be observed. Also, pulled-out trace is fairly unusual in this case indicating the existence of good interphase bonding.

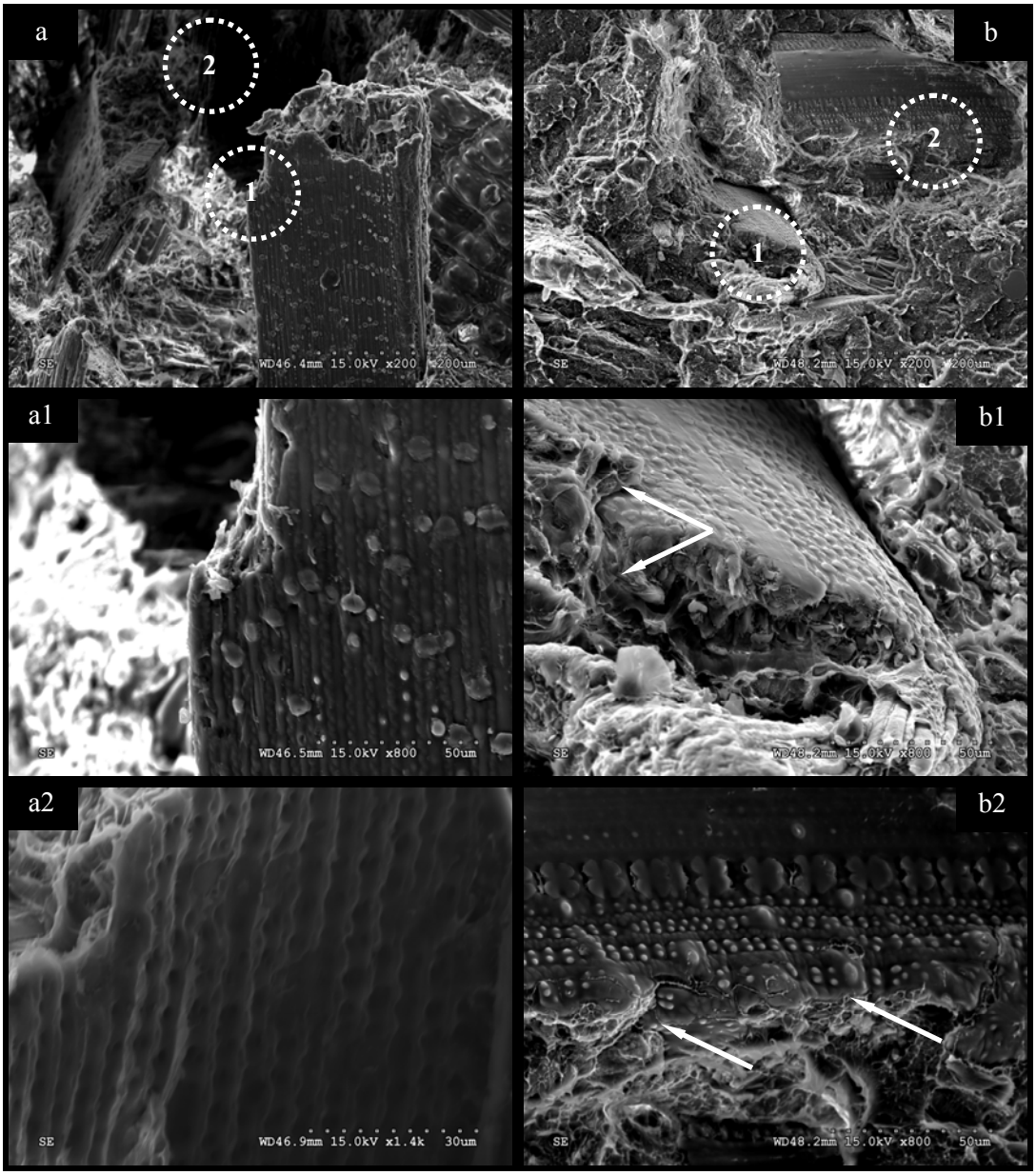

Fig. 6.1 SEM micrograph of impact-fractured surfaces of various HDPE/RS composites: (a) without compatibilizer; (b) modified by PE-g-MA. Compatibilizer content was fixed at 4.3% based on total composite weight. Images a1 and a2, and b1 and b2 are local details corresponding to circles in images a and b, respectively. Solid arrows indicate local interphase improved by compatibilizer; dashed arrows indicate deformation of local matrix.

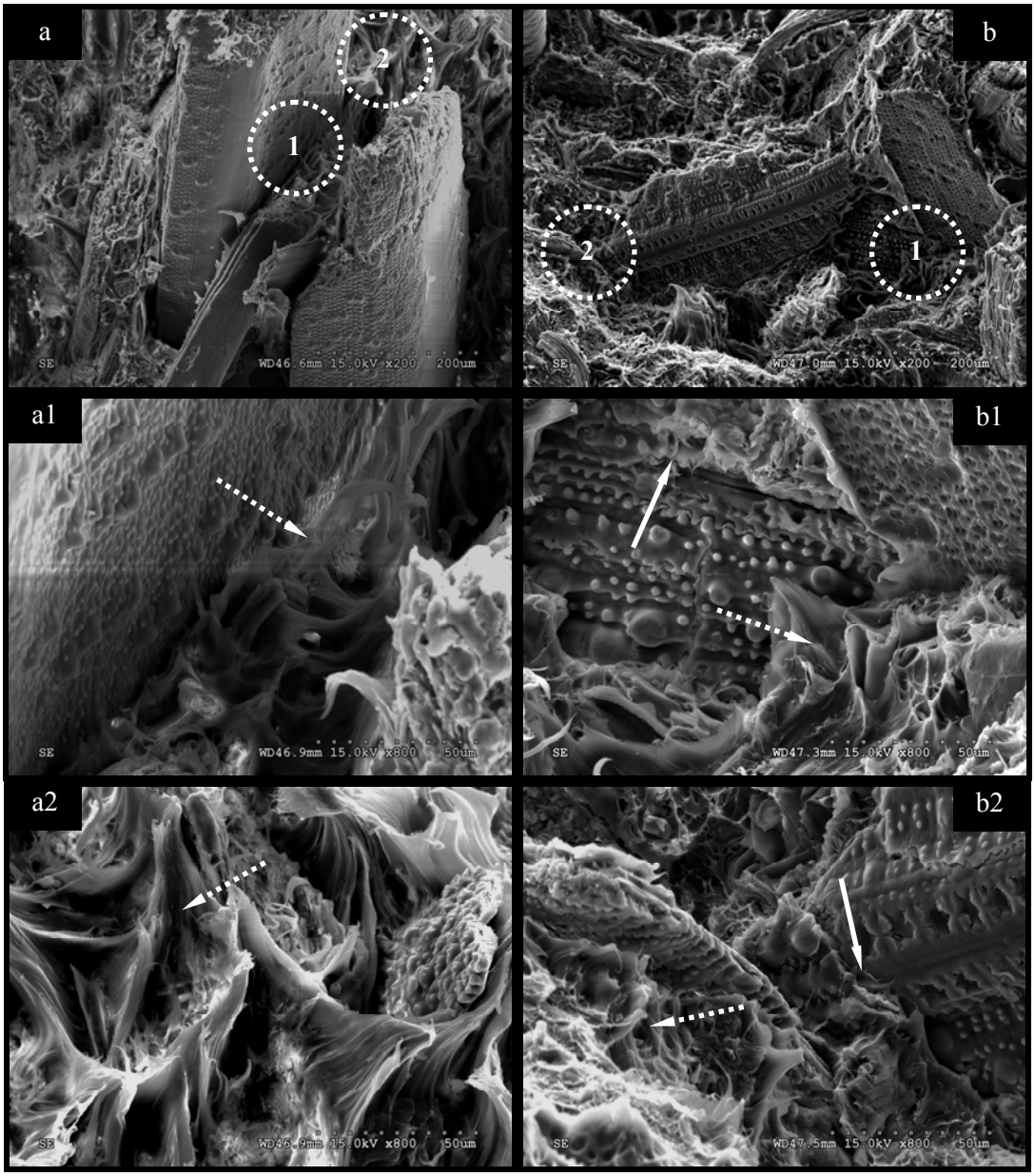

Fig. 6.2 SEM micrograph of impact-fractured surfaces of various HDPE/RS composites: (a) modified by uEPR, and (b) modified by EPR-g-MA. Compatibilizer content was fixed at 4.3% based on total composite weight. Images a1 and a2, and b1 and b2 are local details corresponding to circles in images a and b, respectively. Solid arrows indicate local interphase improved by compatibilizer; dashed arrows indicate deformation of local matrix.

6.3.1.4 Dynamic Modulus

Fig. 6.3 shows the dynamic mechanical spectrum of pure HDPE, unmodified HDPE/RS composites, and modified composites with 1.5wt% compatibilizer, respectively. As expected, the magnitude of storage modulus E' increased with the incorporation of rigid RS fiber into HDPE due to the enhanced stiffness. Among these composites, the unmodified system exhibited the maximum E', while the PE-g-MA system showed the lowest E' during most temperature range. The curves of uEPR and EPR-g-MA modified HDPE/RS composites were in the middle and fairly close to each other. This trend was in agreement with that obtained from the static mechanical data (Table 6.2).

The loss modulus, corresponding to viscous modulus of viscoelastic material, offers relaxation transition information of composites under alternative temperature. As shown in Fig. 6.3, a relaxation transition peak located around 47°C is α -relaxation point of HDPE. The α -relaxation points listed in this figure were obtained from approximate peak positions of corresponding smoothed E'' curves. It is known that α -relaxation is associated with complex multi-relaxation process which was mainly concerned with the molecular motion of PE crystalline region (Huang et al. 2004). Also, it indicated that entire composite started to lose stiffness intensively and was easily deformed when surrounding temperature reached around 50°C. Obviously, α -relaxation temperature shifted to higher temperatures after the introduction of RS fiber into HDPE, which may be attributed to the restriction effect brought by fiber on reducing the segmental mobility of polymer molecules at the relaxation temperatures (Mohanty et al. 2006). However, there was no remarkable difference between different composites, which may imply that the restriction effect caused by compatibilizer is considerably weak compared to that caused by fiber. The unmodified composite and pure HDPE also exhibited the highest and

lowest E'', which is in agreement with results obtained from the static mechanical test (Table 6.2).

The damping factor, $\tan\delta$, which is the ratio of the loss modulus to the storage modulus, reflects the viscoelastic characteristic of certain material. Therefore, lower $\tan\delta$ of composites indicated better elastic characteristic of composites than pure HDPE; however, the difference between composites was not remarkable.

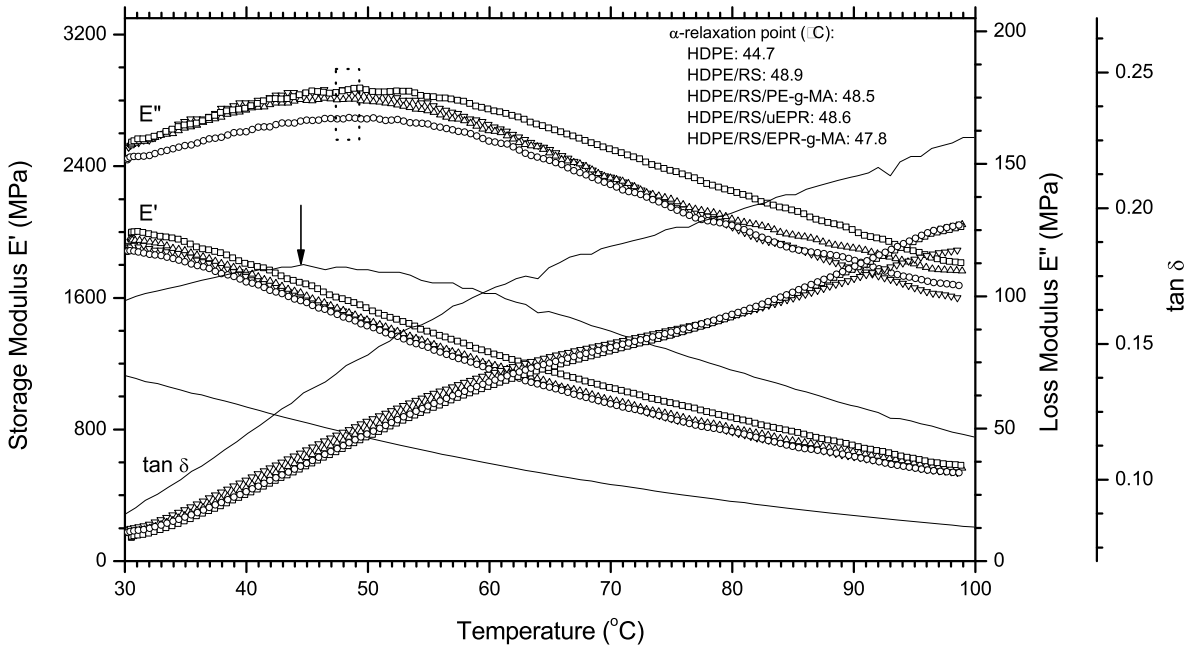

Fig. 6.3 Storage modulus (E'), loss modulus (E'') and damping factor ($\tan\delta$) of pure HDPE (solid line), unmodified HDPE/RS composite (□), and modified HDPE/RS composites with 1.5wt% compatibilizer (PE-g-MA: ○; uEPR: Δ; and EPR-g-MA: ∇). Arrow and rectangular indicated E'' peak position of pure HDPE and composites, respectively. The listed α-relaxation points were obtained from peak positions of corresponding smoothed E'' curves.

6.3.1.5 Thermal Melting and Stability Properties

DSC test was employed to investigate the crystallization degree and temperature of matrix in resultant composites using a similar approach as that presented in Chapter 5. As shown in Table 6.3, the crystallization temperature of HDPE matrix in different systems changed slightly while crystallization degree showed obvious decrease, 6.9 and 5%, respectively, when PE-g-MA and EPR-g-MA were blended in systems. It suggested that the function group MA reduced the perfection of HDPE crystals which is consistent with previous research in wood-flour/HDPE system (Lei et al. 2007). In addition, RS fiber itself and uEPR were observed having no considerable effect to crystallization of matrix. Crystallization degree results calculated from enthalpy of second heating run were fairly close to that from cooling run, which confirmed the above-mentioned observation. The TGA test showed that onset and peak temperatures, T_o and T_p, for degradation stage of rice straw in composites were around 260 and 305°C, respectively, while T_p of HDPE degradation was around 465°C. No obvious difference on the characteristic temperatures was observed between composites, suggesting that no improvement was brought by the compatibilizers.

6.3.2 Effect of Combined Compatibilizer Systems

The effect of combined PE-g-MA and EPR systems on mechanical properties of composites at two fixed total content levels (i.e., 1.5 and 4.3wt%) is summarized in Table 6.4. Statistical ranking showing treatment effect on each property category is also shown in this table.

For tensile and flexural strength of two systems at a fixed total compatibilizer content, it was observed that the HDPE/RS/PE-g-MA/EPR-g-MA system had better performance than the HDPE/RS/PE-g-MA/uEPR system at almost all PE-g-MA/EPR ratios. Also, the strength properties were improved when the total compatibilizer content was increased from 1.5 to 4.3wt% in both combined systems.

Table 6.3 DSC and TGA results of virgin HDPE and resultant HDPE/RS composites modified by individual compatibilizer at content of 4.3wt%

System	DSC [a]				TGA		
	Cooling		2nd Heating		Rice Straw		HDPE
	T_c (°C) [b]	X_R (%)	T_m (°C)	X_R (%)	T_o (°C)	T_p (°C)	T_p (°C)
Pure HDPE	116.0	100	132.1	100	-	-	464.3
HDPE/RS w/o compatibilizer	116.2	99.1	132.6	98.4	260.7	306.5	466.4
HDPE/RS/PE-g-MA	116.4	93.1	130.9	91.4	260.2	302.6	462.2
HDPE/RS/uEPR	116.7	99.7	131.2	96.1	256.6	306.5	465.5
HDPE/RS/EPR-g-MA	115.6	95.0	132.6	93.6	258.7	305.8	466.6

[a] The heating rates were 10 °C/min for all DSC and TGA tests.

[b] Subscript c, R, m, o, and p stand for crystallization, relative, melting, onset and peak, respectively.

It was observed that HDPE/RS/PE-g-MA/EPR-g-MA systems had better impact strength than the HDPE/RS/PE-g-MA/uEPR ones at a given fixed total compatibilizer content. Also, strength increased after increasing total content from 1.5 to 4.3wt%. However, the influence on strength by PE-g-MA/EPR ratio was different in the two cases. For instance, the ratio of 2:1 appeared to be best for the HDPE/RS/PE-g-MA/uEPR system as revealed by the highest strength value at each of the two total compatibilizer contents. For the HDPE/RS/PE-g-MA/EPR-g-MA system, however, the best ratio was 1:1. This phenomenon may be associated with specific individual requirement of two different systems. As discussed in the last section, uEPR failed to improve impact strength effectively at comparatively low content level due to the absence of effective interphase bonding. Therefore, some interfacial compatibilizer was requested by uEPR and, consequently, the impact resistance of its composites was enhanced at higher PE-g-MA percentage because of superior interphase bonding ability of the latter. SEM micrographs of impact-fractured surfaces, which were taken from samples with the PE-g-MA/uEPR ratio of 2:1 under total compatibilizer content of 4.3wt%, also supported this result. As shown in Fig. 6.4a, the matrix-RS interphase was obviously improved (solid arrow) as indicated by rare pulled-out trace and good matrix coverage. The cooperation of better stress transfer by enhanced interphase bonding and energy absorption by deformation of local matrix (dashed arrow) made the best impact strength of the PE-g-MA/uEPR system obtained at this ratio. However, it is noteworthy that higher total compatibilizer content (i.e., 4.3wt% or maybe higher) is recommended due to the fact that impact strength only received moderate improvement at lower total compatibilizer content level (i.e., 1.5wt%). Slightly different with the HDPE/RS/PE-g-MA/uEPR system, a balance between interphase enhancement and matrix toughening might be more favorable in the case of HDPE/RS/PE-g-MA/EPR-g-MA system because EPR-g-MA itself was functionalized

Table 6.4 Effect of PE-g-MA/EPR ratio on mechanical properties of resultant HDPE/RS composites modified by combined PE-g-MA and EPRs

System [a]	Total compatibilizer content [d] (%)	PE-g-MA/EPR Ratio	Strength property			Modulus property	
			Tensile Strength (MPa)	Flexural Strength (MPa)	Impact Strength (KJ/m^2)	Tensile Modulus (GPa)	Flexural Modulus (GPa)
Control group							
Virgin HDPE			18.9(.2)G [b,c]	21.3(.1)G	8.12(.21)A	0.26(.02)F	0.80(.01)J
HDPE/RS without compatibilizer			20.3(.4)F	31.7(.8)F	3.20(.14)G	3.36(.10)AB	2.72(.06)A
HDPE/RS/PE-g-MA/uEPR							
		2:1	21.5(.4)E	37.3(.7)D	3.82(.20)F	3.11(.56)BC	1.97(.08)G
	1.5	1:1	23.4(.5)CD	32.5(.9)F	3.83(.17)F	3.29(.38)B	2.20(.06)DE
		1:2	22.4(1.1)DE	31.6(.6)F	2.89(.09)H	3.38(.11)AB	2.57(.07)B
		2:1	24.7(.8)B	38.3(.7)B	4.81(.31)D	2.67(.19)E	1.77(.01)I
	4.3	1:1	23.1(1.4)CD	38.2(.9)BC	4.43(.28)E	2.83(.16)CDE	2.06(.06)F
		1:2	23.0(.3)CD	37.3(.7)D	4.41(.22)E	2.57(.06)E	2.29(.04)C
HDPE/RS/PE-g-MA/EPR-g-MA							
		2:1	21.8(.4)E	37.6(.3)BCD	3.72(.20)F	3.05(.19)BCD	2.17(.03)DE
	1.5	1:1	23.9(.1)BC	36.1(.8)E	4.78(.11)D	2.90(.45)CDE	2.21(.03)D
		1:2	21.6(.5)E	35.7(.3)E	3.32(.09)G	3.66(.05)A	2.55(.04)B
		2:1	25.8(1.4)A	40.6(.1)A	4.99(.10)CD	2.78(.07)CDE	1.87(.02)H
	4.3	1:1	26.4(.9)A	39.8(.4)A	5.50(.16)B	2.69(.11)DE	1.93(.05)HG
		1:2	25.6(.3)A	37.4(.4)CD	5.19(.15)C	2.64(.28)E	2.13(.03)E

[a] HDPE/RS = 60:40 (wt%) fixed for all composites;
[b] Mean values with the same capitalized letter for each property are not significantly different at the 5% significance level;
[c] Numbers in the parenthesis are standard deviation based on five specimens;
[d] The content was based on the total composite weight.

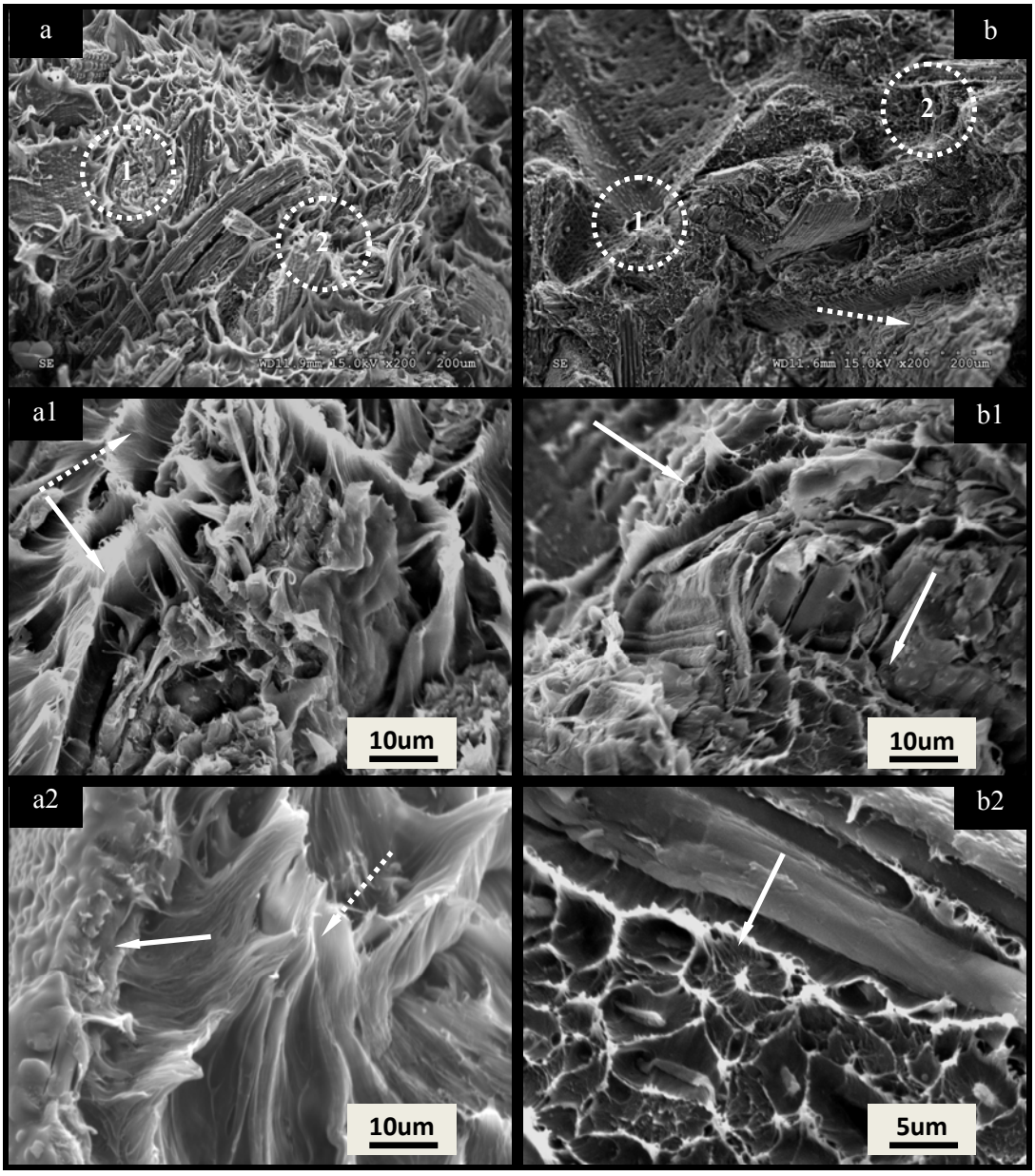

Fig. 6.4 SEM micrograph of impact-fractured surfaces of two HDPE/RS composites: (a) modified by uEPR, and (b) modified by EPR-g-MA. Total compatibilizer content is fixed at 4.3% based on total composite weight. PE-g-MA/EPR ratios for (a) and (b) are 2:1 and 1:1, respectively. Images a1 and a2, b1 and b2 are local details corresponding to circles in images a and b, respectively. Solid arrows indicate local interphase improved by compatibilizer; dashed arrows indicate deformation of local matrix.

with interphase modifier, MA function group. The balance ratio of PE-g-MA/EPR-g-MA was suggested as 1:1 based on experimental data. As shown in Fig. 6.4b, corresponding SEM micrographs of impact-fractured surfaces also presented good interphase bonding (solid arrow). The polymer deformation, however, appeared not as obvious as that shown in Fig. 6.4a, implying a difference between matrixes of the two systems. It was also observed that tensile and flexural strength values were quite acceptable under the respective best ratio, especially at the total compatibilizer content of 4.3wt%.

It should be pointed out that under the optimum ratio composites modified by combined compatibilizers showed better strength and impact toughness (Table 6.4) compared to those of the systems modified by either EPR or EPR-g-MA alone (Table 6.2). This is possibly attributed to better interphase bonding brought by the MA group. On the other hand, under the optimum ratio, the combination of PE-g-MA and EPR-g-MA provided composites better tensile and impact strength than PE-g-MA alone, with acceptable flexural strength decrease.

In general, tensile moduli of modified composites were decreased compared to the unmodified HDPE/RS composite (Table 6.4). Also the two systems almost had no significant difference under accordant PE-g-MA/EPR-g-MA ratio and total compatibilizer content, probably due to the insensitivity of tensile modulus to interfacial nature. Similar to tensile modulus, flexural moduli of modified composites were also comparatively lower than those of unmodified composites. Also, flexural modulus was somewhat improved with increasing EPR percentage to 2/3 in both combined systems. As shown in Fig. 6.5, where the total compatibilizer content was fixed at 4.3wt% for both systems, dynamic mechanical result seemed to support this observation based on E' and E'' values. In addition, the temperature range of α -relaxation shifted to about 50°C for both combined compatibilizer systems.

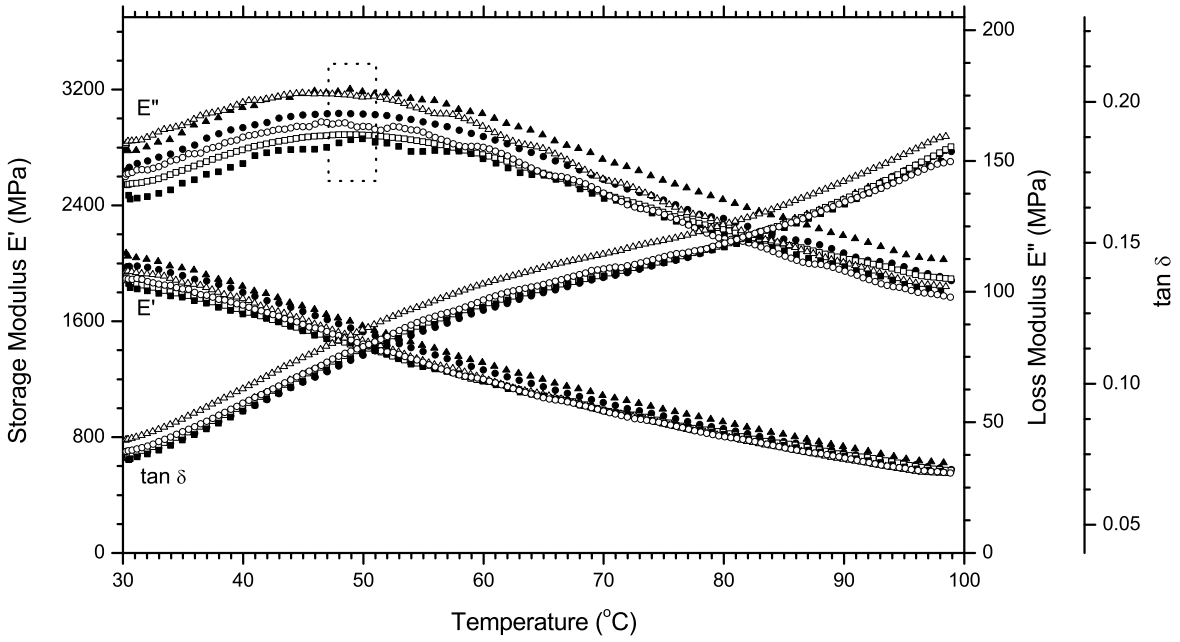

Fig. 6.5 Storage modulus (E'), loss modulus (E'') and damping factor ($\tan\delta$) of combined PE-g-MA/uEPR (solid scatter) and PE-g-MA/EPR-g-MA (hollow scatter) modified HDPE/RS composites at different PE-g-MA/EPR ratios (2:1: square; 1:1: circle; and 1:2: triangle) under fixed total compatibilizer content of 4.3wt%. Dashed rectangular indicated E'' peak position of various composites.

Under the optimum ratio, moduli of composites modified by combined compatibilizers were slightly lower than those modified by uEPR and EPR-g-MA alone. However, the combination of PE-g-MA and EPRs provided composites better tensile and flexural modulus than PE-g-MA alone, especially at a total compatibilizer content of 1.5wt%.

Crystallization behavior and thermal stability of resultant composites containing 4.3wt% combined compatibilizers are summarized in Table 6.5. In general, the addition of combined compatibilizers slightly decreased the crystallization degree of HDPE matrix in composites compared to pure HDPE as indicated by both cooling and second heating run. Comparing two combined compatibilizer systems, however, no obvious difference can be found. Within each

Table 6.5 DSC and TGA results of virgin HDPE and resultant HDPE/RS composites modified by combined compatibilizers with loading level of 4.3wt%

System	PE-g-MA/EPR Ratio	DSC [a]				TGA		
		Cooling		2nd Heating		Rice Straw		HDPE
		T_c (°C) [b]	X_R (%)	T_m (°C)	X_R (%)	T_o (°C)	T_p (°C)	T_p (°C)
Pure HDPE		116.0	100	132.1	100	-	-	464.3
HDPE/RS w/o compatibilizer		116.2	99.1	132.6	98.4	260.7	306.5	466.4
HDPE/RS/PE-g-MA/uEPR								
	2:1	116.6	99.4	131.7	98.8	260.0	306.0	463.9
	1:1	117.1	95.4	132.4	94.9	260.1	306.2	464.3
	1:2	117.8	96.9	132.2	96.5	259.7	305.9	463.2
HDPE/RS/PE-g-MA/EPR-g-MA								
	2:1	116.2	96.3	132.3	97.2	260.4	305.9	466.2
	1:1	116.4	95.5	132.3	94.8	260.2	306.1	466.9
	1:2	115.8	99.5	132.8	99.7	260.5	305.8	466.6

[a] The heating rates were 10 °C/min for all DSC and TGA tests.
[b] Subscript c, R, m, o, and p stand for crystallization, relative, melting, onset and peak, respectively.

combined compatibilizer system, different PE-g-MA/EPR ratios appeared somewhat influence (around 4% between maximum and minimum) on crystallization degree of matrix in composites, which may be associated with the specific magnitude of elastomer in composites. Similar to the situation in Section 6.3.1, different combined compatibilizer systems did not show significant influence on thermal stability of composite as indicated by close onset and peak degradation temperatures between composites. Based on above-mentioned observation, some basic characteristics related to matrix in composites such as crystallization, decrystallization, melting and degradation, etc, were not significantly changed by varied PE-g-MA/EPR ratios.

6.3.3 Optimized PE-G-MA/EPR Coupling System

In general, significantly improved system tensile and flexural strength were observed when the total compatibilizer content was increased from 1.5 to 4.3 wt%, especially in the case of the HDPE/RS/PE-g-MA/EPR-g-MA system, based on data shown in Table 6.6. However, the improvement was not significant when the total content was increased from 4.3 to 5.7wt% as indicated by statistical ranking, implying the existence of enhancement limit. Within a certain total content limit, increasing compatibilizer can lead to increasing interphase bonding strength up to their ultimate strength. However, adding too much compatibilizer into a system may cause part of the compatibilizer entering the matrix instead of interphase due to wettability difference, and consequently cannot help increase the interphase strength. Therefore, a control on total compatibilizer content to a moderate level (e.g., around 5-6wt%) is recommended. Compared to HDPE/RS composites without compatibilizer, the addition of 5.7wt% PE-g-MA/uEPR combined compatibilizer increased tensile and flexural strengths by 23 and 18%, respectively, while the addition of 5.7wt% PE-g-MA/EPR-g-MA increased two strengths by 29 and 30%, respectively.

Table 6.6 Effect of total compatibilizer content on mechanical properties of resultant HDPE/RS composites based on the optimum PE-g-MA/EPR ratio with respect to impact strength

System [a]	Total compatibilizer content[d] (%)	Strength property			Modulus property	
		Tensile strength (MPa)	Flexural strength (MPa)	Impact strength (KJ/m^2)	Tensile modulus (GPa)	Flexural modulus (GPa)
Control group						
Virgin HDPE		18.9(.2)G [b,c]	21.3(.1)H	8.12(.21)A	0.26(.02)E	0.80(.01)H
HDPE/RS w/o compatibilizer		20.3(.4)F	31.7(.8)G	3.20(.14)G	3.36(.10)A	2.72(.06)A
HDPE/RS/PE-g-MA/uEPR under PE-g-MA/uEPR = 2:1						
	1.5	21.5(.4)E	37.3(.7)E	3.82(.20)F	3.11(.56)AB	1.97(.08)CD
	2.9	24.5(.4)BC	38.3(.4)CD	4.32(.19)E	2.80(.22)BCD	1.87(.06)E
	4.3	24.7(.8)B	38.3(.7)CD	4.81(.31)D	2.67(.19)CD	1.77(.01)F
	5.7	24.9(.3)B	37.5(.4)DE	5.21(.07)C	2.39(.23)D	1.55(.05)G
HDPE/RS/PE-g-MA/EPR-g-MA under PE-g-MA/EPR-g-MA = 1:1						
	1.5	23.9(.1)C	36.1(.8)F	4.78(.11)D	2.90(.45)BC	2.21(.03)B
	2.9	23.2(.4)D	38.8(1.1)C	4.84(.13)D	2.88(.49)BC	2.01(.08)C
	4.3	26.4(.9)A	39.8(.4)B	5.50(.16)B	2.69(.11)BCD	1.93(.05)DE
	5.7	26.2(.5)A	41.2(.5)A	5.54(.22)B	2.69(.11)BCD	1.91(.03)DE

[a] HDPE/RS = 60:40 (wt%) fixed for all composites;
[b] Mean values with the same capitalized letter for each property are not significantly different at the 5% significance level;
[c] Numbers in the parenthesis are standard deviation based on five specimens;
[d] The content was based on the total composite weight.

Similar to tensile and flexural strength, the most-concerned impact strength also presented increasing trend when more compatibilizer was introduced, reflecting enhanced matrix-RS interphase. Compared to HDPE/RS composites without compatibilizer, the addition of 5.7wt% PE-g-MA/uEPR and PE-g-MA/EPR-g-MA combined compatibilizers increased impact strength by 63 and 73%, respectively.

As expected, tensile and flexural moduli were both decreased when increasing the total compatibilizer content in the case of HDPE/RS/PE-g-MA/uEPR system, while tensile moduli of HDPE/RS/PE-g-MA/EPR-g-MA composites were not remarkably influenced by the total content based on statistical results. Compared to HDPE/RS composites without compatibilizer, the addition of 5.7wt% PE-g-MA/uEPR combined compatibilizer decreased tensile and flexural moduli by 29 and 43%, respectively. The values were higher than the moduli decreased due to the addition of 5.7wt% PE-g-MA/EPR-g-MA (20 and 30%, respectively).

6.4 CONCLUSIONS

Three compatibilizers, unfunctionalized EPR (uEPR), maleic anhydride grafted EPR (EPR-g-MA), and PE-g-MA as well as their combinations were introduced into HDPE/rice-straw (RS) composites. The weight ratio of HDPE/RS was fixed at 60/40 throughout the experiments.

For the effect of individual compatibilizer, it was found that the incorporation of either PE-g-MA or EPR-g-MA alone enhanced both tensile and flexural strengths and impact toughness of resultant composites, compared to HDPE/RS system without compatibilizers. The use of uEPR showed negative effect on both strengths despite moderate improvement on impact toughness at a high content, 4.3wt%. The introduction of each individual modifier caused a decrease in tensile and flexural moduli of HDPE/RS composites to a different extent. Different interphase morphologies were observed in different compatibilizer systems. Dynamic mechanical analysis results were consistent with the static mechanical tests.

The PE-g-MA/EPR ratio affected mechanical properties of composites modified by combined compatibilizers. The optimum PE-g-MA/EPR ratio was considered as 2:1 and 1:1 for PE-g-MA/uEPR and PE-g-MA/EPR-g-MA modified composites, respectively. At the optimum ratio, composites modified by the combined compatibilizer system showed better strength and impact toughness, and acceptable modulus compared to those modified by either EPR or EPR-g-MA alone, possibly due to better interphase bonding brought by MA. Also, composites modified by combined PE-g-MA/EPR-g-MA showed better impact strength than that modified by PE-g-MA alone. The study further found that, at the optimum compatibilizer ratio, increasing total combined compatibilizer content improved strength but decreased modulus of composites.

DSC and TGA study showed that different compatibilizers and their combination had no significant effect on crystallization behavior of HDPE matrix and thermal stability of resultant composites.

6.5 REFERENCES

Danyadi, L., Renner, K., Szabo, Z., Nagy, G., Moczo, J., and Pukanszky, B. (2006). "Wood flour filled PP composites: adhesion, deformation, failure." *Polymers for advanced technologies*, 17(11-12), 967-974.

Dubnikova, I. L., Berezina, S. M., and Antonov, A. V. (2002). "The effect of morphology of ternary-phase polypropylene/glass bead/ethylene-propylene rubber composites on the toughness and brittle-ductile transition." *Journal of Applied Polymer Science*, 85(9), 1911-1928.

Ganan, P., and Mondragon, I. (2003). "Thermal and degradation behavior of fique fiber reinforced thermoplastic matrix composites." *Journal of Thermal Analysis and Calorimetry*, 73(3), 783-795.

Grozdanov, A., Buzarovska, A., Bogoeva-Gaceva, G., Avella, M., Errico, M. E., and Gentille, G. (2006). "Rice straw as an alternative reinforcement in polypropylene composites." *Agronomy for Sustainable Development*, 26(4), 251-255.

Habibi, Y., Ei-Zawawy, W. K., Ibrahim, M. M., and Dufresne, A. (2008). "Processing and characterization of reinforced polyethylene composites made with lignocellulosic fibers from Egyptian agro-industrial residues." *Composites Science and Technology*, 68(7-8), 1877-1885.

Huang, Y. Q., Jiang, S. L., Wu, L. B., and Hua, Y. Q. (2004). "Characterization of LLDPE/nano-SiO2 composites by solid-state dynamic mechanical spectroscopy." *Polymer Testing*, 23(1), 9-15.

Kaci, M., Cimmino, S., Silvestre, C., Duraccio, D., Benhamida, A., and Zaidi, L. (2006). "Ethylene butyl acrylate glycidyl methacrylate terpolymer as an interfacial agent for isotactic poly(propylene)/wood flour composites." *Macromolecular Materials and Engineering*, 291(7), 869-876.

Kamel, S. (2004). "Preparation and properties of composites made from rice straw and poly(vinyl chloride) (PVC)." *Polymers for Advanced Technologies*, 15(10), 612-616.

Kazayawoko, M., Balatinecz, J. J., and Matuana, L. M. (1999a). "Surface modification and adhesion mechanisms in woodfiber-polypropylene composites." *Journal of Materials Science*, 34(24), 6189-6199.

Kazayawoko, M., Balatinecz, J. J., and Sodhi, R. N. S. (1999b). "X-ray photoelectron spectroscopy of maleated polypropylene treated wood fibers in a high-intensity thermokinetic mixer." *Wood Science and Technology*, 33(5), 359-372.

Kazayawoko, M., Balatinecz, J. J., and Woodhams, R. T. (1997). "Diffuse reflectance Fourier transform infrared spectra of wood fibers treated with maleated polypropylenes." *Journal of Applied Polymer Science*, 66(6), 1163-1173.

Lai, S. M., Yeh, F. C., Wang, Y., Chan, H. C., and Shen, H. F. (2003). "Comparative study of maleated polyolefins as compatibilizers for polyethylene/wood flour composites." *Journal of Applied Polymer Science*, 87(3), 487-496.

Lei, Y., Wu, Q., ClemonS, C. M., Yao, F., and Xu, Y. (2007). "Influence of nanoclay on properties of HDPE/Wood composites." *Journal of Applied Polymer Science*, 106(6), 3958-3966.

Li, Q. X., and Matuana, L. M. (2003). "Surface of cellulosic materials modified with functionalized polyethylene coupling agents." *Journal of Applied Polymer Science*, 88(2), 278-286.

Liu, H., Wu, Q., Han, G., Yao, F., Kojima, Y., and Suzuki, S. "Compatibilizing and toughening bamboo flour-filled HDPE composites: Mechanical properties and morphologies." *Composites Part A: Applied Science and Manufacturing*, In Press, Corrected Proof.

Lu, J. Z., and Wu, Q. L. (2005). "Surface and interfacial characterization of wood-PVC composite: Imaging morphology and wetting behavior." *Wood and Fiber Science*, 37(1), 95-111.

Lu, J. Z., Wu, Q. L., and Negulescu, II. (2005). "Wood-fiber/high-density-polyethylene composites: Coupling agent performance." *Journal of Applied Polymer Science*, 96(1), 93-102.

Matuana, L. M., Balatinecz, J. J., Sodhi, R. N. S., and Park, C. B. (2001). "Surface characterization of esterified cellulosic fibers by XPS and FTIR spectroscopy." *Wood Science and Technology*, 35(3), 191-201.

Matuana, L. M., Woodhams, R. T., Balatinecz, J. J., and Park, C. B. (1998). "Influence of interfacial interactions on the properties of PVC cellulosic fiber composites." *Polymer Composites*, 19(4), 446-455.

Mohanty, S., Verma, S. K., and Nayak, S. K. (2006). "Dynamic mechanical and thermal properties of MAPE treated jute/HDPE composites." *Composites Science and Technology*, 66(3-4), 538-547.

Okada, O., Keskkula, H., and Paul, D. R. (2001). "Mechanical properties of blends of maleated ethylene-propylene rubber and nylon 6." *Polymer*, 42(21), 8715-8725.

Oksman, K. (1996). "Improved interaction between wood and synthetic polymers in wood/polymer composites." *Wood Science and Technology*, 30(3), 197-205.

Oksman, K., and Clemons, C. (1998). "Mechanical properties and morphology of impact modified polypropylene - Wood flour composites." *Journal of Applied Polymer Science*, 67(9), 1503-1513.

Oksman, K., and Lindberg, H. (1998). "Influence of thermoplastic elastomers on adhesion in polyethylene wood flour composites." *Journal of Applied Polymer Science*, 68(11), 1845-1855.

Oksman, K., Lindberg, H., and Holmgren, A. (1998). "The nature and location of SEBS-MA compatibilizer in polyethylene-wood flour composites." *Journal of Applied Polymer Science*, 69(1), 201-209.

Park, B. D., and Balatinecz, J. J. (1997). "Mechanical properties of wood-fiber/toughened isotactic polypropylene composites." *Polymer Composites*, 18(1), 79-89.

Rana, A. K., Mandal, A., and Bandyopadhyay, S. (2003). "Short jute fiber reinforced polypropylene composites: effect of compatibiliser, impact modifier and fiber loading." *Composites Science and Technology*, 63(6), 801-806.

Sombatsompop, N., Yotinwattanakumtorn, C., and Thongpin, C. (2005). "Influence of type and concentration of maleic anhydride grafted polypropylene and impact modifiers on mechanical properties of PP/wood sawdust composites." *Journal of Applied Polymer Science*, 97(2), 475-484.

Wang, J., Tung, J. F., Fuad, M. Y. A., and Hornsby, P. R. (1996). "Microstructure and mechanical properties of ternary phase polypropylene/elastomer/magnesium hydroxide fire-retardant compositions." *Journal of Applied Polymer Science*, 60(9), 1425-1437.

Wang, Y., Yeh, F. C., Lai, S. M., Chan, H. C., and Shen, H. F. (2003). "Effectiveness of functionalized polyolefins as compatibilizers for polyethylene/wood flour composites." *Polymer Engineering and Science*, 43(4), 933-945.

Wu, J. S., Yu, D. M., Chan, C. M., Kim, J. K., and Mai, Y. M. (2000). "Effect of fiber pretreatment condition on the interfacial strength and mechanical properties of wood fiber/PP composites." *Journal of Applied Polymer Science*, 76(7), 1000-1010.

CHAPTER 7 PREPARATION AND PROPERTIES OF RICE STRAW REINFORCED HIGH DENSITY POLYETHYLENE/NYLON-6 COMPOSITES

7.1 INTRODUCTION

It is well-known that natural fiber is subject to thermal degradation during polymer composite processing. This is considered one of the major disadvantages of natural fiber as filler of polymer composites. The problem has limited the application of natural fiber to some engineering thermoplastics with higher melting temperatures, such as nylon-6 (~215°C) and nylon 6-6 (~264°C) (Lu et al. 2007). However, composites strength and modulus change caused by degradation of natural fiber under different processing conditions has not been clearly quantified so far.

Limited research has been done in this field. Sapiaha et al. (1989) investigated the strength properties of composites made of untreated cellulose fibers and linear low density polyethylene (LDPE) as a function of processing parameters. They found that the strength properties of composites increased with processing time and temperature. Due to the observation of linear relationship between the infrared absorbance and yield strength of composites, they further concluded that the increase in strength should be attributed to oxidation at interfaces, which enhanced adhesion between the cellulose and polyethylene matrix. Myers et al. (1991) investigated the effects of extrusion blending temperature (190°C to 250°C) on the mechanical properties of extruded and injection-molded polypropylene-wood flour composites. They found that high extrusion temperature led to a decrease of wood particle surface polarity, small changes of composite strength, and loss of impact resistance. Moreover, the volatiles were concerned for environmental pollution and porous products. Gonzalez and Myers (1993) further investigated the effect of wood thermolysis during melt processing on the properties of wood-plastic composites. In their study, oven-dried sugar pine wood strips were exposed in a temperature

range of 220-260°C from 4096 to 4 minutes in a free-oxygen stirred molten metal bath. They found that toughness was most affected by the degradative treatment, which was followed by bending strength and then bending modulus. However, losses in wood mechanical properties during a single composite extrusion did not significantly alter composite properties, while multiple melt processing steps may have deleterious effect. Moran et al. (2007) studied the influence of multiple extrusion cycles (five cycles) on the behavior of 20wt % flax fiber filled polypropylene blends in low processing temperature (<190°C). They found that the matrix suffered significant mechanical degradation, but the degradation had only a small influence on its mechanical properties. They suggested that three extrusion cycles were enough for attaining a good fiber dispersion and distribution. Also, composite flexural and tensile elastic moduli as well as tensile strength after the first processing cycle were lower than those after other cycles (i.e., second to fifth), while impact strength showed a reverse trend.

Previous research provided some information about composite mechanical properties change caused by thermal degradation of natural fiber under various processing conditions (e.g., temperature, time, and processing cycles, etc.). However, the information is not sufficient for a quantitative understanding of the effect caused by fiber degradation, due to failing to predict degradation level of fiber under the processing conditions. Therefore, it still remains unclear that how to quantitatively link mechanical property change with fiber degradation level. In addition, previous research primarily focused on wood and pure cellulose systems, and little research has been done on rice straw fiber. Therefore, it is necessary to investigate degradation tolerance of rice straw system in order to apply rice straw in engineering plastics with high melting temperatures.

Potential negative effects of fiber degradation on mechanical properties change under high processing temperature and multiple processing cycles did not stop the exploration of

natural fiber filled nylon composites. McHenry and Stachurski (2003) investigated compression-molded (230°C) nylon-6 fiber composites filled with 2.5-10wt% wood fiber and without any additives. They found that the strength and stiffness of the composites began to decline at higher weight fractions of wood fiber after achieving the maximum strength and modulus of elasticity at 2.5wt% fiber loading. They claimed that bundles of wood fibers with internal voids prevent achieving maximum mechanical properties concluded from SEM observation. Santos et al. (2007) manufactured short or long curaua fiber filled nylon-6 composites by twin-screw extrusion-molding and compression-molding at 230°C. They claimed that non-dried raw materials improved fiber/matrix interfacial adhesion. Consequently, drying step can be eliminated to reduce costs and energy use. Chen and Gardner (2008) investigated the dynamic mechanical properties of extruded nylon/wood composites and found that the composites had good temperature-dependent properties. In order to avoid negative effect by degradation of natural fiber during processing, attempts on applying low temperature compounding (LTC) technique (Caulfield et al. 2001; Jacobson et al. 2001) and some low melting temperature nylon, such as nylon-12 (Lu et al. 2007), have also been made in natural fiber filled nylon composites field.

Moreover, the combination of non-polar polyethylene with nylon via melt-blending to produce polymer blends is expected to reduce the processing temperature and to improve the performance of the polyolefin matrix. Polymer blends have gained significant commercial growth due to several economic benefits including desired mechanical, chemical, barrier properties; better processability of difficult-to-form, high performance polymers by reducing the viscosity and/or the processing temperature; and, new types of materials (Utracki 1995). Therefore, the combination of polymer blends with natural fibers appears attractive based on considerations of the above-mentioned benefits. Unfortunately, little work has been focused on this aspect so far. In addition, the utilization of interfacial modifiers is usually required to

overcome immiscibility between polymers. Many polyolefin-based compatibilizers have been attempted, among which PE-g-MA (Chiono et al. 2003; Jiang et al. 2003) and SEBS-g-MA (Filippi et al. 2004; Yordanov and Minkova 2005) have been proven to be effective in achieving finer domain dispersion.

It will be economically favorable and practically convenient if untreated rice straw (RS) fiber can be directly used in polymer blends containing engineering plastics (e.g., nylon) within acceptable and predictable composite strength/modulus loss due to degradation of fibers. The study described in this chapter provides a preliminary feasibility study of such a process. The specific objectives were: (1) to predict weight loss of RS under various processing conditions; (2) to establish the processing temperature limit by using HDPE/RS composite as example and (3) to study the feasibility of applying one-step high-temperature extrusion processing to RS filled HDPE/nylon-6 blends using temperature limit information developed.

7.2 EXPERIMENTAL

7.2.1 Material and Experimental Design

Rice straw (RS) was obtained from Louisiana State University (LSU) Ag Center's Crowley Rice Research Station in Crowley, LA. The harvested whole rice straw was washed with water to remove the impurity and then dried in an oven at 85°C for 24 h. Oven-dried materials were ground with a Wiley mill, and then screened. The samples with the particle size between 20 and 28 meshes were collected for composite.

Technical information of HDPE, nylon-6, and two compatibilizers used in the study are listed in Table 7.1. Maleic anhydride grafted hydrogenated styrene/ethylene-butylene/styrene triblock polymer (SEBS-g-MA) has a styrene/rubber ratio equal to 30/70 (w/w). Maleic anhydride grafted polyethylene (PE-g-MA) is the same as the one used for the study described in the last chapter.

Table 7.1 Characteristics of polymeric resins used in this study

Polymer	Commercial designation	Property	Manufacturer
HDPE	HD6706.17	MFR(190°C/2.16kg) = 6.1g/10min, density = 0.952 g/cm^3	ExxonMobil Chemical Co. (Houston, TX)
Nylon-6	Aegis® H8202NLB	T_m =220°C, density = 1.13 g/cm^3	Honeywell International, Inc. (Morristown, NJ)
SEBS-g-MA	Kraton® FG1901X	MFR(230°C/5kg) = 22g/10min, 1.4~2.0wt% MA.	Kraton Polymers U.S. LLC, (Houston, TX)
PE-g-MA	Epolene™ G2608	MFR(190°C/2.16kg) = 6~10g/10min, M_w = 65,000g/mol, acid number = 8 mgKOH/g	Eastman Chemical Co. (Kingsport, TN)

Experiment design included two factorial experiments. The first experiment was carried out to investigate the effect of three extrusion temperatures (190, 225 and 245°C) for HDPE/RS composites, based on a fixed HDPE/RS ratio of 75/25 (w/w) and without any compatibilizer. The second experiment was designed to study the effect of different processing methods, consisting of 8 blends covering two processing methods (one-step and two-step method), two HDPE/nylon-6 ratios (80/20 and 70/30, w/w), and two rice straw contents (20 and 30 based on total composite weight). The concentration of SEBS-g-MA was fixed at 4wt% based on nylon-6 weight, while the content of PE-g-MA was fixed at 3wt% based on RS weight in each blend. Due to varied contents of nylon-6 and RS with respect to the total composite weight in each blend, the actual content of SEBS-g-MA and PE-g-MA with respect to the total composite varied among blends. However, the ratio of SEBS-g-MA/nylon-6 and PE-g-MA/RS was controlled in each blend as 4/100 and 3/100 (w/w), respectively. The design was based on the functionality of two compatibilizers. SEBS-g-MA and PE-g-MA were used to modify HDPE-nylon and matrix/RS interphase, respectively. Therefore, in the cases of all HDPE/nylon-6 based composites, the final content of the nylon-6 varied between 14 and 24 wt% with respect to the total composite weight.

7.2.2 Sample Preparation

Rice straw was oven-dried at 80°C for 12h, while Nylon-6 was thoroughly oven-dried at 103°C for 24h prior to compounding. Melt compounding was performed using an intermesh, counter-rotating Brabender twin-screw extruder (Brabender Instruments Inc., Hackensack, NJ) with a fixed screw speed of 40rpm.

The extrusion temperature and process varied in different experiments. In the first experiment, material was extruded at 190, 225 and 245°C (temperature of each barrel was fixed as the same), respectively, for three blends. The extrudates were quenched in a cold water bath and then pelletized into granules. In the one-step process of the second experiment, all material was fed simultaneously into the extruder and obtained extrudates were quenched and pelletized. The temperature profile of barrels ranged from 225 to 235°C in this process. In the two-step process, HDPE, nylon-6 and SEBS-g-MA were first extruded, quenched and pelletized into granules in the first extrusion step. Obtained granules were then oven-dried at 100°C for 24h and extruded again with RS and PE-g-MA in the second extrusion step. The temperature profiles of barrels ranged form 225 to 235°C and from 175 to 190°C in two steps, respectively.

After being oven-dried at 100°C for 12 and 24h, respectively, the granules from the first and the second experiment were injection molded into standard mechanical test specimens using Batenfeld Plus 35 injection molding machine (Batenfeld Inc, NJ). The injection temperatures were fixed at 190°C for all blends in both experiments. All specimens were then conditioned for 72 h at a temperature of 23 ± 2°C and a relative humidity of 50 ± 5% for later characterization.

7.2.3 Characterization

7.2.3.1 Static Mechanical Tests

Tensile strength and modulus of type-I dumbbell-shape specimens with a typical dimension of 165×12.5×3mm were measured using an Instron 5582 testing machine (Instron Co,

Norwood, MA) following ASTM D638. A crosshead speed of 5 mm/min and a gauge length of 50mm were used for the test. Using the same machine, flexural strength and modulus of 80×13×3mm specimens were determined under three-point bending with a crosshead speed of 1.3mm/min and a span length of 50mm according to ASTM D790. Izod impact strength of 63.5×12.5×3mm specimens with a notch angle of 45° and a "V"-type notch depth of 2.5mm was measured using a Tinius Olsen Mode 1892 impact tester (Tinius Olsen Inc., Horsham, PA) following ASTM D256. Five replicates were carried out for each test and each blend. The average values along with corresponding standard deviations were reported.

7.2.3.2 Scanning Electron Microscopy (SEM) Analysis

The scanning electron microscope (Hitachi S-3600N VP-SEM, Japan) was employed to analyze the morphology of impact-fracture surfaces of resultant composites. Prior to observation, the fractured surfaces of the impact test specimens were coated with gold to improve the surface conductivity. The acceleration voltage used was 15 KV.

7.2.3.3 Dynamic Mechanical Analysis (DMA)

Storage modulus E' and loss modulus E'' as well as $\tan\delta$ of specimens (63.5×12.5×3mm) were determined by TA Instruments DMA Q800 (New Castle, DW) using dual cantilever mode with a span of 35mm. The measurements were carried out in a temperature range of 25-100°C at a frequency of 1 Hz.

7.2.3.4 Differential Scanning Calorimetry (DSC) Analysis

Crystallization and melting behaviors were investigated using a TA Q100 differential scanning calorimeter (TA Instruments, New Castle, DE). Each sample (4.5±0.3 mg) was heated in a DSC pan from room temperature (25±3°C) to 250°C and maintained at the temperature 10 min to eliminate previous thermal history before being cooled to 30°C. The sample then underwent a second heating from 30 to 250°C. All scans were carried out at a heating rate of

10°C/min. The crystallization and melting temperatures were determined as the peak temperatures of cooling and second heating cycles, respectively. The normalized crystallization degree of HDPE, X_R, was determined using the relationship:

$$X_R = (\Delta H / \Delta H_M) \times 100\% \quad (7.1)$$

where ΔH is the melting (or crystallization) enthalpy of composite sample and ΔH_M is the melting (or crystallization) enthalpy of neat matrix.

7.2.3.5 Thermogravimetric Analysis (TGA)

The thermal stability of resultant composites was analyzed by a TA Q50 thermal gravimetric analyzer (TA Instruments, New Castle, DE). Oven-dried samples with initial amount of 8-10 mg were scanned from room temperature to 800^{o}C at a heating rate of 10°C/min in a nitrogen atmosphere. A high purity nitrogen stream (99.5% nitrogen, 0.5% oxygen content) was continuously passed into the furnace at a flow rate of 60 mL/min at room temperature and atmospheric pressure. Before starting each run, the nitrogen was used to purge the furnace for 30 min to establish an inert environment in order to prevent any unwanted oxidative decomposition.

7.2.4 Statistics Method

Duncan's multiple range tests for pair-wise comparison and analysis of variance (ANOVA) were used to test the effect of various treatments on the composite properties using Statistical Analysis Software (SAS Institute Inc., NC).

7.3 RESULTS AND DISCUSSION

7.3.1 Effect of Extrusion Temperature on HDPE/RS Composites

Experiment one was to study the effect of extrusion temperature on properties of resultant HDPE/RS composites. Based on results from dynamic and isothermal degradation analysis of rice straw (Chapter 3 and 4), rice straw probably suffered acceptable degradation if processing temperature was well controlled. The initial weight loss of RS was predicted as 0.1-0.2, 2.6-6.4

and 11-19.2% for 190, 225 and 245°C, respectively, using the non-isothermal model (Table 7.2). It reflected the possible weight loss of RS during heating from room temperature to designed extrusion temperature. Those values were calculated from $\alpha - T$ relationship (Eq. (3.9)) and adjusted conversion rate α_{WL} equation (Eq. (3.17)) of the non-isothermal model, by substituting corresponding parameters, i.e., activation energy value E_a of $195.5\,kJ/mol$, parameter n in $RO(n) = (1-\alpha)^n$ of 5.81, $\ln A$ of $46.57 \ln s^{-1}$, and the residue of 34% (according to Table 2.3). The assumed heating rate was 40-120°C/min. The extrusion weight loss was calculated first from $\alpha - t$ relationship of the isothermal model by substituting corresponding parameters, i.e., activation energy value E_a of $116\,kJ/mol$, parameter n in $RO(n) = (1-\alpha)^n$ of 3.0, and $\ln A$ of $18.7 \ln s^{-1}$ in Eq. (4.6), and then from converting α to weight loss by inserting residue obtained from Fig. 4.4. The assumed degradation time was $150\,s$. It reflected the possible weight loss of RS during melt-blending processing. The total weight loss was calculated by adding initial and extrusion weight loss. It reflected the possible weight loss of RS after whole extrusion.

It is observed that most mechanical properties of HDPE/RS composites showed no significant difference when increasing extrusion temperature from 190 to 225°C. Thus, up to around 7% weight loss of the RS dry mass was acceptable in terms of maintaining fiber strength and stiffness. Further increasing extrusion temperature to 245°C, tensile and impact properties showed some significant decrease, while flexural modulus showed no significant change. The decrease in tensile strength and modulus, and impact strength were 14, 16 and 33%, respectively, compared to those of composites extruded at 190°C. The weight loss in this temperature is probably caused by the degradation of hemicelluloses from amorphous union of several heteropolymers to suger monomers (e.g., xylose, galactose) with releasing low molecular weight volatiles. This chemical process probably affects the adhesion between matrix and RS, and

Table 7.2 Effect of processing temperature on RS degradation and mechanical properties of resultant HDPE/RS composites

Extrusion temperature [a] (°C)	Degradation			Strength Property			Modulus Property	
	Initial WL[d] (%)	Extrusion WL (%)	Total WL (%)	Tensile strength (MPa)	Flexural strength (MPa)	Impact strength (KJ/m^2)	Tensile modulus (GPa)	Flexural modulus (GPa)
190	0.1-0.2	0	0.1-0.2	22.3(.2)A [b, c]	33.6(1.8)A	4.81(.26)A	1.95(.16)A	1.46(.04)A
225	2.6-6.4	0.6	3.2-7.0	20.8(.4)B	32.6(2.5)A	4.68(.29)A	1.90(.17)A	1.45(.10)A
245	11.0-19.2	2.3	13.3-21.5	19.1(.4)C	32.6(1.4)A	3.23(.13)B	1.64(.04)B	1.53(.03)A

[a] HDPE/RS=75/25 (wt%) fixed for all composites;
[b] Mean values with the same capitalized letter for each property are not significantly different at the 5% significance level;
[c] Numbers in the parenthesis are standard deviation based on five specimens;
[d] WL means weight loss. Initial WL is calculated from non-isothermal model demonstrated in Chapter 3 assuming heating rates from 40-120°C/min; Extrusion WL is calculated from isothermal model demonstrated in Chapter 4 assuming degradation time of 150s; Total WL is obtained by adding Initial and Extrusion WL.

consequently, cause toughness loss. However, the remaining flexural strength and modulus implied that the cellulose, which primarily provides stiffness, still remained undegraded. This observation indicates that high processing temperature can be applied for RS in manufacturing some engineering plastic based composites.

DMA results confirmed the trend of composite flexural modulus. As shown in Fig. 7.1, composites extruded at 245°C showed the highest storage modulus E' and loss modulus E'', which is in agreement with the results obtained from static mechanical tests. Located between 47 and 50°C, the α -relaxation temperatures (peak position of E'' curve) of composites did not show obvious change, indicating insensitivity of matrix to extrusion temperature. DSC data showed that no change on matrix crystallization property was found by either extrusion temperature or RS degradation caused by high temperature (Table 7.3). However, TGA data showed that composites extruded at 245°C exhibited higher onset temperature, T_o, of RS degradation. Considering the fact that peak temperatures, T_p, of RS and matrix degradation were both unchanged, increased T_o of RS may be associated with the lower hemicellulose content in that composite. In terms of T_o, the composite extruded at 245°C showed better thermal stability.

It should be pointed out that composites extruded at 225°C did not show significant difference in mechanical and thermal properties compared to those at 190°C. This implies that comparatively higher temperature (i.e., 225 or even 235°C) may be applied in RS/polymer composites. According to the model, RS experienced 7-13% degradation (initial: 5.8-12.2wt%; extrusion: 1wt%) during the whole extrusion processing at 235°C. Its upper bound was close to 13-21% degradation level caused by extrusion at 245°C and may reach the strength loss limit. In the next section, the influence of different processing methods on various properties of HDPE/nylon-6/RS composites is further discussed.

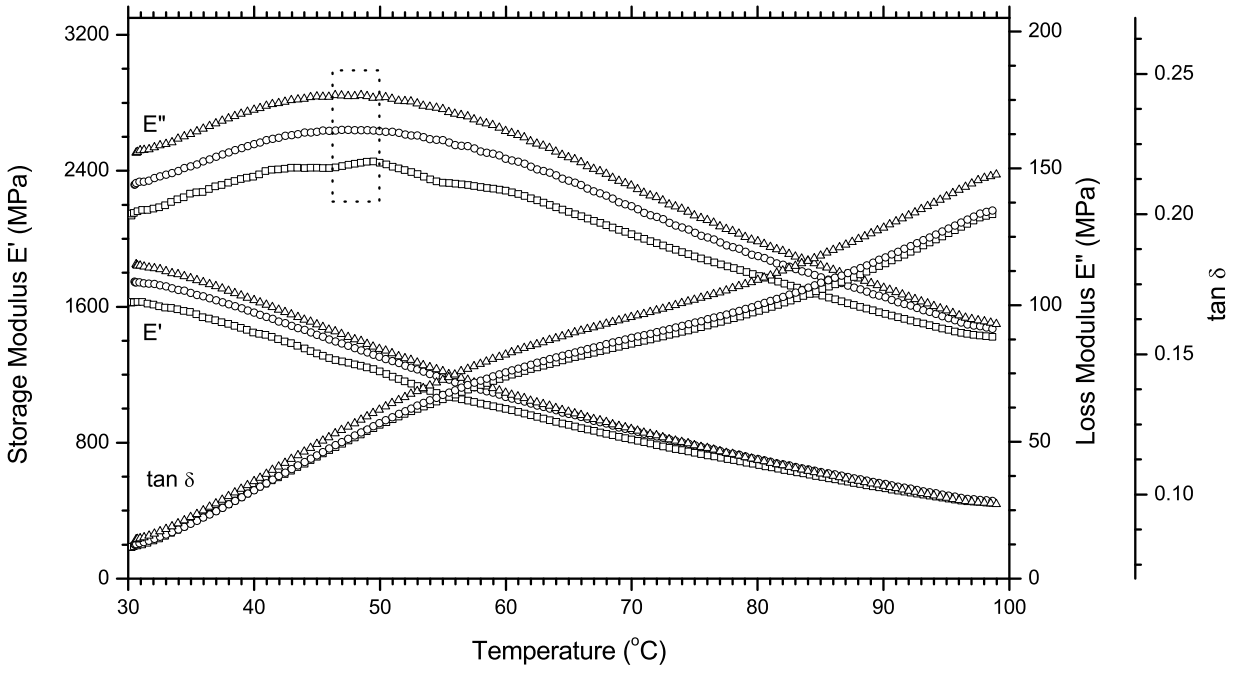

Fig. 7.1 Storage modulus (E'), loss modulus (E'') and damping factor (tan δ) of HDPE/RS composite made at different extrusion temperature: 190°C (□), 225°C (○) and 245°C (Δ). The weight ratio of HDPE/RS was fixed at 75/25. No compatibilizer was added in composites. Rectangular indicated E'' peak position of composite.

Table 7.3 DSC and TGA results of HDPE/RS composites extruded at different temperature

Extrusion temperature [c, d]	DSC [a]				TGA		
	Cooling		2nd Heating		Rice Straw		HDPE
(°C)	T_c (°C) [b]	X_R (%)	T_m (°C)	X_R (%)	T_o (°C)	T_p (°C)	T_p (°C)
Pure HDPE	116.0	100	132.1	100	-	-	464.3
190	116.4	97.3	133.0	91.6	264.9	313.3	465.2
225	117.3	97.5	132.1	91.8	264.8	313.2	464.8
245	117.0	97.8	132.1	91.8	272.1	315.4	465.2

[a] The heating rates were 10 °C/min for all DSC and TGA tests;
[b] Subscript c, R, m, o, and p stand for crystallization, relative, melting, onset and peak, respectively;
[c] Extrusion temperature for pure HDPE (as control) is 170°C;
[d] The weight ratio of HDPE/RS is fixed at 75/25 for all composites.

7.3.2 Effect of Processing Method on HDPE/Nylon-6/RS Composites

Mechanical strength and modulus properties of resultant HDPE/nylon-6/RS composites modified by two compatibilizers (SEBS-g-MA and PE-g-MA) are summarized in Table 7.4 along with statistical information for each category and three main factors. The mechanical properties of HDPE/nylon-6 matrix modified by two compatibilizers are also listed as a control group.

ANOVA data showed that processing method significantly influenced four mechanical properties (three strength properties and tensile modulus). Detailed statistical ranking showed that composites made by one-step method had significantly better strengths than these by two-step method at fixed HDPE/nylon ratio and RS content, while the latter showed slightly better modulus. Compared to the control group, composites made by one-step method had obviously better tensile and flexural properties, especially at a HDPE/nylon ratio of 70/30 (w/w). Their impact strengths were however, significantly lower. It remains unclear that if the degradation of RS during high-temperature extrusion caused toughness loss. Therefore, SEM micrographs of impact-fractured surfaces of HDPE/nylon-6 blends (a) and HDPE/nylon-6/RS composites (b), respectively, are compared in Fig. 7.2. Generally, impact strength is highly related to filler dispersion and strength, and interphase bonding. As shown, nylon-6 balls were dispersed uniformly in HDPE matrix in HDPE/nylon-6 blends (Fig. 7.2a1). However, no strong interphase bonding is observed between nylon-6 ball and matrix (Fig. 7.2a2). The picture of xylene etched HDPE/nylon-6 surface (Fig. 7.2a3) showed fairly uniform dispersion of nylon-6 balls in inner matrix. Therefore, dispersion of nylon-6 in matrix was not responsible for the poor impact strength. As a result, the poor HDPE-nylon interphase caused by the strong polarity difference between the two polymers is probably responsible for it. During impact test, the crack propagated rapidly along the gap between matrix and nylon-6 balls as indicated by undeformed

Table 7.4 Summary of mechanical properties of HDPE/nylon-6 and HDPE/nylon-6/RS composites

HDPE/nylon ratio (w/w)	Rice straw content [c] (wt%)	Strength Property			Modulus Property	
		Tensile strength (MPa)	Flexural strength (MPa)	Impact strength (KJ/m^2)	Tensile modulus (GPa)	Flexural modulus (GPa)
Control group						
80/20		22.0(.4)C [a, b]	23.9(.4)G	4.33(.28)A	0.44(.01)D	0.78(.03)G
70/30		23.8(.6)B	28.7(.3)F	4.41(.12)A	0.49(.01)D	0.97(.07)F
One-step						
80/20	20	19.5(.5)D	31.7(.9)E	3.12(.15)C	1.91(.13)C	1.36(.07)E
	30	19.6(.7)D	35.9(.6)CD	3.04(.15)C	2.82(.57)B	2.02(.01)A
70/30	20	24.4(.5)B	38.1(1.3)B	3.59(.18)B	2.22(.19)C	1.53(.07)D
	30	26.2(.2)A	41.9(.3)A	3.14(.14)C	2.80(.14)B	1.81(.02)C
Two-step						
80/20	20	18.6(.4)E	29.5(.6)F	3.10(.20)C	2.18(.10)C	1.39(.05)E
	30	19.7(.3)D	31.3(.4)E	2.98(.07)C	3.29(.42)A	1.80(.07)C
70/30	20	22.3(.4)C	35.5(.4)D	3.07(.06)C	2.15(.14)C	1.53(.02)D
	30	22.7(.8)C	36.6(.7)C	2.76(.16)D	2.95(.22)AB	1.90(.03)B
Main factor ANOVA[d]						
Processing method		***	***	**	*	0.4417
HDPE/nylon ratio		***	***	0.2337	0.8363	0.1254
RS content		0.7783	*	***	***	***

[a] Mean values with the same capitalized letter for each property are not significantly different at the 5% significance level;
[b] Numbers in the parenthesis are standard deviation based on five specimens;
[c] RS content is based on total composite weight;
[d] 3-way ANOVA under H_0: not significant *vs.* H_1: not H_0. Signs for P-value of accepting H_0 are: *: P <0.05; **: P <0.01; ***: P <0.0001. P-values higher than 0.05 are listed numerically.

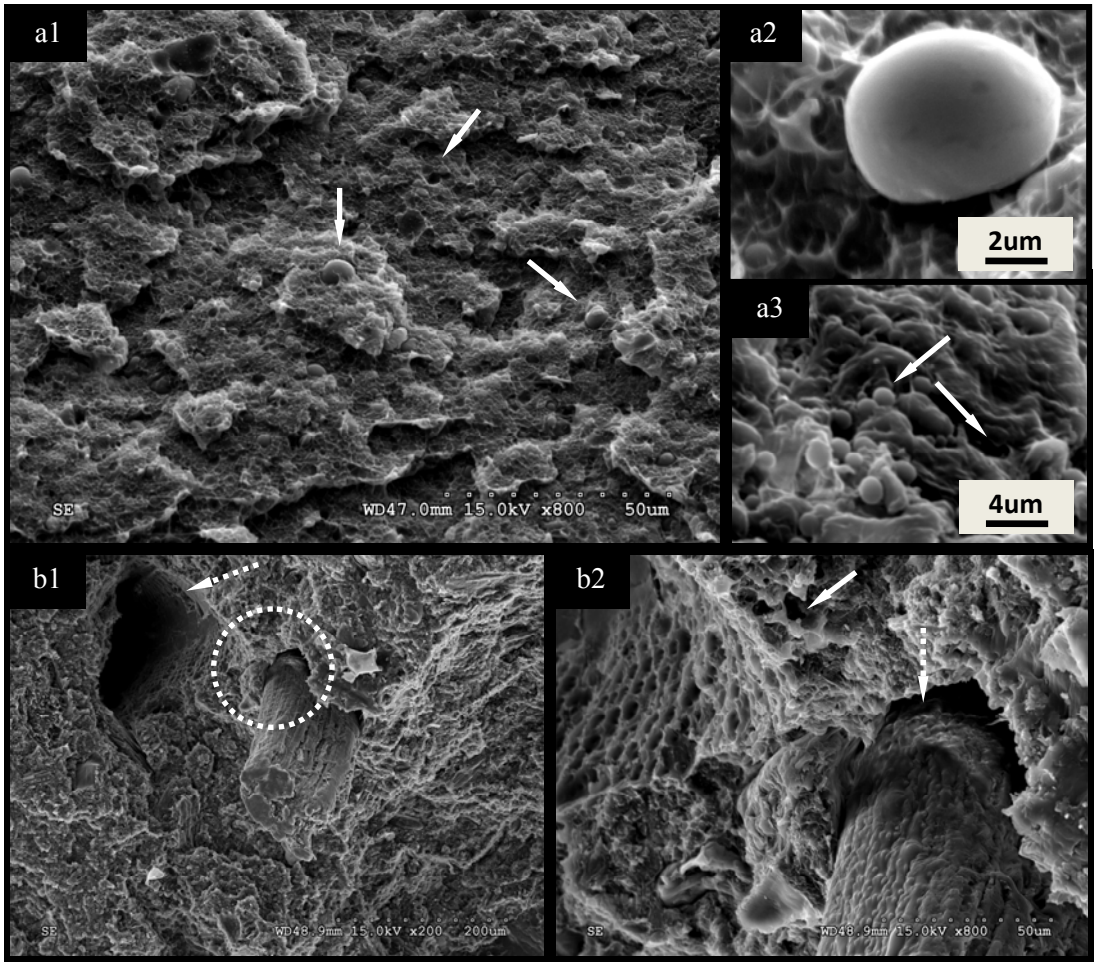

Fig. 7.2 SEM micrograph of impact-fractured surfaces of HDPE/nylon-6 and HDPE/nylon-6/RS composites: (a1) HDPE/nylon-6 surface; (a2) detailed nylon-6 ball; (a3) xylene etched HDPE/nylon-6 surface; (b1) HDPE/nylon-6/RS surface; (b2) local detail corresponding to the dashed circle shown in b1. Solid arrows indicate nylon-6 balls or holes; dashed arrows indicate poor local matrix-RS interphase.

matrix and exposed nylon-6 balls and holes. After introduction of RS, the matrix-RS interphase became the weakest one. As shown in Fig. 7.2b1, for a typical impact-fractured surface of composites, RS fiber was pulled-out and remained unbroken. Detailed image (Fig. 7.2b2) showed smooth fiber surface and gaped matrix-RS interphase, as well as nylon-6 balls and holes, and fiber disfigurement was not observed. Therefore, the interphase compatibility of HDPE/nylon-6/RS ternary system was still poor, although compatibilizers were added and obviously improved the dispersion of nylon-6. Thus, more effective compatibilizer for the ternary system should be the priority for improving impact strength. On the other hand, high-temperature processing (e.g. 235°C) should be safe for RS fiber (the total weight loss ca. 7-13wt % at this temperature) since fiber disfigurement was not obviously.

Statistical analysis also confirmed that RS content significantly influenced mechanical properties of composites (Table 7.4). Obviously, increasing RS content from 20 to 30wt%, tensile and flexural strengths and moduli were increased, while impact strength was decreased for all composites. HDPE/nylon-6 ratio showed no significant influence on impact strength and two moduli by statistical analysis. However, increasing nylon-6 content in the matrix, the tensile and flexural strength of composites were significantly increased.

Fig. 7.3 shows the dynamic mechanical spectrum of HDPE/nylon-6 and HDPE/nylon-6/RS composites with fixed matrix/RS ratio of 70:30 (w/w). As expected, the magnitude of storage modulus E' was obviously increased with the incorporation of rigid RS fiber into HDPE/nylon-6 matrix due to the enhanced stiffness. Among these composites, the one-step extruded composites with HDPE/nylon-6 ratio of 80/20 (w/w) exhibited the maximum E', while two-step extruded composites with HDPE/nylon-6 ratio of 70/30 (w/w) had the second high E' during most temperature range. This trend was in agreement with that obtained from the static mechanical data (Table 7.4). Obtained from the loss modulus (E'') curves, the α -relaxation

temperature of HDPE/nylon-6 matrix located around 45°C. Obviously, it shifted to higher temperatures (rectangular) after introduction of RS fiber into matrix, which may be attributed to the restriction effect caused by fiber on reducing the segmental mobility of polymer molecules at the relaxation temperatures (Mohanty et al. 2006). However, there was no remarkable difference between different composites, implying that the restriction effect was not changed by the processing method. The one-step extruded composites with HDPE/nylon-6 ratio of 80/20 (w/w) exhibited the highest E'', which is in agreement with results obtained from static mechanical test (Table 7.4). Also, the lower $\tan\delta$ of composites shown in Fig. 7.3 indicated better elastic characteristic of composites than HDPE/nylon-6 matrix, and the difference between various composites was not remarkable.

The DSC test showed that the crystallization and melting temperatures of nylon-6 in composites were slightly decreased after the addition of fiber (Table 7.5). In addition, crystallization temperatures of nylon-6 in composites made by one-step method appeared to be lower than those made by the two-step method. The relative crystallization degree X_R of nylon-6 in composites had remarkable difference. Compared to HDPE/nylon-6 matrix (set as base, i.e., 100% crystallization), the one-step method decreased the X_R of nylon-6, while the two-step method increased them. It was possibly attributed to the different mixing results of HDPE/nylon matrix caused by different methods. For HDPE, the addition of fiber obviously decreased its crystallization degree. The TGA test indicated that, compared to the one-step method, the two-step method slightly increased the peak temperatures, T_p, of degradation stage of rice straw in composites, but it also decreased the T_p of HDPE. No obvious difference on the T_p of degradation stage of nylon-6 in composites was observed. Also, the onset degradation temperatures, T_o, of fiber were not affected by the processing method.

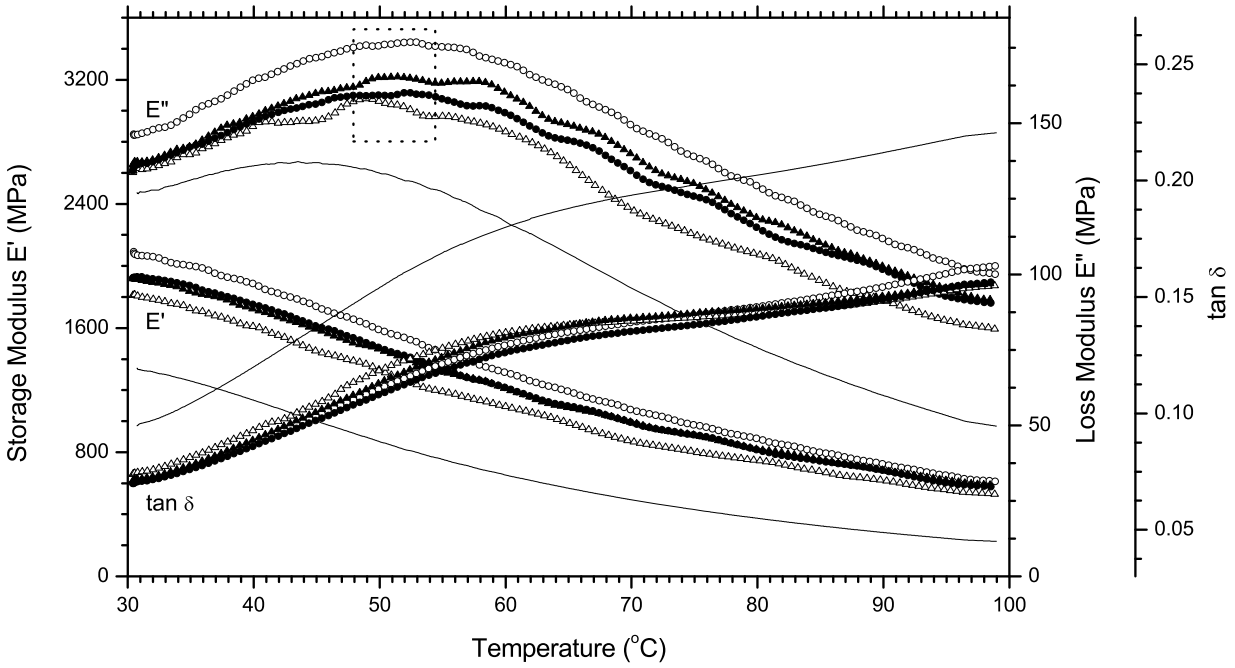

Fig. 7.3 Storage modulus (E'), loss modulus (E'') and damping factor (tan δ) of HDPE/nylon-6 (solid line) and HDPE/nylon-6/RS composites (symbols, ○: one-step, HDPE/nylon = 80:20; Δ: one-step, HDPE/nylon = 70:30; ●: two-step, HDPE/nylon = 80:20; and ▲: two-step, HDPE/nylon = 70:30). Dashed rectangular indicated E'' peak position of composites. The matrix/RS ratio is fixed at 70:30.

Table 7.5 DSC and TGA results of HDPE/nylon-6/RS composites manufactured by different extrusion process

System [c]	DSC [a]						TGA			
	T_c (°C) [b]		T_m (°C)		X_R (%)		Rice Straw		HDPE	Nylon-6
	HDPE	Nylon-6	HDPE	Nylon-6	HDPE	Nylon-6	T_o (°C)	T_p (°C)	T_p (°C)	T_p (°C)
HDPE/nylon-6 = 80/20 (w/w)										
No fiber	116.3	188.8	132.6	221.8	100	100	-	-	-	467.7
One-step	116.2	185.6	132.1	219.7	80.6	88.4	267.3	315.6	415.7	469.4
Two-step	116.2	186.8	131.5	219.5	78.8	125.7	266.3	318.2	412.5	469.9
HDPE/nylon-6 = 70/30 (w/w)										
No fiber	117.0	189.3	132.1	221.5	100	100	-	-	-	467.9
One-step	116.2	185.7	131.3	219.7	81.6	89.5	267.8	316.7	415.3	469.5
Two-step	116.4	187.5	131.6	219.9	80.5	107.5	266.5	318.9	412.7	469.7

[a] The heating rates were 10 °C/min for all DSC and TGA tests;
[b] Subscript c, R, m, o, and p stand for crystallization, relative, melting, onset and peak, respectively;
[c] The weight ratio of matrix/RS is 80/20 for all composites.

7.4 CONCLUSIONS

Processing temperature limit and corresponding weight loss of rice straw (RS) fiber during extrusion were investigated. The limit was used to aid manufacturing HDPE/nylon-6/RS composites. The weight loss under the condition was calculated by the model obtained in the previous chapters.

It was found that 13% weight loss seems to be the limit for RS to maintain its strength. Based on thermal degradation model, the temperature limit was established to be around 235°C, assuming heating rate in initial period of 40-120°C/min and melt-blending time of 150s. Under this limit, high-temperature one-step extrusion was feasible for manufacturing HDPE/nylon-6/RS composites without significant strength loss caused by thermal degradation of fiber. A two-step method, which intended to reduce the degradation of RS and promote the compatibility of HDPE/nylon-6 combined matrix, failed to exhibit better performance than the one-step method. The weight loss limit, 13%, and the thermal degradation model developed could be practically employed in natural fiber reinforced polymer composite manufacturing.

7.5 REFERENCES

Caulfield, D. F., Jacobson, R. E., Sears, K. D., and Underwood, J. H. (2001). "Fiber reinforced engineering plastics." *In: the 2nd International Conference on Advanced Engineered Wood* Composites, Maine, ME, USA.

Chen, J. M., and Gardner, D. J. (2008). "Dynamic mechanical properties of extruded nylon-wood composites." *Polymer Composites*, 29(4), 372-379.

Chiono, V., Filippi, S., Yordanov, H., Minkova, L., and Magagnini, P. (2003). "Reactive compatibilizer precursors for LDPE/PA6 blends. III: ethylene-glycidylmethacrylate copolymer." *Polymer*, 44(8), 2423-2432.

Filippi, S., Yordanov, H., Minkova, L., Polacco, G., and Talarico, M. (2004). "Reactive compatibilizer precursors for LDPE/PA6 blends, 4(a) - Maleic anhydride and glycidyl methacrylate grafted SEBS." *Macromolecular Materials and Engineering*, 289(6), 512-523.

Ganan, P., and Mondragon, I. (2003). "Thermal and degradation behavior of fique fiber reinforced thermoplastic matrix composites." *Journal of Thermal Analysis and Calorimetry*, 73(3), 783-795.

Gonzalez, C., and Myers, G. E. (1993). "Thermal-degradation of wood fillers at the melt-processing temperatures of wood-plastic composites - effects on wood mechanical-properties and production of volatiles." *International Journal of Polymeric Materials*, 23(1-2), 67-85.

Jacobson, R. E., Caulfield, D. F., Sears, K. D., and Underwood, J. H. (2001). "Low temperature processing of cellulose pulp fibers into nylon-6 and other thermoplastics." *In: the Sixth International Conference on Wood fiber-Plastic Composites*, Forest Products Society, Madison, WI, USA, 127-133.

Jiang, C. H., Filippi, S., and Magagnini, P. (2003). "Reactive compatibilizer precursors for LDPE/PA6 blends. II: maleic anhydride grafted polyethylenes." *Polymer*, 44(8), 2411-2422.

Lu, J. Z., Doyle, T. W., and Li, K. (2007). "Preparation and characterization of wood-(nylon 12) composites." *Journal of Applied Polymer Science*, 103(1), 270-276.

McHenry, E., and Stachurski, Z. H. (2003). "Composite materials based on wood and nylon fibre." *Composites Part a-Applied Science and Manufacturing*, 34(2), 171-181.

Mohanty, S., Verma, S. K., and Nayak, S. K. (2006). "Dynamic mechanical and thermal properties of MAPE treated jute/HDPE composites." *Composites Science and Technology*, 66(3-4), 538-547.

Moran, J., Alvarez, V., Petrucci, R., Kenny, J., and Vazquez, A. (2007). "Mechanical properties of polypropylene composites based on natural fibers subjected to multiple extrusion cycles." *Journal of Applied Polymer Science*, 103(1), 228-237.

Myers, G. E., Chahyadi, I. S., Gonzalez, C., Coberly, C. A., and Ermer, D. S. (1991). "Wood flour and polypropylene or high-density polyethylene composites - influence of maleated polypropylene concentration and extrusion temperature on properties." *International Journal of Polymeric Materials*, 15(3-4), 171-186.

Santos, P. A., Spinace, M. A. S., Fermoselli, K. K. G., and De Paoli, M. A. (2007). "Polyamide-6/vegetal fiber composite prepared by extrusion and injection molding." *Composites Part a-Applied Science and Manufacturing*, 38(12), 2404-2411.

Sapieha, S., Pupo, J. F., and Schreiber, H. P. (1989). "Thermal-degradation of cellulose-containing composites during processing." *Journal of Applied Polymer Science*, 37(1), 233-240.

Utracki, L. A. (1995). "History of commercial polymer alloys and blends (from a perspective of the patent literature)." *Polymer Engineering and Science*, 35(1), 2-17.

Yordanov, C., and Minkova, L. (2005). "Fractionated crystallization of compatibilized LDPE/PA6 blends." *European Polymer Journal*, 41(3), 527-534.

CHAPTER 8 CONCLUSION

The study described in this dissertation intends (1) to investigate and model thermal decomposition process of common natural fibers with detailed analysis on rice straw (RS) system; and (2) to investigate the influence of different rice straw components, and compatibilizers on various properties of rice-straw based polymer composites.

The conclusions of this study are as follows:

(1) Assuming a global model occurring within the entire degradation of natural fibers with consideration of fiber as one pseudo-component, $RO(n>1)$ model can be used to describe the non-isothermal degradation process of most selected fibers. The kinetic parameters include activation energy range of 160-170 kJ/mol; parameter n in $RO(n)=(1-\alpha)^n$ of 3-4; and $\ln A$ between 35 and 42 $\ln s^{-1}$. The obtained predictive weight loss curves simulated the thermal weight loss process of natural fibers within an acceptable error limit of 5%.

(2) Within acceptable error limit of less than 3%, $RO(n>1)$ model described the isothermal degradation process of rice straw fiber in a temperature range of less than approximately 265°C. The kinetic parameters include activation energy value of 116±5 kJ/mol; parameter n in $RO(n)=(1-\alpha)^n$ of 3.0±0.2; and $\ln A$ of 18.7±0.1 $\ln s^{-1}$. For temperature range higher than 265°C, the model did not perform well due to pre-degradation during instrument setting period. The model obtained has practical significance for introducing straw fiber into some engineering plastics with comparatively lower melting temperature.

(3) The cumulative percentage distribution of length and aspect ratio of various fibers after milling fitted a lognormal distribution well with two parameters defining the curve location and shape. Rice straw fibers can work well with both VHDPE and RHDPE as reinforcing filler.

Also, different components of rice straw had no significant influence on mechanical properties of composites. This implies the application prospect of conveniently introducing rice straw into thermoplastic composite industry. However, it also implies that special attention should be paid to rice husk composites due to their different mechanical behavior with composites made by other rice straw components.

(4) The PE-g-MA/EPR ratio affected mechanical properties of composites modified by combined compatibilizers. The optimum PE-g-MA/EPR ratio was considered to be 2:1 and 1:1 for PE-g-MA/uEPR and PE-g-MA/EPR-g-MA modified composites, respectively. At the optimum ratio, composites modified by combined compatibilizers showed better strength and impact toughness, and acceptable modulus compared to those modified by either EPR or EPR-g-MA, possibly due to better interphase bonding brought by the MA group. Also, composites modified by combined PE-g-MA/EPR-g-MA systems showed better impact strength than that modified by PE-g-MA alone. The study further showed that, at the optimum compatibilizer ratio, increasing total combined compatibilizer content improved strength but decreased modulus of composites. DSC and TGA study indicated that different compatibilizers and their combination had no significant effect on crystallization behavior of HDPE matrix and thermal stability of resultant composites.

(5) It was found that 13% weight seemed to be the limit for rice straw to maintain its strength in a composite system. Based on thermal degradation model, the temperature limit was around 235°C assuming heating rate in initial period of 40-120°C/min and melt-blending time of 150s. Under this limit, high-temperature one-step extrusion was feasible for manufacturing HDPE/nylon-6/RS composites without significant strength loss caused by thermal degradation of fiber. The two-step method, which intended to reduce the degradation of RS and promote the compatibility of HDPE/nylon-6 combined matrix, failed to exhibit better performance than the

one-step method. The weight loss limit, 13%, and the thermal degradation model developed could be practically employed in natural fiber reinforced polymer composite manufacturing.

Based on limitations of this study, future work is suggested as:

(1) For modeling of natural fiber thermal degradation process, fundamental research on elementary reactions of fiber degradation is intensively needed. These elementary reactions are probably related to the chemical components and molecular structures of cellulose, hemicelluloses and lignin, and minor components. The reactants, reaction type, rate, conditions and products of involved elementary reactions need to be clearly defined and precisely measured. This is the key to reveal the secret of fiber thermal process.

(2) For natural fiber reinforced polymer composites, more effective compatibilizers for improving matrix-fiber interphase bonding are strongly needed. The research on dispersion of these compatibilizers in resultant composites is also very necessary. Moreover, the influence of fiber shape and size on various properties of composites needs to be carefully investigated. It has been realized that fiber shape and size affects not only mechanical property but also thermal degradation of fiber. In addition, research on improving thermal stability of natural fiber is strongly needed.

APPENDIX LETTER OF PERMISSION

ELSEVIER LICENSE
TERMS AND CONDITIONS

Aug 19, 2008

This is a License Agreement between Fei Yao ("You") and Elsevier ("Elsevier"). The license consists of your order details, the terms and conditions provided by Elsevier, and the payment terms and conditions.

Supplier	Elsevier Limited The Boulevard,Langford Lane Kidlington,Oxford,OX5 1GB,UK
Registered Company Number	1982084
Customer name	Fei Yao
Customer address	Rm227, School of Renewable Natural Resources, Baton Rouge, LA 70803
License Number	2012631414000
License date	Aug 19, 2008
Licensed content publisher	Elsevier
Licensed content publication	Polymer Degradation and Stability
Licensed content title	Thermal decomposition kinetics of natural fibers: Activation energy with dynamic thermogravimetric analysis
Licensed content author	Fei Yao, Qinglin Wu, Yong Lei, Weihong Guo and Yanjun Xu
Licensed content date	January 2008
Volume number	93
Issue number	1
Pages	9
Type of Use	Thesis / Dissertation
Portion	Full article
Format	Electronic
You are an author of the Elsevier article	Yes
Are you translating?	No
Purchase order number	
Expected publication date	Dec 2008
Elsevier VAT number	GB 494 6272 12
Permissions price	0.00 USD
Value added tax 0.0%	0.00 USD

Total 0.00 USD

Terms and Conditions

INTRODUCTION

1. The publisher for this copyrighted material is Elsevier. By clicking "accept" in connection with completing this licensing transaction, you agree that the following terms and conditions apply to this transaction (along with the Billing and Payment terms and conditions established by Copyright Clearance Center, Inc. ("CCC"), at the time that you opened your Rightslink account and that are available at any time at <http://myaccount.copyright.com>).

GENERAL TERMS

2. Elsevier hereby grants you permission to reproduce the aforementioned material subject to the terms and conditions indicated.

3. Acknowledgement: If any part of the material to be used (for example, figures) has appeared in our publication with credit or acknowledgement to another source, permission must also be sought from that source. If such permission is not obtained then that material may not be included in your publication/copies. Suitable acknowledgement to the source must be made, either as a footnote or in a reference list at the end of your publication, as follows:

“Reprinted from Publication title, Vol /edition number, Author(s), Title of article / title of chapter, Pages No., Copyright (Year), with permission from Elsevier [OR APPLICABLE SOCIETY COPYRIGHT OWNER].” Also Lancet special credit - “Reprinted from The Lancet, Vol. number, Author(s), Title of article, Pages No., Copyright (Year), with permission from Elsevier.”

4. Reproduction of this material is confined to the purpose and/or media for which permission is hereby given.

5. Altering/Modifying Material: Not Permitted. However figures and illustrations may be altered/adapted minimally to serve your work. Any other abbreviations, additions, deletions and/or any other alterations shall be made only with prior written authorization of Elsevier Ltd. (Please contact Elsevier at permissions@elsevier.com)

6. If the permission fee for the requested use of our material is waived in this instance, please be advised that your future requests for Elsevier materials may attract a fee.

7. Reservation of Rights: Publisher reserves all rights not specifically granted in the combination of (i) the license details provided by you and accepted in the course of this licensing transaction, (ii) these terms and conditions and (iii) CCC's Billing and Payment terms and conditions.

8. License Contingent Upon Payment: While you may exercise the rights licensed immediately upon issuance of the license at the end of the licensing process for the transaction, provided that you have disclosed complete and accurate details of your proposed use, no license is finally effective unless and until full payment is received from you (either by publisher or by CCC) as provided in CCC's Billing and Payment terms and conditions. If full payment is not received on a timely basis, then any license preliminarily granted shall be deemed automatically revoked and shall be void as if never granted. Further, in the event that you breach any of these terms and conditions or any of CCC's Billing and Payment

terms and conditions, the license is automatically revoked and shall be void as if never granted. Use of materials as described in a revoked license, as well as any use of the materials beyond the scope of an unrevoked license, may constitute copyright infringement and publisher reserves the right to take any and all action to protect its copyright in the materials.

9. Warranties: Publisher makes no representations or warranties with respect to the licensed material.

10. Indemnity: You hereby indemnify and agree to hold harmless publisher and CCC, and their respective officers, directors, employees and agents, from and against any and all claims arising out of your use of the licensed material other than as specifically authorized pursuant to this license.

11. No Transfer of License: This license is personal to you and may not be sublicensed, assigned, or transferred by you to any other person without publisher's written permission.

12. No Amendment Except in Writing: This license may not be amended except in a writing signed by both parties (or, in the case of publisher, by CCC on publisher's behalf).

13. Objection to Contrary Terms: Publisher hereby objects to any terms contained in any purchase order, acknowledgment, check endorsement or other writing prepared by you, which terms are inconsistent with these terms and conditions or CCC's Billing and Payment terms and conditions. These terms and conditions, together with CCC's Billing and Payment terms and conditions (which are incorporated herein), comprise the entire agreement between you and publisher (and CCC) concerning this licensing transaction. In the event of any conflict between your obligations established by these terms and conditions and those established by CCC's Billing and Payment terms and conditions, these terms and conditions shall control.

14. Revocation: Elsevier or Copyright Clearance Center may deny the permissions described in this License at their sole discretion, for any reason or no reason, with a full refund payable to you. Notice of such denial will be made using the contact information provided by you. Failure to receive such notice will not alter or invalidate the denial. In no event will Elsevier or Copyright Clearance Center be responsible or liable for any costs, expenses or damage incurred by you as a result of a denial of your permission request, other than a refund of the amount(s) paid by you to Elsevier and/or Copyright Clearance Center for denied permissions.

LIMITED LICENSE

The following terms and conditions apply to specific license types:

15. **Translation**: This permission is granted for non-exclusive world **English** rights only unless your license was granted for translation rights. If you licensed translation rights you may only translate this content into the languages you requested. A professional translator must perform all translations and reproduce the content word for word preserving the integrity of the article. If this license is to re-use 1 or 2 figures then permission is granted for non-exclusive world rights in all languages.

16. **Website**: The following terms and conditions apply to electronic reserve and author websites:
Electronic reserve: If licensed material is to be posted to website, the web site is to be password-protected and made available only to bona fide students registered on a relevant

course if:
This license was made in connection with a course,
This permission is granted for 1 year only. You may obtain a license for future website posting,
All content posted to the web site must maintain the copyright information line on the bottom of each image,
A hyper-text must be included to the Homepage of the journal from which you are licensing at http://www.sciencedirect.com/science/journal/xxxxx or the Elsevier homepage for books at http://www.elsevier.com , and
Central Storage: This license does not include permission for a scanned version of the material to be stored in a central repository such as that provided by Heron/XanEdu.

17. **Author website** for journals with the following additional clauses:
This permission is granted for 1 year only. You may obtain a license for future website posting,
All content posted to the web site must maintain the copyright information line on the bottom of each image, and
The permission granted is limited to the personal version of your paper. You are not allowed to download and post the published electronic version of your article (whether PDF or HTML, proof or final version), nor may you scan the printed edition to create an electronic version,
A hyper-text must be included to the Homepage of the journal from which you are licensing at http://www.sciencedirect.com/science/journal/xxxxx , or the Elsevier homepage for books at http://www.elsevier.com and
Central Storage: This license does not include permission for a scanned version of the material to be stored in a central repository such as that provided by Heron/XanEdu.

18. **Author website** for books with the following additional clauses:
Authors are permitted to place a brief summary of their work online only.
A hyper-text must be included to the Elsevier homepage at http://www.elsevier.com
This permission is granted for 1 year only. You may obtain a license for future website posting,
All content posted to the web site must maintain the copyright information line on the bottom of each image, and
The permission granted is limited to the personal version of your paper. You are not allowed to download and post the published electronic version of your article (whether PDF or HTML, proof or final version), nor may you scan the printed edition to create an electronic version,
A hyper-text must be included to the Homepage of the journal from which you are licensing at http://www.sciencedirect.com/science/journal/xxxxx , or the Elsevier homepage for books at http://www.elsevier.com and
Central Storage: This license does not include permission for a scanned version of the material to be stored in a central repository such as that provided by Heron/XanEdu.

19. **Website** (regular and for author): “A hyper-text must be included to the Homepage of the journal from which you are licensing at http://www.sciencedirect.com/science/journal/xxxxx.”

20. **Thesis/Dissertation**: If your license is for use in a thesis/dissertation your thesis may be submitted to your institution in either print or electronic form. Should your thesis be published commercially, please reapply for permission. These requirements include permission for the Library and Archives of Canada to supply single copies, on demand, of

the complete thesis and include permission for UMI to supply single copies, on demand, of the complete thesis. Should your thesis be published commercially, please reapply for permission.

v1.2

21. **Other conditions:**

None

ELSEVIER LICENSE
TERMS AND CONDITIONS

Aug 19, 2008

This is a License Agreement between Fei Yao ("You") and Elsevier ("Elsevier"). The license consists of your order details, the terms and conditions provided by Elsevier, and the payment terms and conditions.

Supplier	Elsevier Limited The Boulevard,Langford Lane Kidlington,Oxford,OX5 1GB,UK
Registered Company Number	1982084
Customer name	Fei Yao
Customer address	Rm227, School of Renewable Natural Resources, Baton Rouge, LA 70803
License Number	2012631101205
License date	Aug 19, 2008
Licensed content publisher	Elsevier
Licensed content publication	Industrial Crops and Products
Licensed content title	Rice straw fiber-reinforced high-density polyethylene composite: Effect of fiber type and loading
Licensed content author	Fei Yao, Qinglin Wu, Yong Lei and Yanjun Xu
Licensed content date	July 2008
Volume number	28
Issue number	1
Pages	10
Type of Use	Thesis / Dissertation
Portion	Full article
Format	Electronic
You are an author of the Elsevier article	Yes
Are you translating?	No
Purchase order number	
Expected publication date	Dec 2008
Elsevier VAT number	GB 494 6272 12
Permissions price	0.00 USD
Value added tax 0.0%	0.00 USD
Total	0.00 USD
Terms and Conditions	

INTRODUCTION

1. The publisher for this copyrighted material is Elsevier. By clicking "accept" in connection with completing this licensing transaction, you agree that the following terms and conditions apply to this transaction (along with the Billing and Payment terms and conditions established by Copyright Clearance Center, Inc. ("CCC"), at the time that you opened your Rightslink account and that are available at any time at <http://myaccount.copyright.com>).

GENERAL TERMS

2. Elsevier hereby grants you permission to reproduce the aforementioned material subject to the terms and conditions indicated.

3. Acknowledgement: If any part of the material to be used (for example, figures) has appeared in our publication with credit or acknowledgement to another source, permission must also be sought from that source. If such permission is not obtained then that material may not be included in your publication/copies. Suitable acknowledgement to the source must be made, either as a footnote or in a reference list at the end of your publication, as follows:

“Reprinted from Publication title, Vol /edition number, Author(s), Title of article / title of chapter, Pages No., Copyright (Year), with permission from Elsevier [OR APPLICABLE SOCIETY COPYRIGHT OWNER].” Also Lancet special credit - “Reprinted from The Lancet, Vol. number, Author(s), Title of article, Pages No., Copyright (Year), with permission from Elsevier.”

4. Reproduction of this material is confined to the purpose and/or media for which permission is hereby given.

5. Altering/Modifying Material: Not Permitted. However figures and illustrations may be altered/adapted minimally to serve your work. Any other abbreviations, additions, deletions and/or any other alterations shall be made only with prior written authorization of Elsevier Ltd. (Please contact Elsevier at permissions@elsevier.com)

6. If the permission fee for the requested use of our material is waived in this instance, please be advised that your future requests for Elsevier materials may attract a fee.

7. Reservation of Rights: Publisher reserves all rights not specifically granted in the combination of (i) the license details provided by you and accepted in the course of this licensing transaction, (ii) these terms and conditions and (iii) CCC's Billing and Payment terms and conditions.

8. License Contingent Upon Payment: While you may exercise the rights licensed immediately upon issuance of the license at the end of the licensing process for the transaction, provided that you have disclosed complete and accurate details of your proposed use, no license is finally effective unless and until full payment is received from you (either by publisher or by CCC) as provided in CCC's Billing and Payment terms and conditions. If full payment is not received on a timely basis, then any license preliminarily granted shall be deemed automatically revoked and shall be void as if never granted. Further, in the event that you breach any of these terms and conditions or any of CCC's Billing and Payment terms and conditions, the license is automatically revoked and shall be void as if never granted. Use of materials as described in a revoked license, as well as any use of the materials beyond the scope of an unrevoked license, may constitute copyright infringement

and publisher reserves the right to take any and all action to protect its copyright in the materials.

9. Warranties: Publisher makes no representations or warranties with respect to the licensed material.

10. Indemnity: You hereby indemnify and agree to hold harmless publisher and CCC, and their respective officers, directors, employees and agents, from and against any and all claims arising out of your use of the licensed material other than as specifically authorized pursuant to this license.

11. No Transfer of License: This license is personal to you and may not be sublicensed, assigned, or transferred by you to any other person without publisher's written permission.

12. No Amendment Except in Writing: This license may not be amended except in a writing signed by both parties (or, in the case of publisher, by CCC on publisher's behalf).

13. Objection to Contrary Terms: Publisher hereby objects to any terms contained in any purchase order, acknowledgment, check endorsement or other writing prepared by you, which terms are inconsistent with these terms and conditions or CCC's Billing and Payment terms and conditions. These terms and conditions, together with CCC's Billing and Payment terms and conditions (which are incorporated herein), comprise the entire agreement between you and publisher (and CCC) concerning this licensing transaction. In the event of any conflict between your obligations established by these terms and conditions and those established by CCC's Billing and Payment terms and conditions, these terms and conditions shall control.

14. Revocation: Elsevier or Copyright Clearance Center may deny the permissions described in this License at their sole discretion, for any reason or no reason, with a full refund payable to you. Notice of such denial will be made using the contact information provided by you. Failure to receive such notice will not alter or invalidate the denial. In no event will Elsevier or Copyright Clearance Center be responsible or liable for any costs, expenses or damage incurred by you as a result of a denial of your permission request, other than a refund of the amount(s) paid by you to Elsevier and/or Copyright Clearance Center for denied permissions.

LIMITED LICENSE

The following terms and conditions apply to specific license types:

15. **Translation**: This permission is granted for non-exclusive world **English** rights only unless your license was granted for translation rights. If you licensed translation rights you may only translate this content into the languages you requested. A professional translator must perform all translations and reproduce the content word for word preserving the integrity of the article. If this license is to re-use 1 or 2 figures then permission is granted for non-exclusive world rights in all languages.

16. **Website**: The following terms and conditions apply to electronic reserve and author websites:
Electronic reserve: If licensed material is to be posted to website, the web site is to be password-protected and made available only to bona fide students registered on a relevant course if:
This license was made in connection with a course,
This permission is granted for 1 year only. You may obtain a license for future website

posting,
All content posted to the web site must maintain the copyright information line on the bottom of each image,
A hyper-text must be included to the Homepage of the journal from which you are licensing at http://www.sciencedirect.com/science/journal/xxxxx or the Elsevier homepage for books at http://www.elsevier.com , and
Central Storage: This license does not include permission for a scanned version of the material to be stored in a central repository such as that provided by Heron/XanEdu.

17. **Author website** for journals with the following additional clauses:
This permission is granted for 1 year only. You may obtain a license for future website posting,
All content posted to the web site must maintain the copyright information line on the bottom of each image, and
The permission granted is limited to the personal version of your paper. You are not allowed to download and post the published electronic version of your article (whether PDF or HTML, proof or final version), nor may you scan the printed edition to create an electronic version,
A hyper-text must be included to the Homepage of the journal from which you are licensing at http://www.sciencedirect.com/science/journal/xxxxx , or the Elsevier homepage for books at http://www.elsevier.com and
Central Storage: This license does not include permission for a scanned version of the material to be stored in a central repository such as that provided by Heron/XanEdu.

18. **Author website** for books with the following additional clauses:
Authors are permitted to place a brief summary of their work online only.
A hyper-text must be included to the Elsevier homepage at http://www.elsevier.com
This permission is granted for 1 year only. You may obtain a license for future website posting,
All content posted to the web site must maintain the copyright information line on the bottom of each image, and
The permission granted is limited to the personal version of your paper. You are not allowed to download and post the published electronic version of your article (whether PDF or HTML, proof or final version), nor may you scan the printed edition to create an electronic version,
A hyper-text must be included to the Homepage of the journal from which you are licensing at http://www.sciencedirect.com/science/journal/xxxxx , or the Elsevier homepage for books at http://www.elsevier.com and
Central Storage: This license does not include permission for a scanned version of the material to be stored in a central repository such as that provided by Heron/XanEdu.

19. **Website** (regular and for author): “A hyper-text must be included to the Homepage of the journal from which you are licensing at http://www.sciencedirect.com/science/journal/xxxxx.”

20. **Thesis/Dissertation**: If your license is for use in a thesis/dissertation your thesis may be submitted to your institution in either print or electronic form. Should your thesis be published commercially, please reapply for permission. These requirements include permission for the Library and Archives of Canada to supply single copies, on demand, of the complete thesis and include permission for UMI to supply single copies, on demand, of the complete thesis. Should your thesis be published commercially, please reapply for permission.

v1.2

21. **Other conditions:**

None

VITA

Fei Yao was born in December 1979 in Zhenjiang, Jiangsu, People's Republic of China. After completing high school in his hometown, he attended Nanjing Forestry University, Nanjing, China, and graduated with a Bachelor of Engineering in wood science and technology in June 2002. He continued his study at the Graduate School of his alma mater and received his Master of Engineering in wood science and technology in June 2004. Afterward, he worked as an instructor at Nanjing Forestry University for one year. He came to Louisiana State University for his doctoral program in natural fiber reinforced polymer composites in August 2005. Currently, he is a candidate for the degree of Doctor of Philosophy in forestry in the School of Renewable Natural Resources. He will receive his doctoral degree in December 2008.